Technische Universität München

Fakultät für Medizin

Influence of shortened telomeres on the development of the adenocarcinoma of the esophagus and evaluation of telomere length as a biomarker

Vincenz Kajetan Sahm

Vollständiger Abdruck der von der Fakultät für Medizin der Technischen Universität München zur Erlangung des akademischen Grades eines

Doktors der Medizin

genehmigten Dissertation.

Vorsitzender: apl. Prof. Dr. Bernhard Haslinger

Prüfer der Dissertation:
1. Prof. Dr. Michael Quante
2. Prof. Dr. Roland Schmid

Die Dissertation wurde am 09.01.2023 bei der Technischen Universität München eingereicht und durch die Fakultät für Medizin am 18.07.2023 angenommen.

Table of contents

Abstract

Esophageal adenocarcinoma (EAC) is a disease with high mortality and increasing incidence. While exact mechanisms of its development are unknown, longstanding gastroesophageal reflux disease (GERD) with subsequent development of Barrett's esophagus (BE) and more advanced stages hereof (low-grade dysplasia (LGD) and high-grade dysplasia (HGD)) have been postulated as precursor lesions of EAC.

Aim of this thesis was to examine cellular aspects of carcinogenesis of EAC regarding telomere biology. Firstly, we analyzed the influence of shortened telomeres on the carcinogenic process utilizing an established mouse model of the disease (L2-IL-1B mouse model). Secondly, we aimed to translate our findings to human patients. For that, we examined telomere length properties of human BE-, LGD- and EAC samples.

We could demonstrate that engineered telomere dysfunction in the L2-IL-1B mouse model led to an increase of tumor initiation presumably due to chromosomal instability. In human tissue samples we verified prior findings of telomere shortening in preneoplastic histologic stages of the disease and found telomere shortening to be cell-type dependent.

In summary, our data propagate telomere shortening as an important factor during esophageal carcinogenesis and suggest telomere length analysis as a possible approach in surveillance strategies in future studies.

Kurzfassung

Das Adenokarzinom des Ösophagus (EAC) ist eine Krankheit mit hoher Mortalität und zunehmender Inzidenz. Während die genauen Mechanismen ihrer Entstehung nicht bekannt sind, wurden eine langjährige gastro-ösophageale Refluxkrankheit (GERD) mit nachfolgender Entwicklung von Barrett-Ösophagus (BE), leichtgradiger Dysplasie (LGD), hochgradiger Dysplasie (HGD) als Vorläuferläsionen des EAC postuliert.

Ziel dieser Arbeit war es, zelluläre Aspekte der Karzinogenese des EAC in Bezug auf die Telomerbiologie zu untersuchen. Unter Verwendung eines etablierten Mausmodells der Krankheit (L2-IL-1B Mausmodell) analysierten wir zunächst den Einfluss verkürzter Telomere auf dieses Mausmodell für BE. Des Weiteren war es Ziel dieser Arbeit, die Ergebnisse auf menschliche Patienten zu übertragen. Hierfür wurden menschliche Proben von BE, LGD und EAC in Bezug auf die Telomerlängenmerkmale untersucht.

Wir konnten zeigen, dass im L2-IL-1B-Mausmodell künstlich erzeugte Telomerdysfunktion zu einer Zunahme der Tumorinitiierung führte, welche vermutlich auf chromosomale Instabilität zurückzuführen ist. An menschlichen Proben konnten wir frühere Forschungsergebnisse, welche eine Telomerverkürzung in histologisch präneoplastischen Stadien beschrieben hatten, verifizieren. Weiterhin konnten wir zeigen, dass die Telomerverkürzung Zelltyp-abhängig ist.

Zusammenfassend legen unsere Daten nahe, dass die Telomerverkürzung ein wichtiger Faktor in der Karzinogenese des Ösophaguskarzinoms ist und die Telomerlängenanalyse ein möglicher Ansatz für Überwachungsstrategien in zukünftigen Studien darstellt.

1 Introduction

1.1 Adenocarcinoma of the esophagus (EAC) and associated diseases

1.1.1 EAC

EAC is a malignancy with poor prognosis, high mortality and rising incidence (Lambert & Hainaut, 2007). Despite advances in diagnosis and treatment, 5-year survival rates for esophageal cancer remain low at about 15-20% (Pennathur, Gibson, Jobe, & Luketich, 2013). The poor prognosis is partly due to its diagnosis at a late stage (T3 or T4 of Tumor-Nodes-Metastasis (TNM) classification) and its aggressive nature: Direct extension is facilitated by the lack of esophageal serosa – an anatomical barrier – and spreading occurs both lymphatically and hematogenously (Postlethwait, 1983). Almost all esophageal cancers that originate in the esophagus can be classified into either EAC or squamous cell carcinoma (SCC), with other cancer types being on the fringes. Over the past decades epidemiology of the esophageal cancer has changed fundamentally. Over forty years ago the SCC was responsible for more than 90% of cases in the US, by now the EAC has by far overtaken the SCC, representing about 60% of cases in the US and similar rates in other first world countries (Noone AM). However, worldwide, SCC remains the predominant form of esophageal cancer with a ratio of more than 7 to 1 (Arnold, Soerjomataram, Ferlay, & Forman, 2015; Fabian & Leung, 2021). The reason for this deviation can be explained by differences in pathogenesis and risk factors of these two cancer types. The SCC is strongly linked to tobacco use and alcohol consumption (De Stefani, Barrios, & Fierro, 1993; Gammon et al., 1997; Vaughan, Davis, Kristal, & Thomas, 1995). With a combination of both risk factors synergizing to further increase the risk for SCC (C. H. Lee et al., 2007). Together with findings that nutritional deficiencies and poor oral hygiene further contribute make the SCC a disease of people with low socioeconomic status (Abnet et al., 2005; Abnet et al., 2001; Brown et al., 2001; P. R. Taylor et al., 2003). EAC on the other hand can be attributed to the “western lifestyle” with obesity and the associated gastroesophageal reflux disease (GERD) as well as Barrett’s esophagus (BE) constituting the most important risk factors (Engel et al., 2003; Lagergren, Bergstrom, Adami, & Nyren, 2000; Lagergren, Bergstrom, Lindgren, & Nyren, 1999; Reid, Li, Galipeau, & Vaughan, 2010).

1.1.2 Gastroesophageal reflux disease (GERD)

GERD is a common disease in western industrialized countries with a high prevalence which ranges from 10% to 28% and evidence of rising incidence over the last three decades (El-Serag, Sweet, Winchester, & Dent, 2014; Richter & Rubenstein, 2018).

GERD is defined as abnormal reflux of gastric contents, including hydrochloric acid as well as acid- and bile salts which can lead to mucosal damage and symptoms like heartburn, acid regurgitation and dysphagia (Badillo & Francis, 2014; El-Serag et al., 2014). Reflux is usually caused by a transient dysfunction of the lower esophageal sphincter which allows gastric and duodenal juices to enter the esophagus. A mix of both juices is common and more harmful than gastric juices alone (Kauer et al., 1995; Macke et al., 2011). Respective of whether endoscopically visible mucosal damage is found, GERD can further be classified into erosive reflux disease (ERD) with lesions and non-erosive reflux disease (NERD) without lesions (Badillo & Francis, 2014). GERD may induce chronic inflammation in both esophagus and stomach in the form of esophagitis and carditis/gastritis (Quante, Abrams, Lee, & Wang, 2012). This in turn can give rise to BE as a metaplastic tissue alteration. However, it has been found that a considerable amount of more than 50% of patients that complain of symptoms of reflux without visible lesions and therefore lack BE (Koop et al., 2014). Nonetheless, with symptoms of GERD persisting, the odds ratio for developing BE increases (Curvers et al., 2010; Koop et al., 2014; J. B. Taylor & Rubenstein, 2010) and about 5% to 10% of GERD patients are diagnosed with BE (di Pietro, Alzoubaidi, & Fitzgerald, 2014; Kapoor, Lohani, Lee, Agrawal, & Mittal, 2015). Severity of GERD symptoms does not increase the risk for EAC (Nason et al., 2011).

GERD also strongly correlates with body mass index (BMI) (Hajar, Castell, Ghomrawi, Rackett, & Hila, 2012; Hayakawa, Sethi, Sepulveda, Bass, & Wang, 2016). This has been explained in two ways: Firstly, excessive amounts of visceral fat exert direct mechanical pressure onto the stomach, hence increasing intragastric pressure which leads to more frequent relaxation of the lower esophageal sphincter and subsequent reflux (Abdallah, Maradey-Romero, Lewis, Perzynski, & Fass, 2015). Secondly, visceral fat has been shown to produce inflammatory hormones such as IL-6 and TNFα, which are known to be

upregulated in BE (Abdallah et al., 2015; di Pietro et al., 2014; Hayakawa et al., 2016). In a meta-analysis, patients with central adiposity had a higher risk of developing BE compared to patients of normal weight even after adjustment for BMI and GERD, implying a role for central obesity in BE pathogenesis independent of reflux (Singh et al., 2013).

1.1.3 Barrett esophagus (BE)

BE is a known precursor lesion of EAC and is an acquired condition in which the normal stratified epithelium of the distal esophagus is replaced by a metaplastic columnar lined epithelium (CLE) with intestinal differentiation. The latter exhibits three types of cells: A transitional-type epithelium with cardiac mucous-secreting glands, an atrophic gastric-fundic-type epithelium containing parietal and chief cells and specialized columnar epithelium with intestinal-type goblet cells (Paull et al., 1976). There is disagreement among gastroenterological societies whether the presence of goblet cells in metaplastic tissue is mandatory for diagnosis of BE (Fitzgerald et al., 2014; Spechler, Sharma, Souza, Inadomi, & Shaheen, 2011). The reason for this is conflicting data for risk progression of metaplastic tissue: while some studies only found metaplastic tissue with goblet cells to be at risk of progression other studies could show that metaplastic tissue that lack goblet cells can progress to EAC as well.

BE is situated at the junction between squamous esophageal epithelium and columnar gastric/cardia epithelium (see Figure 1). Incidence of BE has been rising rapidly over the last few decades (Brandtner & Quante, 2016) with known risk factors being long-standing GERD, central obesity (Singh et al., 2013), male gender, older age (Rubenstein, Mattek, & Eisen, 2010; Rubenstein et al., 2013) and family history (Chak et al., 2002). BE may over time show histologic signs of dysplasia and then be categorized – according to severity – as low-grade dysplasia (LGD) or high-grade dysplasia (HGD), accompanied by a higher risk of EAC development. The nature of BE as a precursor lesion of EAC and its good accessibility by endoscopic means has spurred thorough investigation. Hereby of interest are not only factors that determine risk of progression, but also knowledge of BE development. Insights in these areas may yield new approaches for BE risk stratification or treatment, respectively.

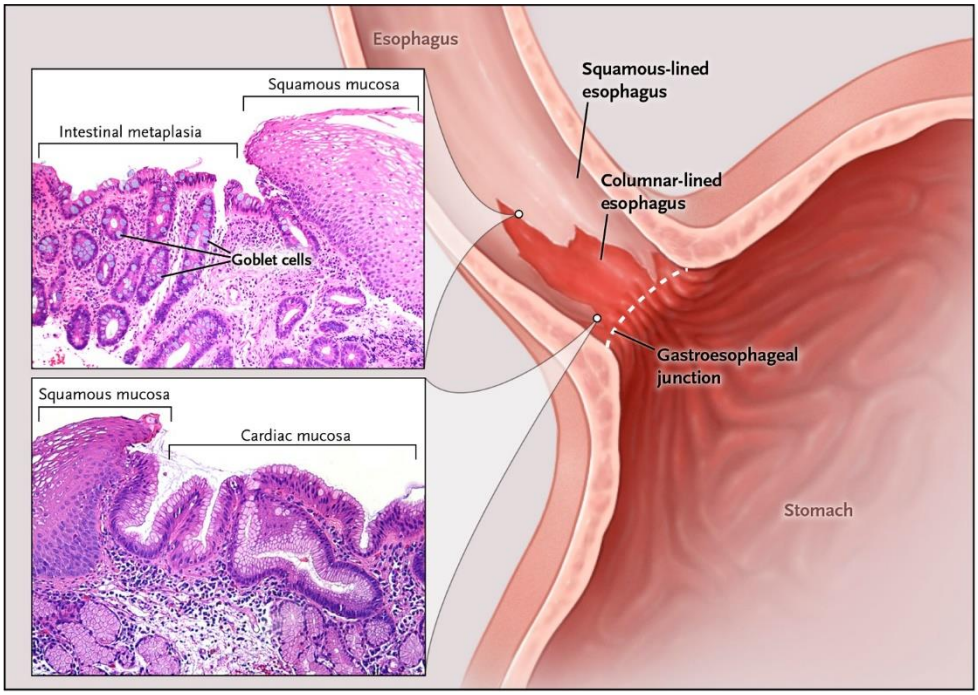

Figure 1 Schematic illustration of Barret Esophagus (BE) and corresponding exemplary histology

This graphic is taken out of a publication by Spechler et al. (Spechler & Souza, 2014). The dashed white line represents the gastroesophageal junction which can be determined macroscopically through endoscopy. It marks the transition zone between the most proximal gastric folds and the squamous-lined esophagus. In the case of BE, columnar-lined mucosa extends in tongue-like shape past the gastroesophageal junction. The histologic samples on the left side show Hematoxylin & Eosin (H&E)-stained tissue originating from two distinct areas of the distal esophagus. The upper specimen displays a portion of squamous esophagus right next to metaplasia with intestinal differentiation (i.e. presence of goblet cells). The other sample, closer to the gastroesophageal junction, depicts the physiological transition of cardiac mucosa with mucus-secreting glands to esophageal stratified epithelium. Differing by guidelines, intestinal metaplasia in the form of goblet cells or cardiac mucosa alone classifies BE.

1.1.3.1 Origin of BE

In recent research, focus has been set on finding the cell of origin of BE. In theory, knowledge of the cell of origin would enable researchers to monitor the suspected stepwise development of BE to EAC and may also yield valuable information on epithelial carcinogenesis in general. Furthermore, it could introduce new approaches of prevention and therapy. Several theories exist regarding the cell of origin in BE and factors that give rise to BE (see Figure 2). The most significant theories are explained in the following sections.

1.1.3.1.1 Trans-differentiation of squamous epithelial cells

One theory postulates BE to be a consequence of trans-differentiation of squamous epithelium stem cells. In this model acid-biliary reflux over time alters squamous stem cells by downregulating their original squamous expression program in favor of a columnar cell expression program hence leading to dedifferentiation. Resident stem cells in the squamous esophagus of adult mice and humans have been found in several studies (Croagh, Phillips, Redvers, Thomas, & Kaur, 2007; Doupe et al., 2012; Kalabis et al., 2008; Pan et al., 2013). Pan et al. (Pan et al., 2013) showed through lineage tracing experiments that small populations of uncommitted, slow cycling cells can be detected in the basal layer of squamous epithelium in metaplastic BE and gastric tissues, as well as in normal esophageal epithelium, indicating a resident stem cell niche. In addition to that, other investigators have suggested that multipotent stem cells reside in the inter-papillary basal layer of the esophageal squamous epithelium (Seery & Watt, 2000). Also, conversion of CLE to stratified squamous epithelium has been reported for the developing mouse esophagus (Barbera et al., 2015; Yu, Slack, & Tosh, 2005), making a reversal of this development seem possible. However, trans-differentiation as defined above has never been observed and the finding that BE heterogeneity results from multiple independent stem- or progenitor-clones likely argues against a trans-differentiation model (Leedham et al., 2008).

1.1.3.1.2 Expansion of residual embryonic cells

Throughout gastrointestinal development a population of embryonic Car4+ cells, some of which with Krt7 expression, remain at the squamocolumnar junction (SCJ) (X. Wang et al., 2011) and are therefore named residual embryonic cells (REC). In a mouse model that lacks the squamous epithelial stem cell survival factor p63, metaplastic tissue is found at the proximal stomach and esophagus,

which exhibits strong histological and molecular similarities to human BE (von Holzen & Enders, 2012; X. Wang et al., 2011). In a setting of reflux mediated inflammation and cell death of squamous cells, these REC may migrate towards the specialized squamous epithelium and give rise to BE (M. Quante, J. A. Abrams, et al., 2012; X. Wang et al., 2011)

1.1.3.1.3 Migration of bone-marrow derived cells (BMDC)

In response to tissue injury and inflammation, bone-marrow derived cells (BMDC) can migrate through peripheral organs (Hutchinson et al., 2011; Quante & Wang, 2008). A study by Hutchinson et al. suggests that stem cells in glands can be replaced by BMDC and give rise to the stromal and epithelial compartment of EAC in mouse and human (Hutchinson et al., 2011). In another study using a rat model for BE, BMDC of male rats were injected into irradiated female rats. Later it was found that some epithelial cells and columnar epithelium of the intestinal metaplasia were of male descent. This suggests that multi-potent progenitor cells from the bone marrow contribute to esophageal regeneration and metaplasia in this mouse model (Sarosi et al., 2008).

1.1.3.1.4 Expansion of submucosal glandular cells

One possible source of origin of BE are submucosal esophageal glands. These glands have been shown to be both genetically and morphologically linked to BE glands (Coad et al., 2005). This theory however is weakened by the fact that also mice and rats, which do not have submucosal glands, can develop BE (Miwa et al., 1996).

1.1.3.1.5 Expansion of gastric cardia cells

This theory has been proposed by Quante et al. upon discoveries in the L2-IL-1B mouse model for BE. The same mouse model was also used in the work at hand and is described in more detail in section 1.1.5.1. Lineage tracing experiments in this model found the progenitor cells of the metaplastic BE tissue that these mice develop to be Lgr5+ stem cells of the gastric cardia (M. Quante, G. Bhagat, et al., 2012). In addition to that a multitude of progenitor markers like Cckbr (Y. Lee et al., 2017), Sox2 (O'Neil, Petersen, Choi, Engevik, & Goldenring, 2017) and Lgr5+ (M. Quante, G. Bhagat, et al., 2012) marks the cardia epithelium a transitional epithelium, a known “hot spot” for preneoplastic lesions in other organ systems (Mirkovic et al., 2015; E. J. Yang et al., 2015) making the SCJ or gastric cardia a likely source of origin for BE.

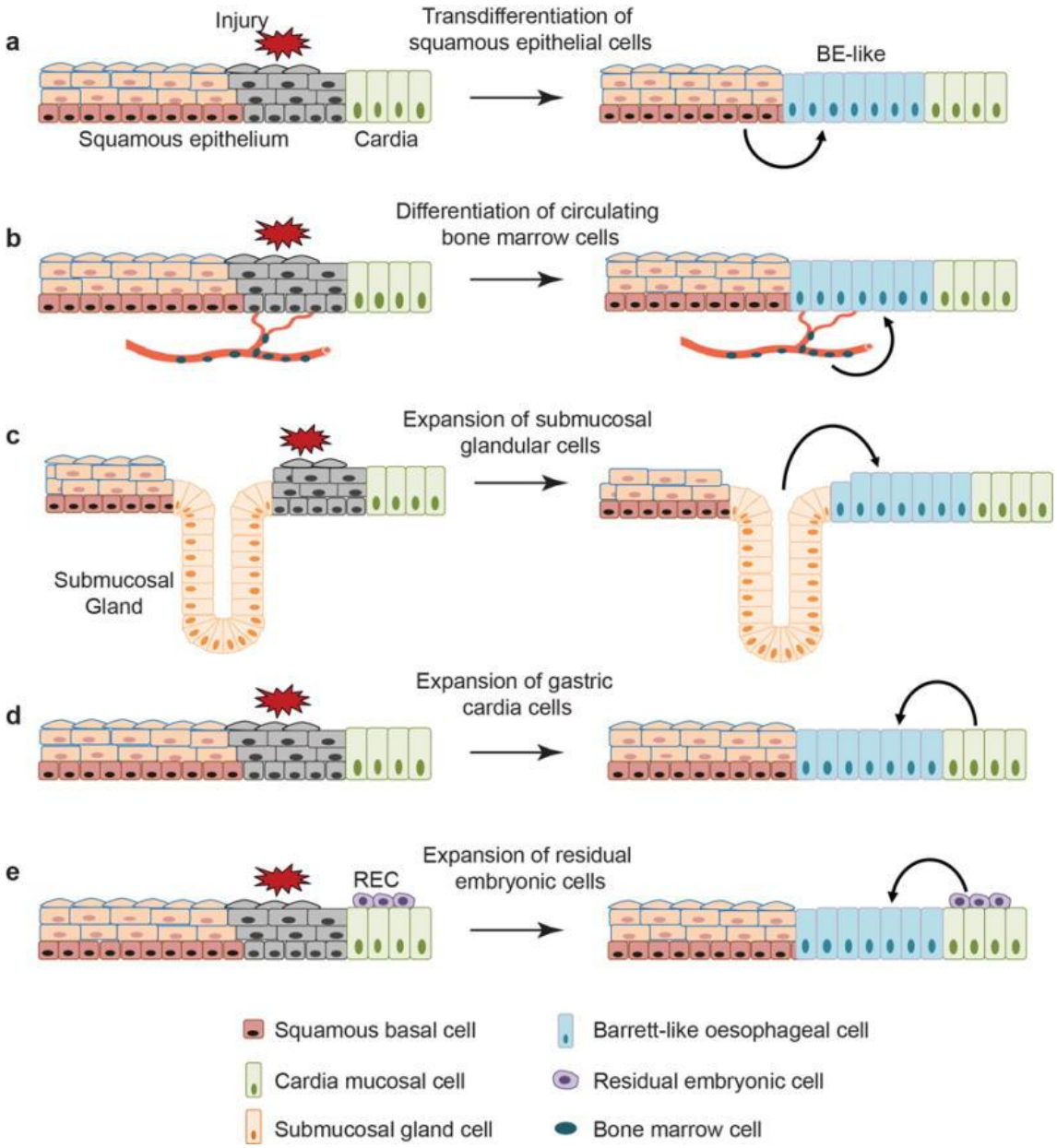

Figure 2 Cell of origin of BE in a schematic overview

This figure is taken from a publication by Jiang, M., et al. (Jiang et al., 2017). It illustrates several proposed theories of BE origin, which are commented on in more detail above. ***a*** *Esophageal squamous cells de-differentiate to form metaplasia.* ***b*** *Bone marrow derived stem cells (BMDC) migrate into the esophagus in response to inflammation.* ***c*** *Stem cells of the submucosal esophageal glands expand and give rise to BE.* ***d*** *Progenitor cells of the gastric cardia migrate into the esophagus triggered by inflammatory signals.* ***e*** *Residual embryonic cells (REC) can give rise to the lesion.*

1.1.3.2 Clinical management of BE

It has been reported that less than 10% of patients with EAC had a prior diagnose of BE (Bhat et al., 2015; Dulai, Guha, Kahn, Gornbein, & Weinstein, 2002; Hvid-Jensen, Pedersen, Drewes, Sorensen, & Funch-Jensen, 2011) and a large portion of patients with BE lack symptoms and remain undetected (Dulai et al., 2002). In one study a share as high as 40% of EAC patients had no history of GERD symptoms (Lagergren et al., 1999). Conversion rate of BE to EAC is relatively low with an incidence between 0.2% to 0.6% annually (di Pietro et al., 2014; M. Quante, G. Bhagat, et al., 2012; Souza, 2010; Spechler, 2013; Yousef et al., 2008). BE nonetheless constitutes a precursor lesion of EAC and therefore guidelines recommend endoscopic surveillance using high-definition white light endoscopy with biopsy of all visible lesions and four-quadrant random biopsies obtained every 2 cm with subsequent histological analysis (Fitzgerald et al., 2014; Shaheen, Falk, Iyer, & Gerson, 2016; Spechler et al., 2011). Intervals between control biopsies however are subject of intense dispute in the scientific community.

BE can be classified as either short segment BE (BE segments <3 cm) or long segment BE (BE segments >3 cm) (Sharma, Morales, & Sampliner, 1998) with long segment BE at higher risk of progression (approximately 14% per cm length of BE) (Gopal et al., 2003).

Histologic assessment of BE biopsies is at the heart of current surveillance strategies (Falk, 2016; Levine, Blount, Rudolph, & Reid, 2000). BE is hereby classified in five categories: Indefinite of dysplasia, non-dysplastic, LGD, HGD and EAC. This classification is strongly tied to the notion of a stepwise dysplasia-to-carcinoma sequence which assumes BE to progress first to LGD then HGD and ultimately EAC. Non-dysplastic BE was found to progress to EAC at a rate of 0.2% to 0.6% per year (di Pietro et al., 2014; M. Quante, G. Bhagat, et al., 2012; Souza, 2010; Spechler, 2013; Yousef et al., 2008). Investigation of dysplastic BE have been giving rates of progression for LGD between 0.4% to 13.4% (Wani, Rubenstein, Vieth, & Bergman, 2016) and approximately 31 % for HGD (Kahn et al., 2015).

Guidelines recommend that diagnosis of dysplasia should be confirmed by an experienced pathologist. If LGD is found and confirmed in a successive endoscopy with biopsy, endoscopic mucosal resection (EMR) and subsequent

radiofrequency ablation (RFA) is recommended (Shaheen et al., 2016; Weusten et al., 2017). Endoscopic therapy has been demonstrated to be effective (Pouw et al., 2010; Shaheen et al., 2009), however a low but real rate of complications (Bulsiewicz et al., 2013) and costs for these interventions (Hur et al., 2012) must be taken into consideration. This, together with the fact that recurrence after ablation is not uncommon (Agoston et al., 2016; Gupta et al., 2013) and the low incidence of BE progression, increase the need for biomarkers to aid decision making regarding surveillance and treatment.

1.1.3.3 Biomarkers of BE

Biomarkers are measurable factors that correlate with a disease or even present with a mechanistic effect that causes or contributes to the disease. Biomarkers can be used in different ways including risk stratification for the development of a disease, prediction of response to a treatment or estimation of prognosis (Vargas & Harris, 2016). Ideally, a biomarker is one that is easily accessible, cost-effective, correlates with the burden of the disease and is both sensitive and specific. In the case of BE, four principled ideas that would prompt development of a biomarker have been proposed by Qureshi et al. (Qureshi, Stachler, Haque, & Odze, 2018):

- Identification of patients who have a greater chance of progression to EAC.
- Increase sensitivity of diagnosis of progression to dysplasia.
- Measure and anticipate response to treatment.
- Single out patients with low risk of progression and therefore lessen costly and possibly harmful surveillance for these individuals.

In the case of BE several biomarkers have been proposed that can be assigned to histologic analysis, genomic alterations and epigenetic changes or protein expression. In the following section the most promising biomarkers or those with relevance to the work are summarized. For a thorough analysis of this broad field, the reader may be referred to recent reviews (Konda & Souza, 2018; Qureshi et al., 2018). Several genomic alterations have been proposed as possible biomarkers. These alterations can be subdivided into different categories. One of it, aneuploidy, is defined as an abnormal number of chromosomes in a cell. Aneuploidy was correlated to disease progression (M. Fang et al., 2004; Rabinovitch, Reid, Haggitt, Norwood, & Rubin, 1989). Loss of heterozygosity (LOH) marks another chromosomal alteration in which both, a gene and the

surrounding chromosomal region is lost. Among the most affected regions in EAC cells are 9p21 (CDKN2A/MTS1/INK4A) and 17p13 (p53) with a prevalence of approximately 75% and 95%, respectively (Galipeau, Prevo, Sanchez, Longton, & Reid, 1999). Maley et al combined genome instability with a measure of clonal expansion and found that both factors together predict progression to EAC better than either factor alone (Maley et al., 2004). Also telomere length of leukocytes as a surrogate marker of oxidative stress has also been proposed (Risques et al., 2007).

The most promising biomarker up to date besides histologic analysis is an aberrant p53 expression. In several different studies overexpression of this tumor suppressor as well lack of expression was found to be predictive of progression to EAC (Davelaar et al., 2015; Kastelein et al., 2013). However, none of these markers has been adopted thus far in clinical practice.

1.1.4 Genome instability, chromosomal instability (CIN) and implications for EAC development

In the update to their landmark paper describing the hallmarks of cancer, Hanahan and Weinberg added genome instability and inflammation as enabling characteristics that facilitate generation of the hallmarks of cancer (Hanahan & Weinberg, 2011). Genome instability refers to a high frequency of mutations within the genome. Depending on the initiating mechanism, different events can be observed, one of which is chromosomal instability (CIN). CIN terms a variation in chromosome number caused by either failure in the chromosome segregation apparatus or the mitotic checkpoint (Aguilera & Gomez-Gonzalez, 2008). One known and frequent driver of CIN is telomere crisis (Maciejowski & de Lange, 2017).

According to recent theories BE progresses to EAC through means of genome instability and clonal diversity in stem- and progenitor cell populations (Sayin, Baumeister, Wang, & Quante, 2018). The harsh environment of inflammation and genome instability selects the fittest stem cells of which one ultimately, through monoclonal expansion gives rise to EAC. This theory is supported by findings that EAC does not develop by single specific driver mutations but rather opportunistic extension due to cumulative mutations and deoxyribonucleic acid (DNA) abnormalities (Ross-Innes et al., 2015; X. Wang et al., 2011). Genome instability has been reported frequently in BE and is more pronounced in later

stages of the disease like LGD, HGD and EAC (Khara et al., 2014; Li et al., 2014). While the mechanisms for EAC transformation remain to be completely elucidated, both telomere shortening and copy number alterations (CNAs) have previously been correlated (Goh et al., 2011; Shammas et al., 2008; Shiraishi et al., 2009). Telomere shortening has been observed in BE at all histologic grades (Finley et al., 2006).

1.1.5 Animal models for BE and EAC

For modelling of BE and EAC in animals, rodents, particularly mice and rats, are commonly used. Main reasons are low cost of maintenance and the possibility of mechanistic studies with genetic modifications. Rodents are generally susceptible to BE and EAC via induction of reflux or introduction of carcinogens. However anatomical differences in comparison to humans like absence of submucosal glands and difference in keratinization must be taken into consideration (Y. Fang et al., 2013).

1.1.5.1 The L2-IL-1B- mouse model

In this transgenic mouse model, esophagitis is induced through chronic inflammation. As these mice age, BE-like metaplasia develops with subsequent transformation to EAC. Detailed characterization of this model and evaluation of its properties was conducted by Quante et al. (M. Quante, J. A. Abrams, et al., 2012; M. Quante, G. Bhagat, et al., 2012).

The model was created using modified human IL-1β cDNA (Bjorkdahl, Akerblad, Gjorloff-Wingren, Leanderson, & Dohlsten, 1999) with insertion downstream of an Epstein-Barr virus (ED-L2) promoter, that targets the oral cavity, esophagus and murine squamous forestomach (Nakagawa et al., 1997). This was done upon prior findings of a strong link between inflammation and cancer (Grivennikov, Greten, & Karin, 2010) and demonstration that IL-1β can induce carcinogenesis in the murine stomach (Tu et al., 2008). Furthermore, up-regulation of IL-1β at the squamocolumnar junction in human BE patients had been described (Fitzgerald, Abdalla, et al., 2002; Fitzgerald, Onwuegbusi, et al., 2002; O'Riordan et al., 2005).

L2-IL-1B-mice present with moderate inflammation and epithelial hyperplasia at six months of age, which develops into severe columnar metaplasia with mucus producing cells at the SCJ after 12 to 15 months. At 20 to 22 months of age, some

mice displayed HGD or intra-mucosal EAC (M. Quante, J. A. Abrams, et al., 2012; M. Quante, G. Bhagat, et al., 2012). The induced murine BE shows striking similarities to human BE: Electron microscopy examination revealed common ultrastructural features (columnar lined epithelium, microvilli, granules and mucins), Tff2 expression, $Muc5ac^+$ - and Periodic-Acid-Schiff (PAS)+, AS^+ cells. In addition, microarray analysis found upregulation of β-catenin, EVI 1 and RRas in these tumors and occasional loss of p16, increased c-Myc expression and stabilization of P53 was observed, all of which is known for human BE (M. Quante, G. Bhagat, et al., 2012). Furthermore, like in human BE, certain genes are upregulated. These include IL-6, TNF-α, Notch, Lgr5, Dclk1, Krt19 and Tff2 (M. Quante, G. Bhagat, et al., 2012). However, in contrast to human BE, the columnar lined metaplasia in L2-IL-1B-mice lack goblet cells.

Lineage tracing of BE-lesions found stem cell progenitors to be Lgr5+ and originating in the cardia (M. Quante, G. Bhagat, et al., 2012) (see 1.1.3.1.5).

1.2 Telomeres

1.2.1 Constitution of telomeres and general function

Telomeres are protective capping structures at the end of linear chromosomes (McClintock, 1939, 1941). Telomeric DNA is composed of GT-rich repeats of which sequence and length varies among different species (Klobutcher, Swanton, Donini, & Prescott, 1981; Zakian, 1989). Vertebrates have the characteristic TTAGGG repeats with great variance in length (humans 7,000 to 10,000 (20,000bp in germ cells) (Allshire, Dempster, & Hastie, 1989) and around 150,000 bp in mice (Kipling & Cooke, 1990)). More recent research revealed a more complex system: In mammals, plants and several lower eukaryotes the single strand overhang may fold back, invade into the preceding telomeric DNA and form loop structures called D-loop and T-loop. It is believed that these loops function as a seal, preventing degradation of telomeres (Cesare, Quinney, Willcox, Subramanian, & Griffith, 2003; Griffith et al., 1999; Munoz-Jordan, Cross, de Lange, & Griffith, 2001). Furthermore, several proteins have shown to be associated with telomere function. In humans, six of them (Telomeric Repeat Factor 1 (TRF1), Telomeric Repeat binding Factor 2 (TRF2), TRF1-interacting factor (TIN2), TIN2-interacting protein 1 (TPP1), Repressor Activator Protein 1 (RAP1) and Protection of Telomere 1 (POT1)) form the shelterin complex, which interacts with a number of other proteins for telomere length regulation (de Lange, 2005). Telomeres can lose their protective capacity and become dysfunctional either through continued cell divisions and the concomitant “end replication problem” (Lundblad, 1997) or through oxidative damage (Kurz et al., 2004; von Zglinicki, 2002). When telomeres become dysfunctional, telomere ends can be recognized as a double strand break which triggers growth arrest and subsequently cellular senescence or apoptosis depending on cell type (Fumagalli et al., 2012; Gong et al., 1999; Stiewe & Putzer, 2001; von Zglinicki, Saretzki, Ladhoff, d'Adda di Fagagna, & Jackson, 2005; Zou, Sfeir, Gryaznov, Shay, & Wright, 2004).

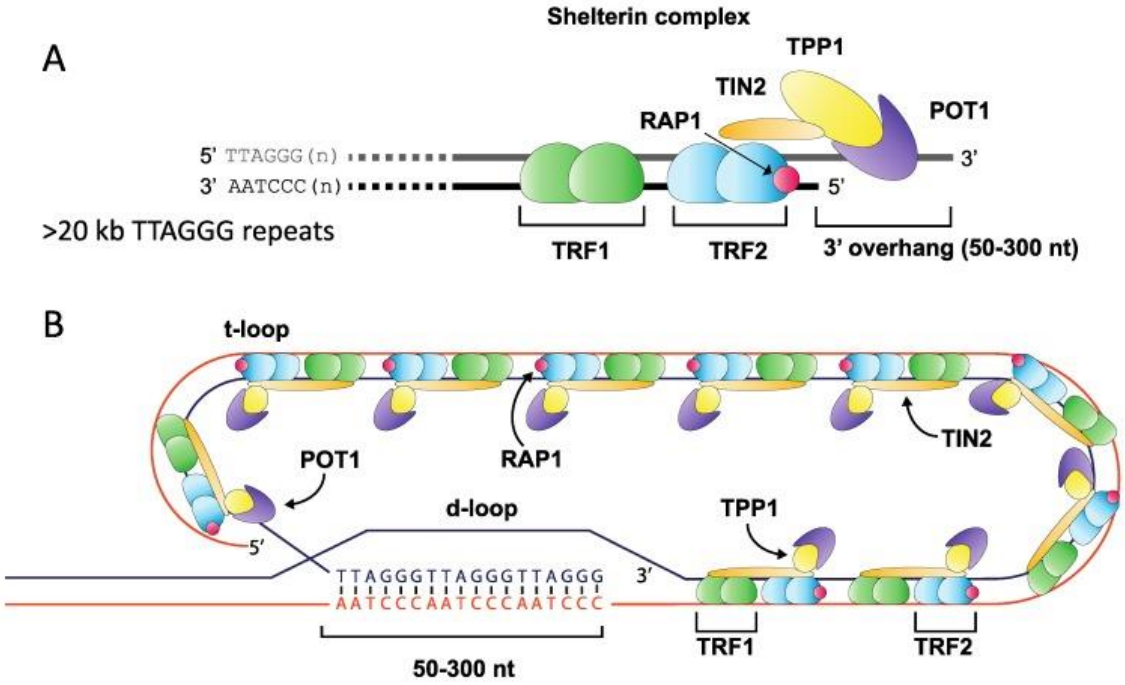

Figure 3 Telomeres, shelterin complex and resultant ultrastructure

This graphic was taken from (Cleal, Norris, & Baird, 2018) and gives a schematic overview of the telomere structure with associated proteins. In A the shelterin-complex at the telomere ends is depicted. Hereby Telomeric Repeat Factor 1 (TRF1) and Telomeric Repeat binding Factor 2 (TRF2) anchor the other shelterin-proteins TRF1-interacting factor (TIN2), Repressor Activator Protein 1 (RAP1 TIN2-interacting protein 1 (TPP1) and Protection of Telomere 1 (POT1) to the chromosome. In B arrays of shelterin-complexes bound to telomeric deoxyribonucleic acid (DNA) form an ultrastructure in the form of the t-loop with the 3' overhang creating a d-loop by invading into the forward strand and hiding the chromosome ends from the DNA repair machinery.

1.2.3 Telomerase

Telomerase is a ribonucleo-protein complex with reverse transcriptase activity that can overcome the “end-replication problem” by adding repeats of the telomere sequence (Shippen-Lentz & Blackburn, 1990). Telomerase consists - among others - of two vital components, the RNA component TERC (or TR) which acts as a telomere-template for reverse transcription (Blasco, Funk, Villeponteau, & Greider, 1995) and the telomerase reverse transcriptase (TERT) component, which is the catalytic subunit with transcriptase activity (Meyerson et al., 1997). Telomerase activity is weak or absent in normal somatic cells but is elevated in germ cells and cancer cells (Counter et al., 1992; N. W. Kim et al., 1994). Cells in telomere crisis need to either activate telomerase or activate the alternative lengthening of telomeres (ALT) pathway to restore genomic stability and proliferative capacity (Maciejowski & de Lange, 2017).

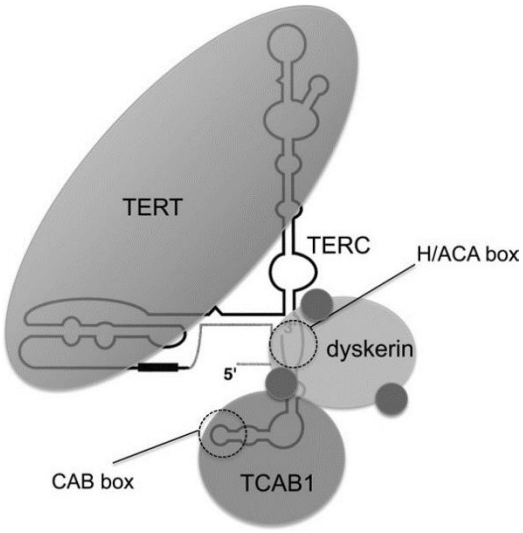

Figure 4 Schematic illustration of telomerase

This schematic presentation of telomerase and its subunits is taken from Artandi et al (Artandi & DePinho, 2010). Telomerase is a ribonucleoprotein (RNP) with several subunits of which telomerase reverse transcriptase (TERT) embodies the catalytic function and TERC providing the template for the addition of TTAGGG repeats.

1.2.4 Telomere dysfunction and implication for carcinogenesis

1.2.4.1 Tumor suppressive capacity of telomere dysfunction

Telomere shortening occurs naturally with ageing due to the “end-replication problem” (Greider & Blackburn, 1985; Harley, Futcher, & Greider, 1990) which also sets a limit to cell divisions known as the ”Hayflick limit” (Hayflick, 1965). Telomere length shorter than the average has been associated with higher incidences of several age-related diseases and shorter life span (Cawthon, Smith, O'Brien, Sivatchenko, & Kerber, 2003; Farzaneh-Far et al., 2008; Z. Yang et al., 2009). Dyskeratosis congenita e.g. is a genetic disorder that leads to shorter telomeres because of a telomerase deficiency and therefore illustrates consequences of telomere dysfunction. The disease is associated with premature graying, predisposition to cancer, vulnerability to infections, progressive bone marrow failure, and premature death in adults (Vulliamy et al., 2001). There are several factors that can lead to accelerated telomere shortening, among others smoking (McGrath, Wong, Michaud, Hunter, & De Vivo, 2007; Song, von Figura, et al., 2010) and obesity (Valdes et al., 2005), which are both believed to be a result of oxidative damage (Shammas, 2011). The link between oxidative damage and telomere shortening is rather well established in vitro (Reichert & Stier, 2017; von Zglinicki, 2002). When telomeres in a cell reach critical length senescence is induced (d'Adda di Fagagna et al., 2003; Zou et al., 2004) which acts as a tumor suppressor. Dysfunctional telomeres lead to activation of DNA-damage response (DDR) which is indicated by p53 upregulation and induction of the cyclin-dependent kinase (CDK) inhibitors p21 and p16 and lead to either senescence or apoptosis with a tumor-suppressive effect (Jacobs & de Lange, 2004; Takai, Smogorzewska, & de Lange, 2003).

1.2.4.2 Carcinogenic capacity of telomere dysfunction

Mere telomere dysfunction with unimpaired tumor suppression pathways has been associated with senescence and apoptosis (see 1.2.4.1) and therefore tumor suppression. If however senescence or apoptosis are bypassed, cells enter a phase of telomere crisis, in which increasing rates of telomere shortening lead to chromosome end-to-end fusions and subsequently mitotic missegregation (Maciejowski & de Lange, 2017). To overcome senescence or apoptosis in human cells, both inactivation of p53 and RB is needed (Jacobs & de Lange, 2004). In murine cells, inactivation of p53 already leads to telomere-based instability (Artandi & DePinho, 2010; Meena, Rudolph, & Gunes, 2015; Rudolph,

Millard, Bosenberg, & DePinho, 2001). This form of telomere-based cause of genome instability has been shown to give rise to aneuploidy, translocations, gene loss (in form of loss of heterozygosity (LOH)) and regional amplification via breakage–fusion–bridge (BFB) cycles (Artandi et al., 2000; Riboni et al., 1997; Roger et al., 2013). Another rather recently discovered event in genome instability that is attributed to telomere crisis is chromothripsis (Maciejowski, Li, Bosco, Campbell, & de Lange, 2015). It marks a novel form of genome instability that leads to tens to hundreds of chromosomal rearrangements in a single catastrophic event (Rode, Maass, Willmund, Lichter, & Ernst, 2016; Stephens et al., 2011). It has been verified as a driver for tumorigenesis in a significant amount of EACs (Nones et al., 2014) and telomere shortening and subsequent chromosomal instability has been proposed as a possible mechanism of chromothripsis (Jones & Jallepalli, 2012; Nones et al., 2014; Rode et al., 2016; Sorzano, Pascual-Montano, Sanchez de Diego, Martinez, & van Wely, 2013).

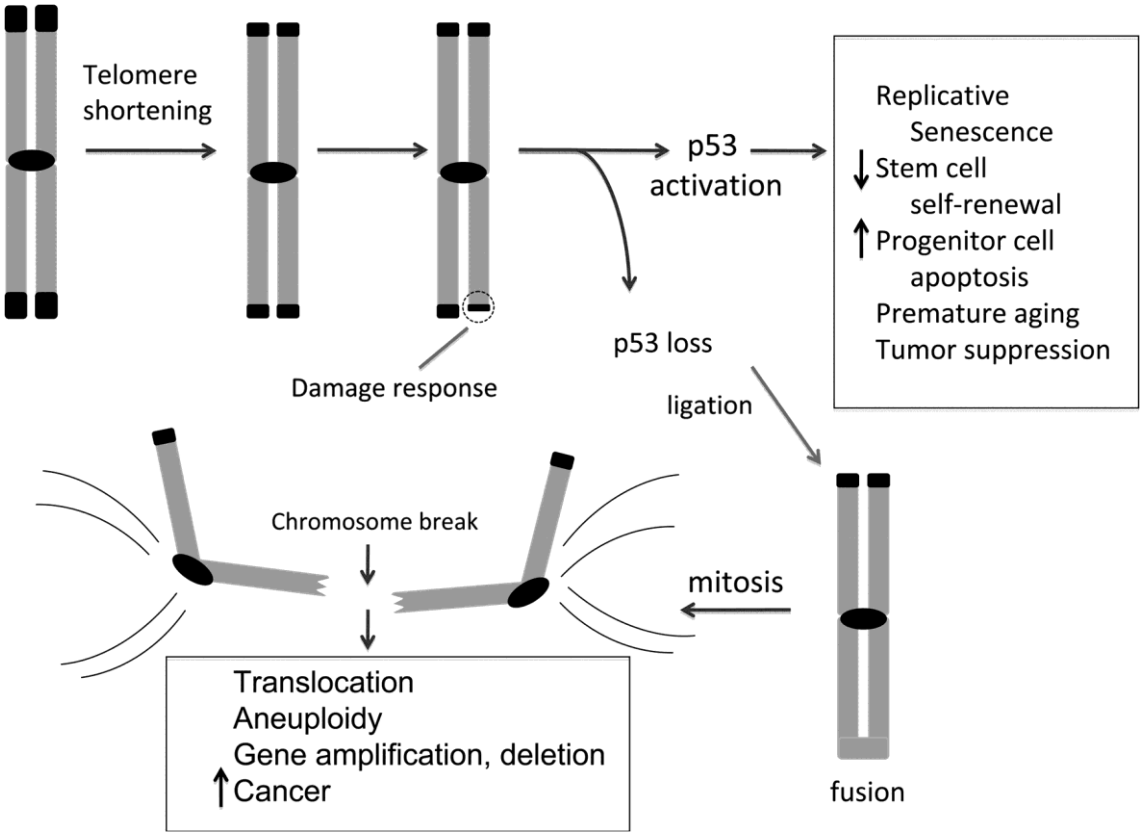

Figure 5 Impact of telomere dysfunction on carcinogenesis

This figure was taken from a publication by Artandi et.al (Artandi & DePinho, 2010). Progressive telomere shortening leads to dysfunctional telomeres and activation of the DNA-damage response system. In the case of intact p53 this entails replicative senescence, decrease of stem cell self-renewal, an increase in cancer progenitor cell apoptosis and therefore tumor suppression as well as premature aging. In the case of a compromised p53-status, chromosomal ends are treated as double strand breaks (DSB) and ligated, which leads to chromosomal breakage during mitosis. The resulting broken chromosome ends are prone to further translocations, focal amplifications and focal deletions in the form of breakage-fusion-bridge-cycles, which drive development of carcinomas.

1.2.5 Methods for telomere length measurement

Since telomere function is tied to telomere length several methods for telomere length assessment have been developed with distinct advantages and disadvantages. The most important techniques are outlined in the following paragraphs.

1.2.5.1 Terminal restriction fragment analysis (TRF-analysis)

Terminal restriction fragment (TRF) analysis was the first widely used technique for determining telomere length and is often described as the “gold standard” method. In this procedure, genomic DNA is thoroughly digested using several different frequent cutting restriction enzymes that lack recognition sites in telomeric and subtelomeric DNA, which is left uncut. The intact telomeres from all chromosomes are then resolved, based on size, using agarose gel electrophoresis, with visualization by either southern blotting or in-gel hybridization. The varying lengths of telomeres present as a smear, of which size and intensity is assessed compared to a DNA ladder comprised of known fragment sizes (Allshire et al., 1989; Harley et al., 1990; Kimura et al., 2010)

1.2.5.2 Polymerase chain reaction (PCR)-based techniques

Polymerase chain reaction (PCR)-based telomere length analysis methods need less DNA for telomere length evaluation than TRF analysis. These procedures include quantitative (real time) PCR (qPCR), monochrome multiplex quantitative PCR (MMqPCR), and absolute telomere length (aTL) quantitation. PCR amplifies a DNA sequence over 20 to 40 cycles using specific primers for the region of interest. With each cycle the quantity of the PCR product (amplicon) doubles. The amount of the DNA sequence of interest is then quantified through the use of a fluorophore that intercalates with double stranded DNA (i.e., SYBR green®), or a probe with an attached fluorophore which is released when the sequence of interest is amplified (i.e., TaqMan probes®). After each cycle, the intensity of emitted fluorescence is measured, which is used to infer the amount of starting material (C. Ding & Cantor, 2004; Montpetit et al., 2014). Polymerase chain reaction is also the foundation of single telomere length analysis (STELA), which is an adaption to the qPCR protocol and can measure very precisely telomere lengths of certain chromosomes (Baird, Rowson, Wynford-Thomas, & Kipling, 2003).

1.2.5.3 Quantitative fluorescence in situ hybridization (Q-FISH)

Quantitative fluorescence in situ hybridization (Q-FISH) of telomeric repeats is used for assessing metaphase chromosomes or interphase nuclei following hybridization with a fluorescent $(CCCTAA)_3$ probe. In contrast to TRF-analyses and PCR-based assays, the substrate for Q-FISH is cells instead of DNA. The cells used for assessment with Q-FISH methods can be fresh frozen, formalin fixed, paraffin-embedded or permeabilized.(Montpetit et al., 2014). The following paragraphs will in short explain two adaptions of this method.

1.2.5.3.1 Metaphase chromosome Q-FISH

In this adaptation, telomeric repeats of single chromosomes can be analyzed by allowing synthetic peptide nucleic acid (PNA) probes with a $(CCCTAA)_3$ sequence to hybridize with telomeric chromatin. The remaining non-telomeric chromatin is counterstained with a non-specific DNA stain like 4',6-diamidino-2-phenylindole (DAPI) (Lansdorp et al., 1996) or propidium iodide (Krejci & Koch, 1998). In addition to being able to visualize all 92 telomeres, the existence of telomere-free chromosomes can be inferred by the lack of telomeric spots at the end of the chromatids. Drawbacks of this technique however constitute the fact that it cannot be used to measure telomeres in cells that are not mitotically active like terminally senescent cells and that its use is limited for samples having a very low proliferation rate (Montpetit et al., 2014).

1.2.5.3.2 Interphase Q-FISH

Interphase Q-FISH is used on interphase cells rather than metaphase chromosomes. This technique is applicable to several different sample types like blood cells, formalin-fixed paraffin embedded tissues and frozen tissue. In addition to a telomeric probe, a centromere probe, attached to a different colored fluorophore can be added, with which signal a Telomere/Centromere ratio can be calculated (Aubert, Hills, & Lansdorp, 2012; Vera & Blasco, 2012) which is believed to allow for greater reproducibility. A clear advantage of using interphase Q-FISH methodology is that it allows to combine telomere length measurement with immunostaining techniques that can label specific cells of interest, sometimes referred to as “telomapping” (Vera & Blasco, 2012). Limits to assessment of the interphase Q-FISH method is the lack of detection of telomere-free ends and telomere overlay prohibits recognition of each single telomere.

1.2.6 Modelling telomere insufficiency in mice

1.2.6.1 mTERC$^{-/-}$ telomerase knockout mice

Telomere shortening and concomitant chromosomal instability was first achieved with the mTERC$^{-/-}$ mouse model, created by Blasco et al. (Blasco et al., 1997). In these mice the TERC component of telomerase is knocked out, which leads to progressive shortening of telomeres resulting in the loss of telomere capping function. Characterization of mice lacking TERC demonstrated that this telomerase component is dispensable for life and that telomerase-knockout mice are remarkably normal (Blasco et al., 1997). The rather unimpaired survival and lack of symptoms in these telomerase knockout mice of the first generation (mTERC$^{-/-}$G1) could be explained with the long telomeres of these laboratory mouse strains. Only mTERC knockout mice of later generations (see method section) showed phenotypical changes. Very late generation mTERC$^{-/-}$ mice (generation (G)5-G6) were infertile, showed high rates of apoptosis in testes and germ cell depletion. Furthermore, diminished proliferation of lymphocytes and impaired bone marrow function has been described (H. W. Lee et al., 1998). Onset and severity of these defects depend on the degree of telomere dysfunction. Early generation mTERC$^{-/-}$ mice with intact telomeres are grossly unaffected while late generation mTERC$^{-/-}$ mice suffer from multi-organ degenerative decline and a shortened life span. In tissues of G5–G6 mTERC$^{-/-}$ mice chromosomal ends without detectable telomere sequence, chromosomal end-to-end fusions and anaphase bridging at mitosis have been observed (Blasco et al., 1997; Hande, Samper, Lansdorp, & Blasco, 1999; H. W. Lee et al., 1998). The severe degenerative tissue defects appear to be linked to impaired proliferation and increased apoptosis in cycling progenitor cells and stem cells and are more pronounced in tissues with fast self-renewal like the intestine which exhibit villus atrophy (Rudolph et al., 1999; Wong et al., 2000). In another study it was demonstrated that hematopoietic stem cells show less transplant potential reduced ability to reconstitute blood after irradiation compared with wildtype controls (Allsopp, Morin, DePinho, Harley, & Weissman, 2003; Choudhury et al., 2007). Late generation mTERC$^{-/-}$ mice also show a moderate increase in the incidence of spontaneous tumors (Blasco et al., 1997). When late generation mTERC$^{-/-}$ mice are intercrossed with wildtype mice to yield mice with half the dose of dysfunctional telomeres, comparable apoptotic and proliferative defects are

seen as in the original late generation they are originating from. This leads to the notion that only a subset of dysfunctional telomeres is needed to drive progenitor cell defects in this model (Hemann, Strong, Hao, & Greider, 2001; Samper, Flores, & Blasco, 2001).

1.2.6.2 Telomerase knockout in cancer prone mouse models

The influence of telomere dysfunction on carcinogenesis has been tested by introduction of the mTERC knockout to some cancer prone mouse models. Here, impairment of tumor development could be observed in most cases (Artandi & DePinho, 2010). Especially late generation telomerase knockout tumor model mice developed less tumors and had a longer life span than mice without the introduction of telomere attrition. Two well researched examples are the Ink4a/Arf mutant mice, which develop lymphomas and sarcomas with short latency and high penetrance (Serrano et al., 1996) and Apc^{Min} mice, which develop gastrointestinal adenomas (Rudolph et al., 2001). Interestingly, Apc^{Min} mice with second generation telomerase knockout suffer from reduced life span and increased micro-adenoma formation in comparison to mere Apc^{Min} mice, implying an increased tumor initiation-capability of mild telomere dysfunction (Rudolph et al., 2001).

1.2.6.3 Combination of telomerase knockout and p53-impairment through the $p53^{R172H}$- mouse model

As already described above, p53 dysfunction takes a crucial part in telomere crisis, which leads to translocations, focal amplifications, and focal deletions in the form of breakage-fusion-bridge-cycles. It has been shown that impairment of p53 together with telomere erosion can accelerate carinogenesis in cancer prone tumor mouse models (Artandi & DePinho, 2010). Many of these studies use a p53-knockout which leads to a loss of function. Mutations in the p53 gene locus however – in contrast to other tumor suppressor genes – are more often point mutations rather than large deletions (Olivier et al., 2002). Furthermore, studies suggest that some p53 mutations can feature a gain of function and further promote tumorigenesis (Aurelio, Kong, Gupta, & Stanbridge, 2000; Dittmer et al., 1993). One common mutation in human cancers is a missense mutation in position 175, the R175H mutation. In murine models this corresponds with a mutation in position 172 (R172H). This $p53^{R172H}$ mouse model was first created independently by Olive et al. (Olive et al., 2004) and Lang et al. (Lang et al., 2004)

to create a model for the Li-Fraumeni syndrome. Analysis of the $p53^{R172H}$ model verified the gain of function in the form of promoted tumorigenesis, a dominant negative effect on the wild type p53, as well as a shift to carcinomas (Lang et al., 2004; Olive et al., 2004). In mouse models for breast- and pancreatic cancer the $p53^{R172H}$ allele led to increased tumor initiation, invasion, and metastasis (M. K. Lee et al., 2012; G. Liu et al., 2000; Lu, Liu, & Xu, 2013; Morton et al., 2010).

2 Aims of this work

As indicated in the introduction, EAC is a disease with rising incidence and high mortality. Furthermore, BE is the only known precursor lesion of EAC with a high prevalence among western countries but only low tendency of malignant transformation. Hence, there is a great need to study all aspects of BE origin and malignant progression to find viable biomarkers for risk stratification or discover new approaches for therapy. Prior findings have demonstrated that chromosomal instability is a major factor in EAC development. It can occur in the face of telomere crisis and previous studies found shortened telomeres, a prerequisite for telomere crisis, in human BE epithelium with one study being able to correlate this to chromosomal instability. Telomere shortening alone with intact p53 has generally been shown to accelerate tumor growth and initiation, nevertheless, functional analysis is lacking. Thus, we aim here to better understand the impact of telomere shortening in the L2-IL-1B mouse model for BE and in human samples of BE, LGD and EAC. The experiments conducted in this piece of work had several aims:

Aim 1: Investigating the impact of shortened telomeres on the phenotype of the L2-IL-1B mouse model for BE and EAC by mTERC knockout.

Aim 2: Evaluation of the p53R172H genetic alteration on the L2-IL-1B.mTERC$^{-/-}$G2 mouse model.

Aim 3: Establishing telomere length measurement on samples of a human cohort of patients who received full length esophagus resection. Exploring differences in telomere length depending on histological grade and establishing a “telomere profile” to track changes in telomere length within one patient.

Aim 4: Examining differences in telomere length of different epithelial cell populations of BE- and LGD samples.

3 Methods and materials

3.1 Methods specific to murine experiments

Macroscopic scoring, histological analysis, immunohistochemical analysis, histopathological evaluation and telomere length analysis were performed on murine samples of the L2-IL-1B- and L2-IL-1B.mTERC$^{-/-}$G2 genotypes. A small cohort of L2-IL-1B.mTERC$^{-/-}$G2.p53^{R172H} was analyzed with regard to macroscopic tumor phenotype and histologic phenotype (H&E staining, see below).

3.1.1 Transgenic mouse strains

The used mouse models L2-IL-1B, mTERC$^{-/-}$ and p53^{R172H} have been described in previous studies (Blasco et al., 1997; Olive et al., 2004; M. Quante, G. Bhagat, et al., 2012). All mice were backcrossed to a C57BL/6 background and if necessary intercrossed to obtain the three different genotypes: L2-IL-1B, L2-IL-1B.mTERC$^{-/-}$G2 and L2-IL-1B.mTERC$^{-/-}$G2. p53^{R172H}. Mice were born at the expected Mendelian ratio and successful recombination was verified by PCR (see 3.1.4 Genotyping of mice). For the work at hand focus was set on evaluating the influence of short telomeres on carcinogenesis of the L2-IL-1B mouse model. For this the tseewo groups of the genotypes L2-IL-1B (n=16) and L2-IL-1B.mTERC$^{-/-}$ G2 (n=17) were analyzed at different time points (9 months and 12 months) representing different stages of disease. Additionally a small cohort of L2-IL-1B.mTERC$^{-/-}$G2.p53^{R172H} (n=9) was analyzed and compared to the L2-IL-1B.,TERC$^{-/-}$G2 model.

3.1.2 Mouse husbandry

Housing of mice was carried out under specific pathogen free (SPF) conditions in an animal facility of Klinikum rechts der Isar of the Technische Universität München (MRI). All animal experiments were done in accordance with the Federation of European Laboratory Animal Science Associations (FELASA) and approved by the local government (Regierung Oberbayern with animal experimental permits (Tierversuchsanträge) 55.2.1.54-2532-125-12 and 55.2-1-54-2532-24-2016.

Mice were kept in groups of up to six animals in Sealsafe NEXT Blue Line Cages (1145T, Scanbur) at constant temperatures of 20°C to 25°C, 50% to 60% humidity and a 12h light/12h dark cycle. Ad libitum access to food (Forti, Altromin

Spezialfutter) and sterile filtered water was provided. Pups were weaned at three or four weeks of age and numerated using ear punches on both ears in specific locations.

Mice were monitored at least weekly with evaluation of health status according to a preformed examination routine. When visual signs and further evidence of severe disease were observed, mice were delivered.

3.1.3 Mouse pairing and mating pattern

Breeding was started earliest at six weeks of age for males and eight weeks of age for females. Telomerase deficiency was introduced into the L2-IL-1B mouse model by breeding mTERC$^{+/-}$ mice with L2-IL-1B mice. This yielded mice with both, IL-1β-expression and heterozygous mTERC knockout (L2-IL-1B.mTERC$^{+/-}$). Breeding of mice with this newly created genotype yielded offspring with a full mTERC knockout in the first generation (L2-IL-1B.mTERC$^{-/-}$G1). The mating pattern is displayed in Figure 6. In the study at hand, L2-IL-1B.mTERC$^{-/-}$G2 were compared to L2-IL-1B mice. To further observe differences in carcinogenesis, both genotypes were subdivided into two groups each, representing two different time points (nine months and twelve months). In addition to these main study cohorts, a small cohort of L2-IL-1B.mTERC$^{-/-}$G2.p53^{R172H} was analyzed. Breeding regime was accordingly to the L2-IL-1B.mTERC$^{-/-}$G2 cohort with the addition of p53^{R172H} -mutation.

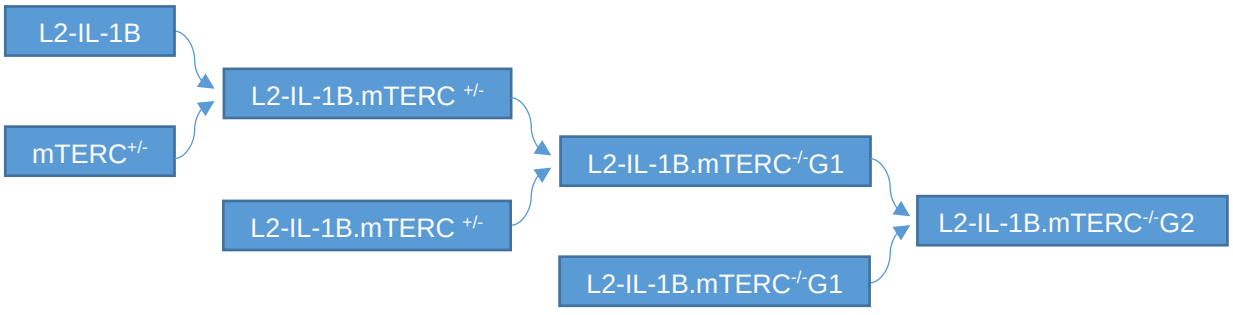

Figure 6 Mating pattern for the L2-IL-1B.mTERC -/- G2 group

L2-IL-1B mice were mated with mTERC$^{+/-}$ mice. Offspring with the genotype L2-IL-1B.mTERC $^{+/-}$ were mated to obtain L2-IL-1B mice with with mTERC- knockout in the first generation: pL2-IL-1

B.mTERC$^{-/-}$ G1. Mating of these mice (L2-IL-1 B.mTERC $^{-/-}$G1) yielded L2-IL-1 B.mTERC $^{-/-}$G2 mice.

3.1.4 Genotyping of mice

Genotype verification was conducted using PCR on murine DNA with primers for either the IL-1β-locus and/or the mTERC- as well as the p53^{R172H}-locus. DNA-extraction was performed on tissue specimens gained from ear clips or tail tips. Samples were lysed in 200 µl DirectPCR-Tail Lysis Reagent (31-102-T, Peqlab) supplemented with 2 µl Proteinase K (03115828001, Roche Diagnostics) overnight at 55°C and 400rpm (Thermomixer compact, Eppendorf). The lysate was then heated at 85°C for 45 minutes (min) to inactivate the proteinase and used for PCR. For each PCR, a total reaction volume of 10 µl was used. 5 µl of either ReadyMixTM REDTaq® PCR Reaction Mix with MgCl2 (R2648, Sigma) or GoTaq® Green Master Mix (M7422, Promega) was mixed with 1 µl of mouse tissue sample as template and 1 mM of each primer. Additional RNAse free water was added to obtain a volume of 10 µl. Each PCR was conducted with a positive and a negative control.

Primers were obtained from Eurofins Genomics as High Purity Salt Free (HPSF) purified lyophilisates and prepared according to manufacturers´ instructions.

PCR followed these steps: Initialization (95°C, 3 min) and denaturation (95°C, 30 sec), annealing (primer specific: mTERC-primer at 58°C, L2-IL-1B primer at 60°C, 30 sec, p53^{R172H} primer at 57°C, 30 sec) and elongation (amplicon size dependent 60 sec at 72°C). In total 35 cycles of denaturation- annealing-elongation cycles were run.

PCR products were visualized on a 1.5% agarose gel containing ethidium bromide in a horizontal electrophoresis system (BioRad). After completion of PCR 10 µl of each sample was loaded in a gel pocket and 5 µl of a 100 kb Ladder (N0467L, BioLabs) was added as a size control. Gels were run at constant voltages of 120V to 150V (depending on the gel-length) until fragment sizes were clearly distinguishable and photographed with a Gel DocTM XR system (Bio-Rad) and the Quantity One software (version 4.5.2 (Basic), Bio-Rad).

3.2 Human tissue samples

Human tissue samples were obtained from the pathology department of TUM/MRI in the form of formalin fixed paraffin embedded (FFPE) samples. Only Specimens from patients who underwent full length esophagectomy were considered. Eight patients were selected, all male, with a mean age of 69.8 ± 9.4 SD years. Of each individual patient one cardia sample and two samples containing metaplastic tissue at different levels of histologic graduation (BE, LGD or EAC) were analyzed. Histological assessment of each specimen was performed by an experienced pathologist.

3.3 Tissue preparation

Mice used for experiments were sacrificed at nine or twelve months after birth or upon notable signs of severe illness. Mice were anesthetized with isoflurane (798-932, cp-pharma) and then sacrificed by cervical dislocation. Organs were removed, washed with phosphate buffered saline (PBS), and conserved. For macroscopic examination, the stomach was opened along the large curvature, food residue was removed by rinsing with PBS, then the stomach was flattened on a Whatman paper with the luminal surface visible. Pictures taken with a digital camera were subject to macroscopic scoring.

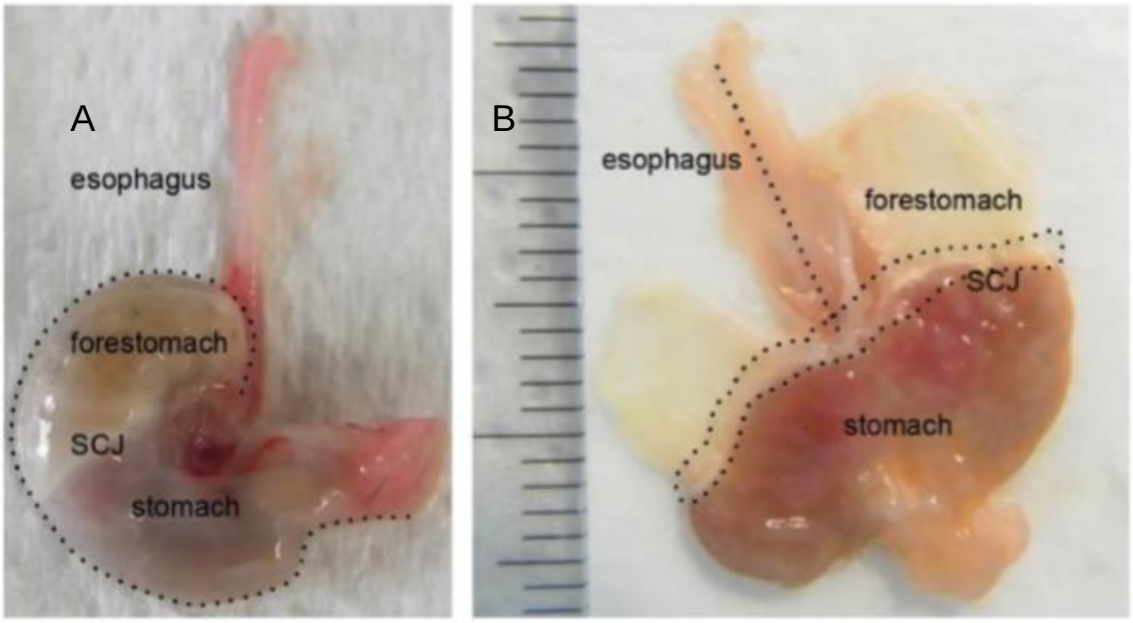

Figure 7 Murine stomach and preparation for macroscopic analysis

***A** Murine stomach and attached esophagus. The dotted line marks the greater curvature alongside which cutting was performed. **B** Murine stomach and esophagus after opening; ruler for size reference. The dotted lines indicate the orientation of the esophagus and the squamocolumnar junction (SCJ) which was subject to macroscopic tumor scoring.*

3.4 Macroscopic tumor evaluation

After preparation (compare figure 7B) murine stomachs were assessed following previously reported scoring system for dysplasia assessment in mice (Münch et al., 2019; M. Quante, G. Bhagat, et al., 2012). This encompasses tumor size and tumor coverage along the SCJ (see Table 1). For estimation of tumor coverage, the SCJ was notionally divided into five segments and checked for macroscopic tumors independent of size. For tumor size evaluation, only the biggest tumor was assessed (see Table 1).

Tumor coverage		Tumor size	
0	No abnormalities	**0**	No abnormalities
1	Focal tumors (<20%)	**1**	>0.5mm
2	Partial tumors (20-50%)	**2**	>1.0mm
3	Increased tumors (>50-80%)	**3**	>2.0mm
4	Continuous tumors (>80%)	**4**	>3.0mm

Table 1 Macroscopic tumor scoring

Tumors were rated macroscopically according to tumor size and coverage along the SCJ with values ranging from 0 to 5 each. High scores in either category imply stronger macroscopic tumor formation.

3.5 Microscopic tumor examination

3.5.1 Histological preparation

The following organs were prepared for histological analysis: stomach with attached esophagus, small intestine, large intestine, liver and spleen. Of these only the stomach and more specifically the SCJ between forestomach and stomach was analyzed.

3.5.1.1 Tissue harvesting and preparation of formalin-fixed paraffin-embedded (FFPE) tissue blocks

Organs were collected and washed in PBS, before small tissue samples were taken. Those samples were snap frozen in liquid nitrogen and kept at -80°C for further possible downstream applications (e.g. RNA extraction, not part of this

thesis). The remaining organs were put into histocasettes (7-0014, neoLab) and transferred into formaldehyde (4%). The stomach was cut open before fixation along the greater curvature and flattened out on a Whatman paper. To assure the flat position of the stomach during the process of fixation a sponge was put on top, which exerts pressure on the tissue when the lid of the histocassette is closed. Small and large intestine were opened longitudinally and washed with PBS to remove feces. After approximately 16h hours of fixation all organs were cut longitudinally except for the stomach with attached esophagus, which had already been prepared. Small and large intestine were shaped to a swiss roll which was then cut crossways into two parts. Preparing the tissue in this fashion ensured that all organs embedded in one histocassete were in the same section. The tissue was dehydrated in increasing concentrations of ethanol, xylene and paraffin in a S300 tissue processing unit (Leica). Next day the samples were embedded into paraffin, creating FFPE blocks.

3.5.1.2 Cutting and downstream applications of FFPE blocks

FFPE blocks were precooled (in a -20°C freezer) and cut into 2 µm sections (for H&E - and PAS -Alcian blue staining) and 5µm sections (for Telomere- FISH, Ki-67- and phosphorylated H2A histone family member X (γH2AX)- staining) using a microtome (MICROM HM 355S, ThermoFisher). After that, sections were transferred to a 45°C warm water bath and mounted on SUPERFROST® PLUS microscope slides (ThermoFisher). Slides were transferred into light protecting boxes and heated to 65°C for 30 min to increase tissue attachment to the slides. Thereafter slides were kept at room temperature.

3.5.2 Hematoxylin and Eosin (H&E) staining

3.5.2.1 H&E staining procedure

Hematoxylin and Eosin staining was carried out to assess histological tissue structure. Paraffin sections were first deparaffinized in xylene (2x 15 min) and then rehydrated in descending concentrations of ethanol (2x 3-5 min 100% ethanol, 2x 3-5 min 96% ethanol, 2x 3-5 min 70% ethanol). Slides were transferred to Mayer's hemalum solution (1.09249.2500; Merck) for 2 min, which stains basophilic structures, followed by a wash step in tap water to halt the staining process (10 min). Acidophilic structures were then counterstained in Eosin (1.7% ethanolische Eosinlösung, Pharmacy of MRI, diluted 1:5 in 96% ethanol) for 3 min. Subsequently, slides were dehydrated in ascending

concentrations of ethanol (2x 2 min 70% ethanol, 2x 2 min 96% ethanol and 2x 2 min 100% ethanol), followed by washes in Xylene (2x 2 min), mounted in Pertex embedding medium (41-4012-00, Medite) and covered with coverslips (MENZEL-Gläser, e.g. BB024032A1, ThermoFisher).

3.5.2.2 Evaluation of H&E-stained tissue

L2-IL-1B mice, as characterized above, express L2-IL-1B in the esophagus, forestomach and SCJ. This induces inflammation, which in turn promotes hyperplasia, metaplasia and at later stages (12-15 months) varying degrees of dysplasia (M. Quante, J. A. Abrams, et al., 2012; M. Quante, G. Bhagat, et al., 2012). Histopathology was evaluated by an experienced mouse pathologist based on a previously described scoring system (Fox et al., 2000). Criteria were inflammation, metaplasia and dysplasia (Michael Quante et al., 2012) (see Table 2)

Score	Inflammation	Metaplasia	Dysplasia
0	no inflammation	no metaplasia	no dysplasia
1	mild inflammation	rare mucus cells	superficial epithelial
2	moderate inflammation	single metaplastic glands	atypia in glandular complexity
3	severe inflammation	multiple metaplastic	low-grade dysplasia
4			high-grade dysplasia

Table 2 Criteria for histopathological scoring

Histopathological evaluation was performed on H&E-stained murine samples.

3.5.3 Periodic Acid Schiff (PAS) staining with Alcian blue

3.5.3.1 PAS-Alcian blue staining procedure

To visualize mucus producing cells and further determine subgroups with different mucins, a combined PAS- and Alcian blue staining was applied to FFPE tissue samples. Alcian blue stains acidic mucins whereas PAS stains neutral mucins. Deparaffinization and rehydration of the tissue was performed identically to the H&E protocol. After rinsing in distilled water, slides were stained in Alcian

blue (101647, Merck Millipore) for 1.5 min, followed by a wash in tab water for 3 min. Periodic acid (HP00.1, Roth) was applied for 10 min with a subsequent washing step of 3 min in tab water. Slides were then exposed to Schiff´s reagent (X900.2, Roth) for 15 min and washed in tab water for 3 min. Subsequently, Hematoxylin, used as a counterstain to visualize nuclei, was applied for 2 min. After a washing step in tab water, slides were dehydrated in an ascending alcohol series and cover-slipped identically to the H&E protocol.

3.5.3.2 Evaluation of PAS- Alcian blue stained tissue

Goblet cell ratio (GC-ratio) was estimated with PAS-/Alcian blue double stained slides. Only epithelial cells with a light blue color were attributed to the “goblet cell fraction” whereas purple stained cells and such with no mucus production were assigned to the “non-goblet-cell fraction”.

3.5.4 Immunohistochemical analysis

3.5.4.1 Immunohistochemnistry (IHC) staining protocols

3.5.4.1.1 Ki-67 staining

Firstly, slides were deparaffinized and rehydrated identically to the H&E protocol. Antigen retrieval was performed in 10mM Sodium Citrate buffer in pH 6.0 using a microwave at 400W for 15 min followed by a cool-down period of 15 min. Subsequently slides were transferred into a washing buffer (PBS). Tissue samples were encircled using a “PAP Pen” (S2002, Dako). Endogenous peroxidases were blocked with addition of 3% H2O2 (1.08597.1000, Merck) for 10 min at room temperature. After a washing step, unspecific antibody binding was blocked using 5% goat serum (solved in tris-buffered saline with Tween20 (TBST)) as a blocking solution for 30 min at room temperature. After washing, the primary antibody (ab15580, abcam) was applied to the slides in a dilution of 1:500 for 1h at room temperature. Three washing steps of 5 min each were performed. Afterwards the biotinylated secondary antibody was applied for 30 min. To enhance the signal, Avidin-Biotin Complex (ABC) solution was used according to manufacturer´s instructions for 30 min on the slides after three washing steps of 5 min each. Slides were washed three times in deionized water. Signal detection was achieved with usage of the 3,3′-Diaminobenzidin (DAB) Peroxidase Substrate Kit (SK-4100, Vector Labs) for 1-4 min at room temperature. Slides were washed for 5 min in deionized water and counterstained for 1 min in Hematoxylin solution (1.05175.2500, Merck). After rinsing in tap water for 5 min,

slides were dehydrated in ascending alcohol series and xylene, mounted and coverslipped as described previously.

3.5.4.1.2 γH2A histone family member X (γH2AX) staining

FFPE tissue sections were deparaffinized in xylene two times for 30 min. Hereafter rehydration was performed in ethanol of descending concentrations (2x 5 min 100% ethanol, 2x 2 min 96% ethanol, 2x 2 min 70% ethanol). Heat-induced antigen retrieval was achieved by microwave heating the slides in 10mM sodium citrate buffer (pH 6) at a power of 900W for 5 min and subsequently at a power of 450W for 10 min, followed by a cool-down period of 30 min. After a washing step with distilled H_2O once for 5 min, tissue samples were encircled using a PAP Pen (S2002, Dako). Endogenous peroxidases were blocked with addition of 3% H2O2 (1.08597.1000, Merck) for 15 min at room temperature. After a washing step with TBST (3x5 min), unspecific antibody binding was blocked using 5% goat serum in 3% bovine serum albumin (BSA, solved in PBS) and 4gtt/ml Streptavidin as a blocking solution for 60 min at room temperature. After discarding the blocking solution, the primary antibody was applied in 3% BSA (solved in PBS) in a concentration of 1:500 with overnight incubation at 4°C. Then, after another washing step with TBST (3x 5 min), the secondary biotinylated antibody (goat-anti rabbit) was applied in a solution of 3% BSA (solved in PBS) with a concentration of 1:1000 with an incubation time of 30 min at room temperature. After a washing step with TBST (3x 5 min), ABC solution was used for signal enhancement according to the manufacturer's instruction for 30 min, followed by a washing step with TBST (3x 5 min). Signal detection was achieved with usage of the DAB Peroxidase Substrate Kit (SK-4100, Vector Labs) for 2 to 3 min at room temperature. Slides were washed for 5 min in deionized water and counterstained for 30 sec in Hematoxylin solution (1.05175.2500, Merck). After rinsing in dH_2O for 1 min, slides were dehydrated in ascending alcohol series (2x 2 min 70%; 2x 2 min 96%; 2x 5 min 100%) and xylene (2x 30 min), mounted and coverslipped as described previously.

3.5.4.2 Evaluation of IHC stainings

Ki-67- and γH2A histone family member X (γH2AX)- stained slides were evaluated by assessing the ratio of DAB positively stained epithelial cells to DAB-unstained epithelial cells in the SCJ region of age matched L2-IL-1B mice compared to L2-IL-1B.mTERC$^{-/-}$G2 mice. For this the default cell counter-tool of

the JAVA-based, open-source image analysis software ImageJ (Rasband) was used.

3.5.5 Telomere length measurement

3.5.5.1 Telomere- Q-FISH

FFPE slides were dewaxed in xylene (3x 5 min) and then rehydrated in descending concentrations of alcohol (1x 5 min 100% ethanol, 1x 5 min 96% ethanol and 1x 5 min 70% ethanol). Samples were then washed 3x 5 min in PBS. Antigen retrieval was performed through heat and enzymatically: sections were transferred into citratbuffer and then pre-heated in a microwave (800W) for 3 min until boiling and then another 10 min at (240W). Slides were left to cool-down for 20 min at room temperature and then transferred into a pre-warmed (37°C) pepsin-solution for 15 min. Hereafter another washing step with PBS was included (3x 5 min). Sections were then dehydrated in ethanol (1x 5 min 70% ethanol, 1x 5 min 96% ethanol and 1x 5 min 100% ethanol) and allowed to air-dry for 5 min. Then 15µl hybridization mix was applied and covered air-bubble free with a cover slip. The next steps were all performed in darkness to prevent probes from fading. Samples were denatured on a hot plate at 80°C for 3 min and then incubated in a humid chamber for 2h. After removing the coverslips, slides were washed in a wash buffer (2x 15 min). Two additional washing steps with tris-buffered saline Tween0.1% (3x 5 min) and PBS (2x 5 min) were carried out. Lastly, slides were mounted and counterstained with 30µl mounting solution Antifade + Dapi (Vectashield, Vector#H1200). Image acquisition was performed one day later.

3.5.5.2 Image acquisition of Telomere-Q-FISH slides

Images were taken latest 24h after staining with a fluorescence microscope (Zeiss Axio Imager Z1 Fluoreszenzmikroskop) at a magnification level of 100x. Optimal exposure times for both DAPI-and Cy3-channels were determined with the Axio-Vision software belonging to the microscope. For this, optimal exposure times as ascertained by the Axio-Vision software belonging to the microscope were averaged. Exposure times were set at 2 ms for the DAPI image for both human and murine tissues and 500 ms for Cy3-labeled telomeres for human tissues and 50 ms Cy3 for murine samples. Exposure times were held constant for all human and murine samples.

3.5.5.3 Telomere-image analysis

Telomere-specific FISH signals are linearly proportional to telomere length and are therefore quantifiable via digital image analysis (Meeker et al., 2002). The digitized fluorescent telomere FISH signals were quantified using the JAVA-based, open-source image analysis software ImageJ (Rasband) and a custom-built plugin called “Telometer” ("Telometer (Version: 3.0.5) last published: 2020-08-28. https://demarzolab.pathology.jhmi.edu/telometer/index.html, 25.06.2021,"). This program uses matching telomere and nuclear DNA grayscale TIFF image files. The images are normalized by background subtraction, subsequently run through a sharpening filter, followed by enhancement using a rolling ball algorithm for contouring of telomere spots. A binarized mask of the telomere signals is then created and applied to the original unfiltered Cy3 telomere fluorescence image for data extraction. For each cell group, a region of interest was manually defined on the DAPI image by use of the freeform drawing tool in ImageJ. Guidance for cell type selection was provided by comparison to a separate two-color merged image showing the combined DNA stain (DAPI) and the telomere stain (Cy3). Quality of signals was then evaluated visually and edited manually when necessary: ”Halos”, which come about when a signal is not in focus are removed (see Figure 8A) and joined signals, that occur when telomere signals are close to one another and are merged by the “Telometer”-software are separated by hand (see Figure 8B).

After editing, all telomere signals that belong to one nucleus are identified by the binary segment mask and measured for size and intensity.

Cells were classified as epithelial when aligned in a typical crypt-like structure, whereas cells that lack a specific formation were considered stroma cells. For some comparisons epithelial cells were subdivided into either “non-mucus” or “mucus”. Cells that were assigned to the latter category presented with a typical vacuole-like auto fluorescence pattern.

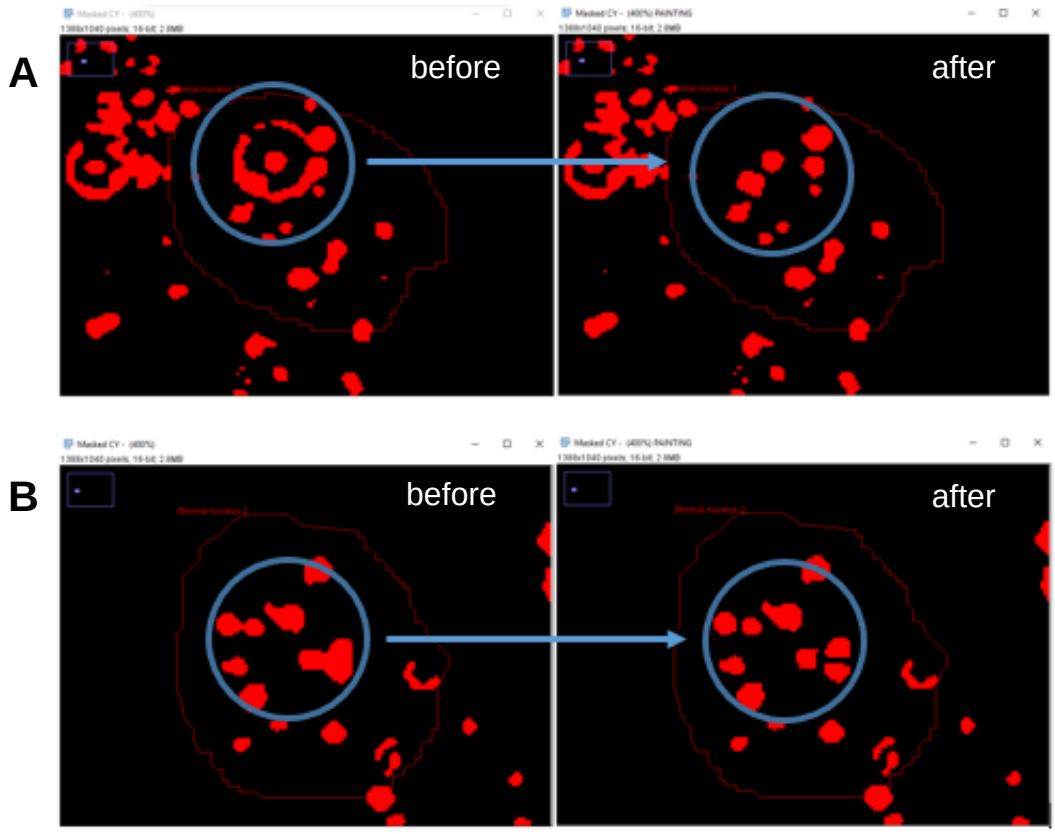

Figure 8 Processing of telomere signals for analysis

*Figure displays two frequently used types of signal processing for later telomere length estimation. Halos, which appear when a signal is not in focus, are removed as shown in (**A**) before and after processing. Nuclei with many out-of-focus telomere signals were avoided, if possible, to minimize effects on telomere spot values. In (**B**) joined signals are separated manually, shown before and after processing. The thin dark red lines in each picture indicate the contour of a single cell nucleus.*

3.5.5.4 Calculation of telomere length values

3.5.5.4.1 Telomere length value per cell

Telomere length was assessed, on a per cell basis (V_N), as the ratio of combined telomere signals in each cell to the total intensity of the DAPI stained nuclear DNA signal in the same cell. Each telomere signal was calculated as the product of area of the telomeric spot and its corresponding brightness. The same is true for the DNA signal, it was calculated as the area of the signal multiplied with its brightness.

$$V_N = \frac{\sum_{k=1}^{n} (I_T \cdot A_T)_k}{I_D \cdot A_D}$$

Legend: V_N= *Telomere value per nucleus*

n= number of telomere signals within one nucleus

I_T= *Intensity of Telomere signal*

A_T= *Area of telomere signal*

I_D= *Intensity of DNA signal*

A_D= *Area of DNA signal*

V_N of all murine cells for both genotypes and each time point were compared. To obtain a single value for each biological specimen, the mean V_N of all cells of one mouse was taken.

3.5.5.4.2 Telomere length ratio analysis

For human specimens V_N were calculated identically to murine cells (see above). Additionally, epithelial cells were in some cases notionally subdivided into either mucus cells or non-mucus cells. Furthermore, V_N of stromal cells (= V_S) were calculated.

Previous analysis of telomere length in BE has revealed much longer telomeres in stromal cells than epithelial cells (Finley et al., 2006). It was therefore considered that calculating the ratio of telomere length of epithelial cells to the telomere length of stromal cells leads to more reproducible results since it may correct for differences in staining and image acquisition (O'Sullivan et al., 2004). To harness this effect, the telomere length value of each epithelial cell within one image was divided by the mean telomere length value of the stromal cells of the same image. This yielded a stroma-corrected value for each epithelial cell. Eventually, the mean of all stroma-corrected epithelial cells of one biological sample was calculated.

$$V_C = \frac{V_E}{\overline{V_s}}$$

Legend: V_C= *Telomere value per nucleus, stroma corrected*

V_E= *Telomere value per nucleus (Epithelial cell)*

$\overline{V_s}$ = *Mean telomere value of stromal cell per image*

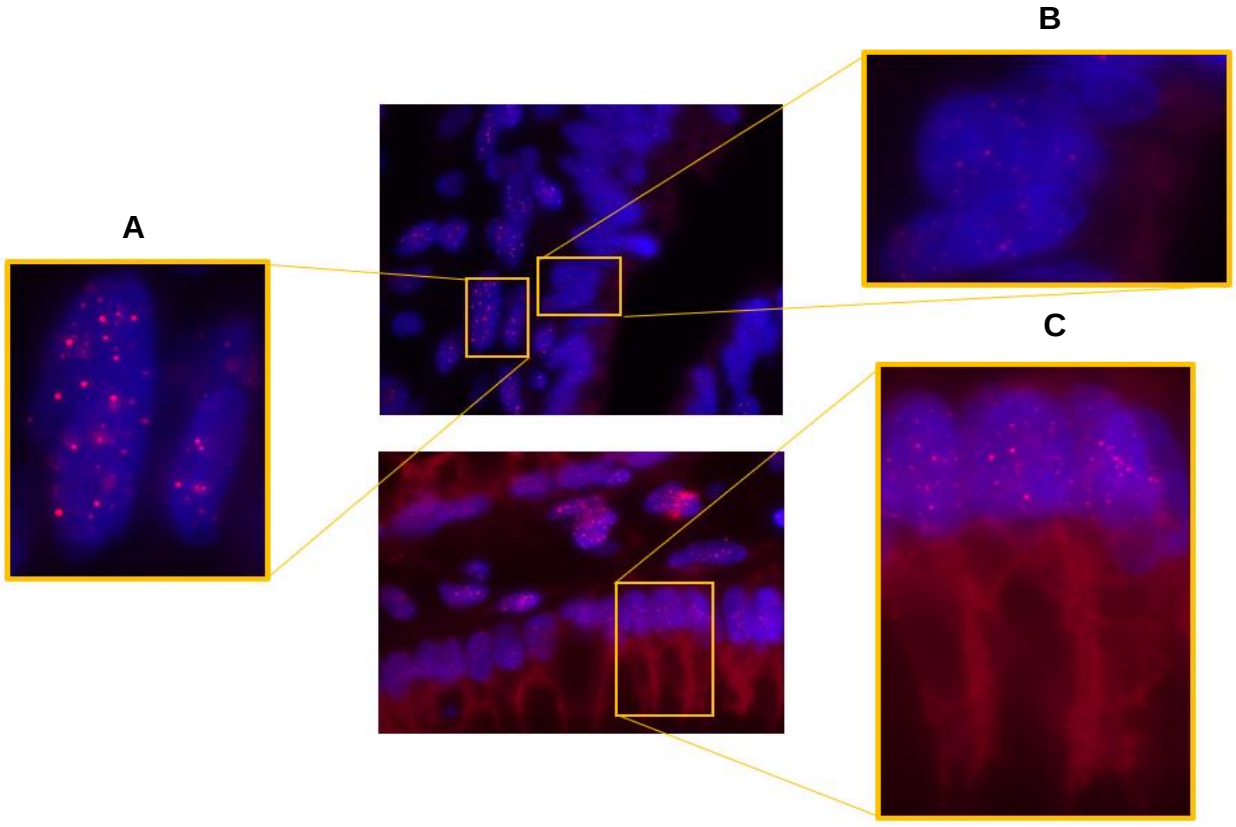

Figure 9 Differentiation of cells according to location and autofluorescence pattern

Graphic shows telomere-FISH images of a human BE sample. Cells can be identified by their location and their autofluorescence pattern. ***A*** *Stromal cells.* ***B*** *Columnar lined epithelial cells arrayed in a gland.* ***C*** *Mucus producing cells, recognizable by their cell formation and vacuole-like autofluorescence pattern.*

For comparison between mucus producing cells and non-mucus cells, epithelium to stroma ratios have been calculated in similar fashion. Telomere length measurement of murine SCJ samples only contained epithelial cells, since differentiation between epithelial and stromal cells could not be performed with enough certainty. However, telomere length was also calculated on a per cell basis and stated as telomere fluorescence intensity (TFI). For this the value given by the program “Telometer” ("Telometer (Version: 3.0.5) last published: 2020-08-28. https://demarzolab.pathology.jhmi.edu/telometer/index.html, 25.06.2021,") was multiplied by 1000.

3.5.5.4.3 Telomere length variation measurements

Cell-to-cell telomere length variation has been proposed in other studies as a potential biomarker for risk assessment in lung cancer, cancer of the biliary tract and breast cancer (Hansel et al., 2006; Sun et al., 2015; Zhou et al., 2012). We therefore examined telomere length variation on our human samples. In prior publications by other researchers two different operating figures have been used to estimate cell-to-cell telomere length variation: On the one hand standard deviation, on the other hand coefficient of variation.

$$c_v = \frac{\sigma}{\mu}$$

Legend: c_v *= Coefficient of variation*

σ *= standard deviation*

μ *= mean*

3.5.6 In vitro examination

In-vitro studies were carried out in form of three-dimensional organoid cell culture from murine SCJ cell isolates. These organoids were cultured and passaged following a protocol tailored for organoid culture using special culture media. Aim of the organoid culture was to investigate differences in organoid forming capacity and proliferation between the L2-IL-1B and L2-IL-1B.mTERC$^{-/-}$G2 mouse models.

3.5.6.1 Media preparation

3.5.6.1.1 Complete medium without growth factors (CM w/o GF)

500 mL Advanced Dulbecco's Modified Eagle Medium (DMEM) /F12 (Life Technologies, Germany) was complemented with 5 mL Glutamax 100 x, 5ml HEPES 1M and 5 mL Penicillin/Streptomycin (Pen/Strep) (10,000 Units/mL Penicillin Stock; 10,000 µg/mL Streptomycin Stock (Life Technologies, Germany)). Complete medium was stored at 4°C for up to four weeks.

3.5.6.1.2 Wnt-conditioned complete medium (Wnt-CCM)

L Wnt-3A fibroblasts were thawed in DMEM and complemented with 10% fetal calf serum (FCS, Life Technologies, Germany) and 1% Pen/Strep and incubated overnight at 37°C. Cells were then detached from the petri dishes using Tripsin-Ethylenediaminetetraacetic-acid (Tripsin-EDTA, Life Technologies, Germany), split at a ratio of 1:15 in new Petri-dishes and re-suspended in fresh DMEM (10% FCS, 1% Pen/Strep. Wnt producing cells were selected for 7 to 10 days with the marker Geneticin, at a concentration of 4 µL/ml. Following the expansion, medium was collected and filtered with a 0.22 µm strainer (Sarstedt, Germany).

3.5.6.1.3 Wnt-CCM with growth factors and Epidermal Growth Factor/Noggin/R-Spondin (Wnt-CCM with GF and ENR)

40 mL of Wnt-CCM was complemented with 800 µL B27 (50X Stock, Thermo Scientific, Germany), 400 µL N-2 (100X Stock, Thermo Scientific, Germany) and 100 µL n-acetylcysteine (500mM Stock). Additionally, 4 µL epidermal growth factor (EGF), 40 µL Noggin and 350 µL R-Spondin were added. The obtained Wnt-CCM with GF and Epidermal Growth Factor/Noggin/R-Spondin (ENR) was aliquoted and frozen at -20°C for future usage.

3.5.6.2 Squamocolumnar junction (SCJ) organoid isolation

Adenomatous SCJ-tissues from resected murine stomachs were detached using a scalpel, transferred into a petri dish containing PBS (Life Technologies,

Germany) and heat inactivated fetal bovine serum (FBS, Life Technologies, Germany) and then further cut into minute fragments using fine tipped scissors. This suspension was then incubated in a falcon tube with 25 mL PBS-EDTA- (Life Technologies, Germany)-EGTA (Roth, Germany) at 4°C for 45 min. Subsequently, 10 mL PBS-FBS was added to the suspension and transferred through a 70-µM strainer into a new falcon tube. The remaining tissue was transferred back from the strainer to the original tube and washed again with 10 mL PBS-FBS and filtered once more through the same strainer. This procedure was repeated five to six times to obtain approximately 80 ml of SCJ cell suspension. The fractions were then centrifuged at 800x g for 8 min at 4°C. After removing the supernatant, pellets were resuspended in Matrigel™ Matrix (BD Biosciences, UK) and pipetted into a prewarmed 24-well-plate with drop sizes of 50µl per well. After a subsequent incubation period of 10 min at 37°C in the incubator, the Matrigel™ had solidified well enough to add 500 µL of Wnt-CCM with growth factor (GF) and ENR at room temperature and returning the plate back to the incubator.

3.5.6.3 Passage of organoids

Passaging of SCJ organoids was carried out every seven to ten days, splitting them at a ratio of approximately 1:2. First, media from each well was discarded, then 4-5 ml of cold (4°C) CM without GF was added to each well and was pipetted up and down multiple times to dissolve the Matrigel™. The suspension was then transferred to a 15 ml falcon tube on ice and pipetted up and down several times more to further separate and dissolve the organoids. Two additional ml of cold medium were added to the tube, which then was centrifuged at 800 x g for 8 min at 4°C. The supernatant was discarded and the pellets were re-suspended in Matrigel™ and pipetted into new wells. The plate was then transferred to the incubator (37°C) for 5-10 min until the Matrigel™ drops had solidified. Then 500µL Wnt-CCM with GF and ENR was added per well and the plate was returned to the incubator.

3.5.6.4 Evaluation of organoid growth

Comparison of organoid forming capacity and differences in morphology was investigated in the third passage to eliminate confounding effects that occur directly after isolation. In order to investigate organoid proliferation, the number of organoids was counted under a microscope 24h after the third passage. Then

counts for both genotypes were normalized by determining an individual factor that yields 100 when multiplied with the original count. This factor was then multiplied with the organoid counts at later time points (24h, 96h, 120h) to get a measure for proliferation.

3.6 Statistical analysis

Statistical analysis was performed with GraphPad Prism 5 for Windows (GraphPad Software, La Jolla California USA). Tests were performed as described in the respective figure legends of the results section of this thesis. In short, one-way ANOVA with Tukey's post hoc test was used when testing multiple groups for telomere length comparisons of murine samples. Unpaired t-test with Welch's correction was used when only two groups were compared. For organoid proliferation-analysis paired t-test was used. Results were considered significant when p-values of statistical tests were ≤ 0.05. A significant difference between two compared groups is marked with a defined number of asterisks: p≤0.05 *, p≤0.01 **, p≤0.001 ***, p≤0.0001 ****. Correction for multiple testing was not performed.

Symbol	Meaning
ns	p > 0.05
*	p ≤ 0.05
**	p ≤ 0.01
***	p ≤ 0.001
****	p ≤ 0.0001

Table 3 Legend of symbols indicating various degrees of significance

4 Results

4.1 Elimination of telomerase in the L2-IL-1B mouse model

4.1.1 In-situ telomere length measurement shows telomere shortening in L2-IL-1B.mTERC$^{-/-}$G2 mice

Telomere length was assayed in-situ according to the method section of this thesis. For this, SCJ-specimens of the transgenic mouse strains L2-IL-1B and L2-IL-1B.mTERC$^{-/-}$G2 at two different time points (9 months and 12 months) were analyzed. In total n=17 samples of L2-IL-1B.mTERC$^{-/-}$G2 mice were examined and compared to the L2-IL-1B control group (n=16). Per mouse two different SCJ-regions were selected microscopically of which two representative photos were chosen. An average of 9.8 ± 0.8 SD nuclei per picture were selected and assayed for telomere length with the JAVA-based software “Telometer” ("Telometer (Version: 3.0.5) last published: 2020-08-28. https://demarzolab.pathology.jhmi.edu/telometer/index.html, 25.06.2021,").

When compared on “cell-level”, that is cells of all mice of the respective genotype and time point pooled together, cells of L2-IL-1B.mTERC$^{-/-}$G2 mice had significantly shorter telomeres than L2-IL-1B cells at both – the 9-months-time point ($p<0.01$, unpaired t-test with Welch’s correction) as well as the 12-months-time-point ($p<0.01$ unpaired t-test with Welch’s correction). Results are presented in Figure 10 A as histograms.

Telomere length means in the 12-months-old groups of both genotypes were less than those of the 9-months-old groups with mean TFIs of 34.3 ± 14.2 SD in the L2-IL-1B.mTERC$^{-/-}$G2 12 months cohort and 43.5 ± 20.9 SD in the L2-IL-1B 12-cohort in contrast to the L2-IL-1B.mTERC$^{-/-}$G2 9-months group (43.5 ± 15.1 SD) and L2-IL-1B 9-months group (51.2 ± 18.3 SD) respectively.

In order to obtain telomere length distributions on a “mouse-level” we calculated the mean TFI of all measured SCJ cells of one mouse. This yields a single value of telomere length per mouse. Figure 10 B and C show plots of these data points. The L2-IL-1B.mTERC$^{-/-}$G2 12-months-old group had significantly shorter telomeres than the L2-IL-1B 9-months-old group ($p<0.01$, one-way ANOVA, Tukey’s post-hoc test) and the L2-IL-1B 12-months-old group ($p<0.05$, one-way ANOVA, Tukey’s post-hoc test). However telomere length means of the L2-IL-

1B.mTERC$^{-/-}$G2 9-months-old group did not differ significantly from any other group.

When data of both time points of each genotype were pooled to obtain a comparison between the two genotypes, the L2-IL-1B.mTERC$^{-/-}$G2 group presented with significantly shorter telomeres than the L2-IL-1B group ($p<0.01$, unpaired t-test, see Figure 10C) .

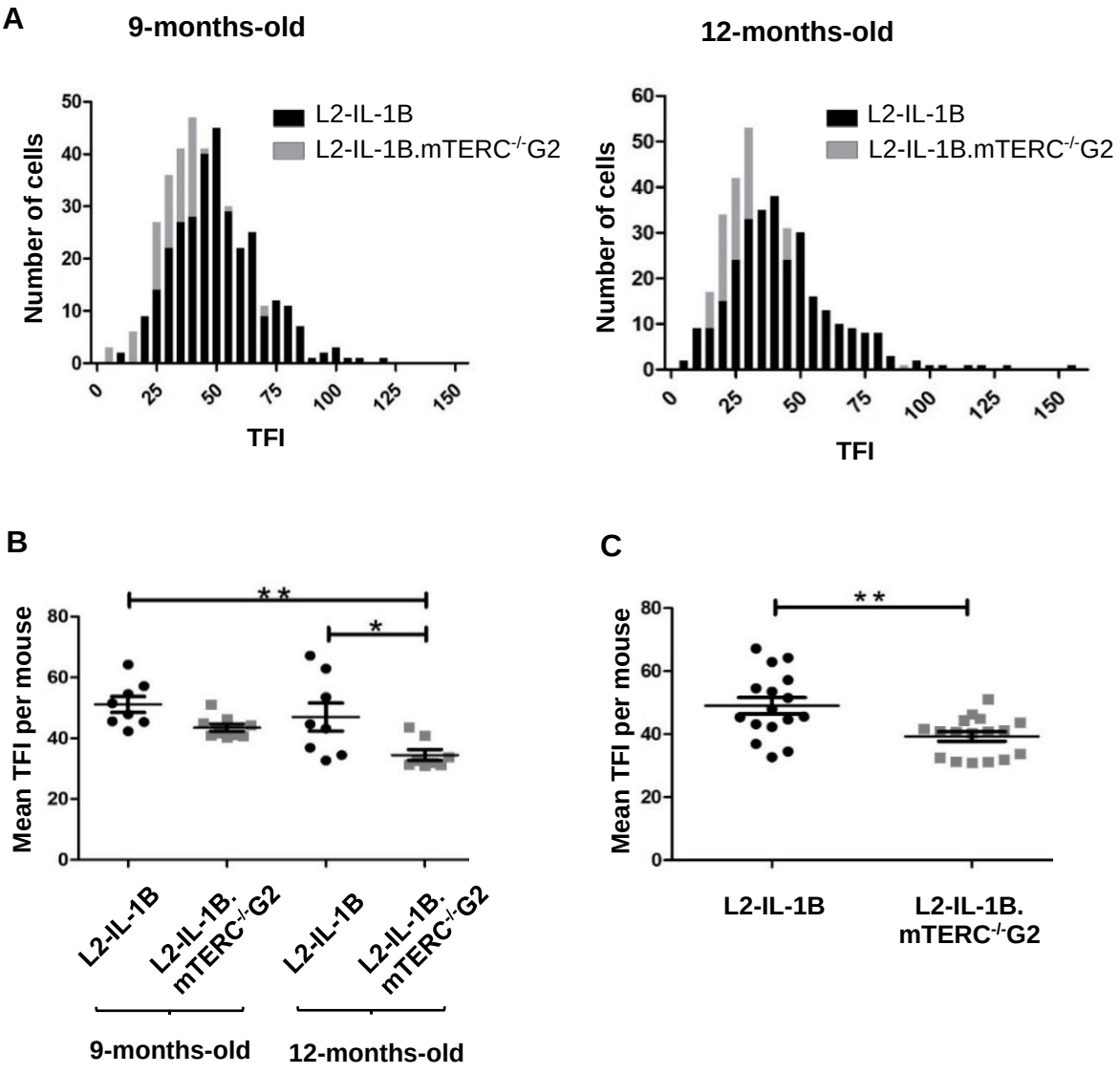

Figure 10 Telomere length analysis of murine epithelial cells of the SCJ

*Figure **A** shows the distributions of SCJ cells according to their telomere length (measured as telomere fluorescence intensity (TFI)) at the 9-months-old time point (left histogram) and 12-months-old timepoint (right histogram). Values are superimposed in the graphs. L2-IL-1B.mTERC$^{-/-}$G2 mice showed a larger portion of cells with shorter telomeres compared to L2-IL-1B mice at both time points (unpaired t-test with Welch's correction, 9-months comparison: p<0.01, 12-months comparison: p<0.01). Figure **B** depicts telomere length as mean TFI of SCJ cells per mouse of both genotypes at both time points. Means and standard deviation are indicated by horizontal bars. The asterisk marks a significant difference. Means differed significantly between 9-months-old L2-IL-1B mice and 12-months-old L2-IL-1B.mTERC$^{-/-}$G2 mice (p<0.01, one-way-ANOVA, Tukey's post-hoc test). Furthermore means of 9-months-old L2-IL-1B.mTERC$^{-/-}$G2 mice and 12-months-old L2-IL-1B.mTERC$^{-/-}$G2 mice differed significantly (p<0.05, one-way ANOVA, Tukey's post-hoc test). **C** depicts telomere length as mean TFI of SCJ cells per mouse of both genotypes with the data of both time points of each genotype pooled to obtain a mere comparison between the two genotypes. L2-IL-1B.mTERC$^{-/-}$G2 mice presented with significantly shorter telomeres than the L2-IL-1B group (p<0.01, unpaired t-test with Welch's correction).*

4.1.2 γH2AX induction implies more DNA damage in L2-IL-1B.mTERC$^{-/-}$G2 mice compared to L2-IL-1B mice

Dysfunctional telomeres, either through uncapping in the absence of TRF2 or when reaching a critical length, can lead to phosphorylation of H2AX (γH2AX) - a damage response factor and indicator of DNA double strand breaks (d'Adda di Fagagna et al., 2003; Takai et al., 2003). In order to evaluate whether the induced shortening of telomeres had a measurable impact on the amount of double strand breaks (DSB), SCJ-tissues of 12-months-old L2-IL-1B.mTERC$^{-/-}$G2 mice and 12-months-old L2-IL-1B mice were assayed for γH2AX-loci and compared. Representative images of γH2AX-stained tissue sections of the 12-months groups of both L2-IL-1B and L2-IL-1B.mTERC$^{-/-}$G2 genotypes are shown in Figure 11. The 12-months-old L2-IL-1B group presented with a mean ratio of γH2AX-positive cells to γH2AX-negative cells of 0.22 ± 0.09 SD (n=8) whereas L2-IL-1B.mTERC$^{-/-}$G2 mice had a mean ratio of γH2AX-positive to γH2AX-negative of 0.36 ± 0.13 SD (n=8). Means were statistically significant different from each other ($p<0.03$, unpaired t-test). This indicates that telomere dysfunction in leads to increased DNA damage.

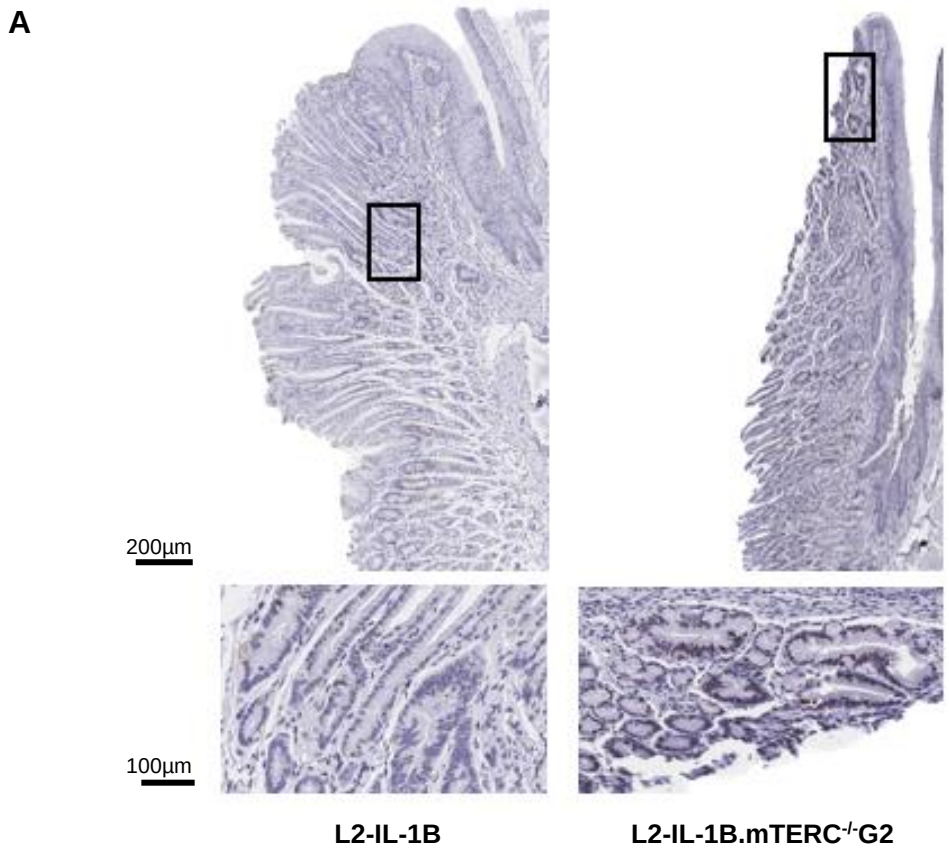

Figure 11 γH2AX-staining of murine SCJ tissue at the 12-months-old time point

*Graphic **A** shows representative scans of SCJ-tissues of 12-months-old L2-IL-1B and L2-IL-1B.mTERC$^{-/-}$G2 mice stained for γH2AX with framed regions magnified in the images below. Dark brown/black (DAB) stained nuclei indicate antibody-binding at γH2AX loci. Graph **B** displays ratios of γH2AX positive to γH2AX negative cells at the SCJ regions of 12-months-old mice of both genotypes. Means and standard deviation are indicated by horizontal bars. The asterisk*

marks a significant difference. 12-months-old L2-IL-1B.mTERC$^{-/-}$G2 mice show a significant higher rate of γH2AX positive cells, compared to 12-months-old L2-IL-1B mice (p< 0.03, unpaired t-test).

4.1.3 Macroscopic tumor coverage is increased with tumor size on par in L2-IL-1B.mTERC$^{-/-}$ G2 genotype compared to the L2-IL-1B genotype

Images of processed murine stomachs were the basis for macroscopic analysis. Both genotypes were examined at the 9-months-time-point (L2-IL-1B: n=8; L2-IL-1B.mTERC$^{-/-}$G2: n=9) and at the 12-months-time-point (L2-IL-1B: n=8; L2-IL-1B.mTERC$^{-/-}$G2: n=8). Regarding tumor coverage along the SCJ, L2-IL-1B mice scored less than L2-IL-1B.mTERC$^{-/-}$G2 mice: L2-IL-1B (9 months 3.13 ±0.83 SD, 12 months 2.88 ± 0.83 SD); L2-IL-1B.mTERC -/- G2 (9 months 3.67 ± 0.50 SD, 12 months 3.88 ± 0.35 SD). One-way ANOVA with Tukey's multiple comparison post-test only revealed significantly stronger tumor coverage in 12-months-old L2-IL-1B.mTERC$^{-/-}$G2 mice compared to 12-months-old L2-IL-1B mice (p< 0.02). When data of both time points were pooled to get a comparison between the two genotypes with a higher number of observations, the stronger tumor coverage in L2-IL-1B.mTERC$^{-/-}$G2 mice became significant (p< 0.002, scores: L2-IL-1B 3.00 ± 0.82 SD n=16, L2-IL-1B.mTERC$^{-/-}$G2 3.77 ± 0.44 SD, n=17).

In respect of tumor size, L2-IL-1B mice mostly scored less than L2-IL-1B.mTERC$^{-/-}$G2 mice: L2-IL-1B (9 months 1.75±0.89 SD, 12 months 2.25 ± 0,71 SD); L2-IL-1B.mTERC$^{-/-}$G2 (9 months 2.11 ± 0.60 SD, 12 months 2.63 ± 0.52 SD). One-way ANOVA with Tukey's multiple comparison post-test revealed no significant differences between the groups (p=0.11). Even after time points of each genotype were pooled to gain a mere comparison between the genotypes, no significant difference was seen (p= 0.17, scores: L2-IL-1B 2.00 ± 0.82 SD n=16, L2-IL-1B.mTERC$^{-/-}$G2 2.35 ± 0.61 SD, n=17). Representative macroscopic images and results are illustrated in Figure 12.

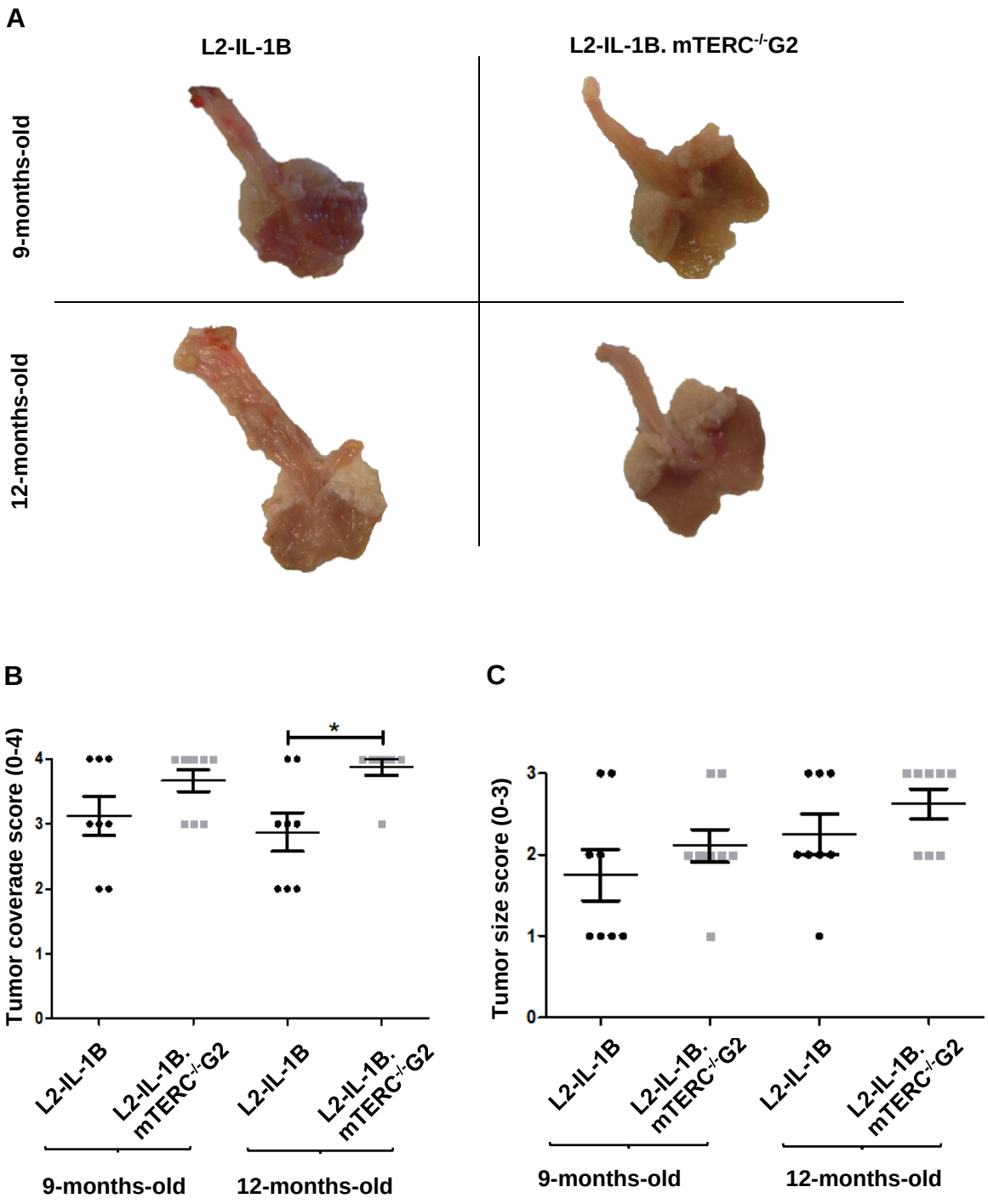

Figure 12 Macroscopic assessment of murine SCJ tumors

*Figure **A** shows exemplary images of processed/opened murine stomachs with attached esophagi of L2-IL-1B- and L2-IL-1B.mTERC-/-G2 mice at both time points. These images were subject to macroscopic analysis with assessment of tumor coverage and tumor size. Figure **B** depicts scores for tumor coverage of both genotypes at both time points. Means and standard deviation are indicated by horizontal bars, the asterisk marks a significant difference. The 12-months-old L2-IL-1B.mTERC-/-G2 group exhibits significantly stronger tumor coverage than the 12-months-old L2-IL-1B group (p=0.02, one-way ANOVA, Tukey's post-test). In graphic **C** scores for tumor size of both genotypes and time points are displayed, means and standard deviation are indicated by horizontal bars. There is a trend of larger tumors in L2-IL-1B.mTERC-/-G2 mice at both time points, however no significant difference (p=0.11, one-way ANOVA, Tukey's post-test).*

4.1.4 Dysplasia is stronger in L2-IL-1B.mTERC$^{-/-}$G2 mice compared to L2-IL-1B mice with similar rates of metaplasia and inflammation

Histological analysis was conducted on H&E- and PAS-Alcian blue stained SCJ-tissue samples, rater blinded by an experienced gastroenterologist and creator of the histological score for this mouse model. H&E-stained SCJ-tissue sections were subject to analysis of inflammation, metaplasia and dysplasia. Regarding inflammation a combined score for signs of chronic as well as acute inflammation was used with a scale ranging from 0 to 3. The L2-IL-1B 9-months-old group received a mean rating of 2.63 ± 0.35 SD, the L2-IL-1B 12-months-old group 2.25 ± 0.27 SD, the L2-IL-1B.mTERC$^{-/-}$G2 9-months-old group 2.78 ± 0.26 SD and the L2-IL-1B.mTERC$^{-/-}$G2 12-months-old group 2.38 ± 0.44 SD. One-way ANOVA with Tukey's post test revealed no significant differences. When both time points of each genotype were pooled to obtain a comparison between the two genotypes with a higher number of observations, there was no significant difference between the two groups (L2-IL-1B (2.44 ± 0.36 SD) and L2-IL-1B.mTERC$^{-/-}$G2 (2.59 ± 0.40 SD), p=0.27, unpaired t-test).

All mice of both genotypes and time points showed signs of metaplasia with only three mice of the L2-IL-1B group not receiving the highest metaplasia score (see Figure 13C). The comparison between the two genotypes irrespective of time points (L2-IL-1B: 2.81 ± 0.40 SD; L2-IL-1B.mTERC$^{-/-}$G2 3.00) reveals no significant differences (p=0.06, unpaired t-test).

In the L2-IL-1B mouse model the dysplasia score is deemed relevant to assess the stage of carcinogenesis. There was no statistically significant difference when all four groups (L2-IL-1B 9-months-old 1.88 ± 1.46 SD; L2-IL-1B 12-months-old 1.25 ± 0.71 SD; L2-IL-1B.mTERC$^{-/-}$G2 9-months-old 2.67 ± 1.00 SD L2-IL-1B.mTERC$^{-/-}$G2 12-months-old 2.25 ± 1.04 SD) were compared to each other but a clear trend towards stronger dysplasia in L2-IL-1B.mTERC$^{-/-}$G2 mice at both time points. When both time points of each genotype were taken together to obtain a comparison between the two genotypes with a larger number of observations, this trend became significant: L2-IL-1B mice had a mean dysplasia score of 1.56 ± 1.15 SD whereas the L2-IL-1B.mTERC$^{-/-}$G2 group scored 2.47 ± 1.01 SD (p=0.02, unpaired t-test).

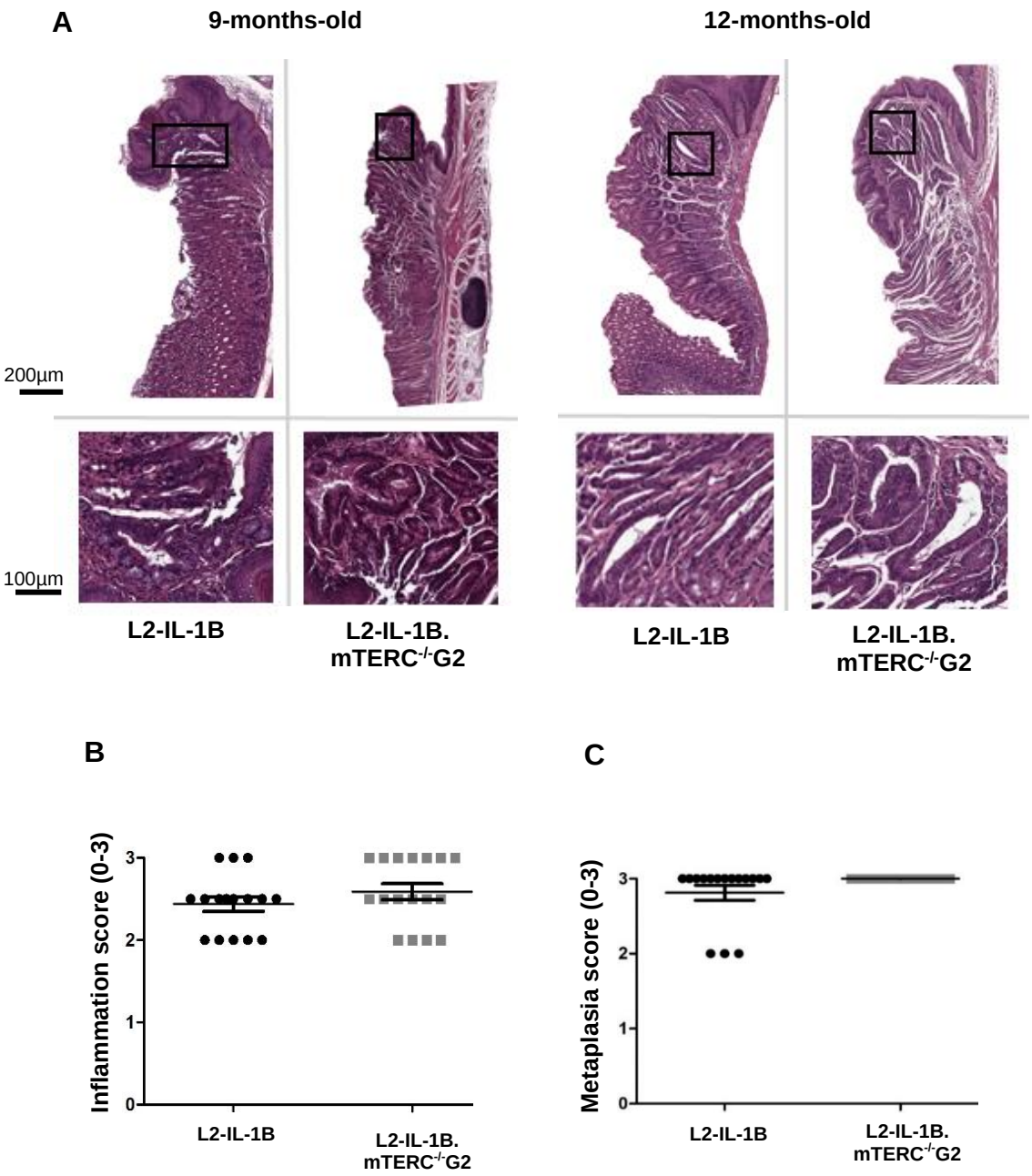

Figure 13 H&E staining of murine SCJ tissue and microscopic scoring

Graphic A shows exemplary scans of H&E-stained murine SCJ-tissue of both genotypes at the 9-months-time-point and at the 12-months-time-point. Framed areas in the upper scans are enlarged below. Figure B displays inflammation scores with data of L2-IL-1B and L2-IL-1B.mTERC-/-G2 mice with both time points pooled to obtain more observations. Means and standard deviation are indicated by horizontal bars. Both genotypes received high scores for inflammation: L2-IL-1B: 2.44 ± 0.36 SD and L2-IL-1B.mTERC-/-G2: 2.59 ± 0.40 SD but no statistical significant difference was seen (p=0.27, unpaired t-test). Figure C displays metaplasia scores for both genotypes. In this data set both time points (9 months and 12 months) have been taken together. All mice of the L2-IL-1B.mTERC-/-G2 cohort got the strongest metaplasia score with all but three of the L2-IL-1B mice receiving the strongest metaplasia score. Means do not differ significantly (p=0.06, unpaired t-test).

D

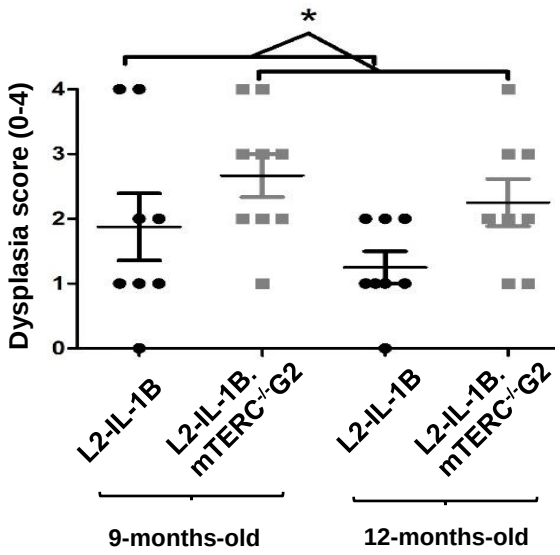

Figure 13 (continuation) H&E staining of murine SCJ tissue and microscopic scoring

*Graphic **D** shows dysplasia scores of SCJ-regions of both genotypes at both time points. There was a trend of stronger dysplasia in each L2-IL-1B.mTERC$^{-/-}$G2 group compared to their age matched L2-IL-1B control group. However, a significant difference was only seen when scores at both time points were pooled (p=0.02, unpaired t-test).*

4.1.5 Intestinal metaplasia differs not significantly between the L2-IL-1B- and L2-IL-1B.mTERC$^{-/-}$G2 mouse model

Intestinal metaplasia is a mandatory feature of BE which manifests itself through different gene expression and goblet cells. The latter was used as a marker for intestinal metaplasia in the L2-IL-1B mouse model. Hereby a higher fraction of goblet cells in SCJ-tissues indicates stronger intestinal metaplasia. Evaluation of tissue specimens was carried out using PAS-Alcian blue double staining. In this double staining, acidic mucins and therefore goblet cells appear in a bright light blue and neutral mucins in a purple color. Figure 13A depicts exemplary SCJ tissue sections of both genotypes and time points stained with PAS-Alcian blue. All four groups presented with comparable amounts of intestinal metaplasia: The 9-months-old L2-IL-1B had a share of 62.50% ± 23.75 SD goblet cells, the L2-IL-1B.mTERC$^{-/-}$G2 of the same age 52.22 % ± 20.48 SD. The 12-months-old L2-IL-1B presented with a mean share of 57.50% ± 19.09 SD goblet cells, the L2-IL-1B.mTERC$^{-/-}$G2 of the same age with 48.75% ± 21.67 SD. Means were not significantly different from each other (p=0.95, one-way ANOVA, Tukey's post-test).

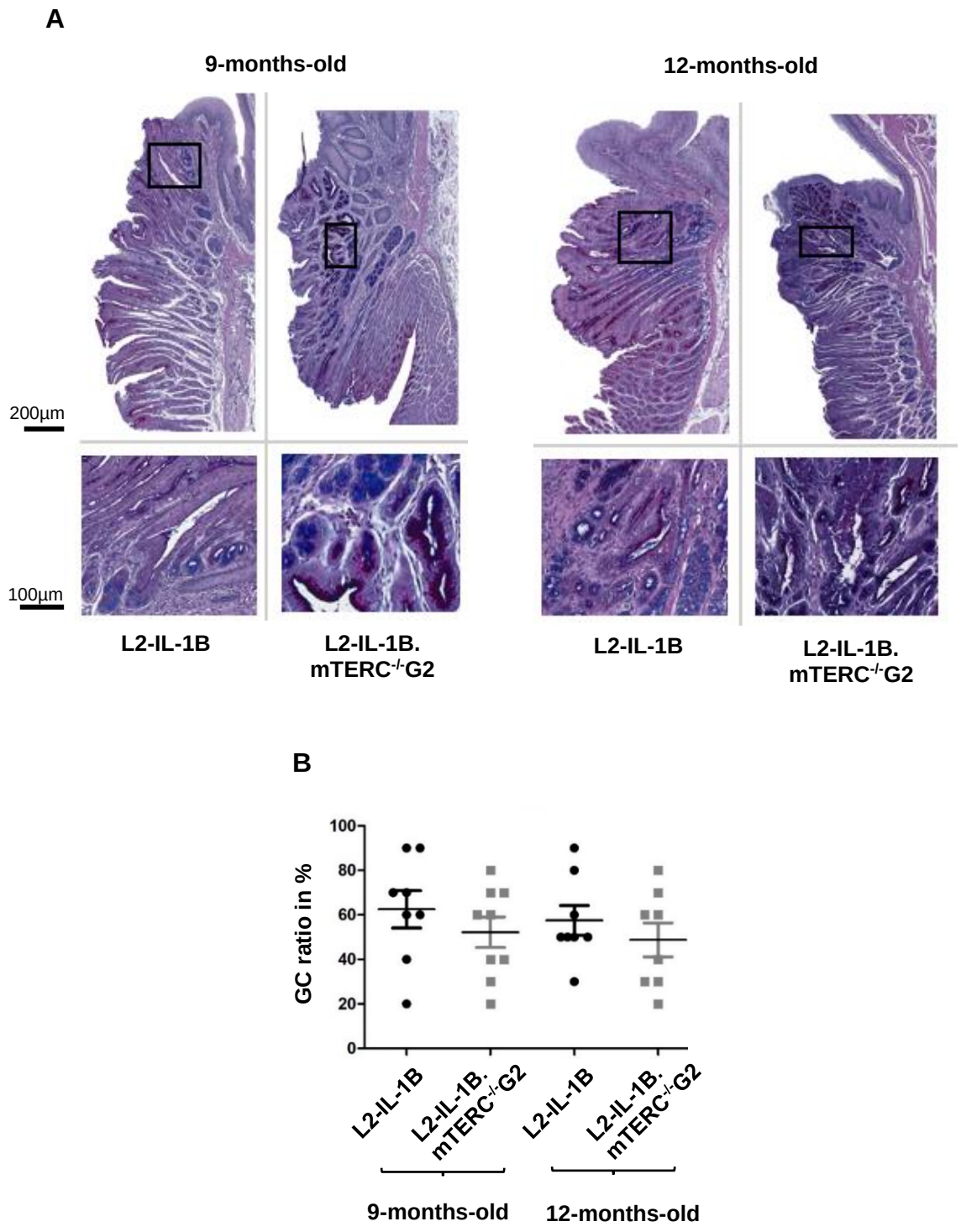

Figure 14 Alcian blue-PAS double staining of murine SCJ tissue and GC-ratio

*Figure **A** shows exemplary scans of PAS-Alcian blue stained SCJ-tissues of L2-IL-1B- and L2-IL-1B.mTERC$^{-/-}$G2 mice at the 9-months- and the 12-months- time point. Framed areas are magnified below. The goblet cell (GC)-ratio marks the rate of light blue stained goblet like epithelial cells in the SCJ region to columnar lined epithelial cells. Figure **B** depicts GC-ratios of both genotypes and time points. Mean and standard deviation are indicated by horizontal bars. There was no significant difference found between the two genotypes (p=0.95, one-way ANOVA, Tukey's post-test).*

4.1.6 Marker for proliferation shows no significant difference between the L2-IL-1B - and L2-IL-1B.mTERC$^{-/-}$G2- model

Tumor proliferation is an important parameter in the characterization of tumor aggressiveness. Dividing cells express the protein Ki-67 which makes it a measure for cell proliferation and a prognostic marker in other tumor entities. In the case of the L2-IL-1B mouse model, Ki-67 is used to monitor changes in tumor proliferation (M. Quante, J. A. Abrams, et al., 2012). Evaluation of Ki-67 was performed according to the methods section. Figure 15A shows representative scans of SCJ tissues stained with a Ki-67 antibody of both genotypes and time points. The SCJ area of both genotypes presented with a high percentage of proliferating cells at both time points. The 9-months-old groups even had a higher rate of Ki-67 positive cells: L2-IL-1B: 0.47 ± 0.14 SD and L2-IL-1B.mTERC$^{-/-}$G2: 0.61 ± 045. At the 12-months time point both genotypes displayed lower rates of Ki-67 positive cells: L2-IL-1B: 0.27 ± 0.08 and L2-IL-1B.mTERC-/-G2: 0.45 ± 0.14. The 9-months-old L2-IL-1B.mTERC-/- G2 contained an outlier, which was kept in the visual presentation of the data (see Figure 15) and for calculations of mean and standard deviation, but was excluded when testing for significant differences. One-way ANOVA revealed no significant differences between the four groups after Tukey's post-test (p=0.08). Even after pooling the data of both time points, we did not see a significant difference between the genotypes (p=0.12, unpaired t-test).

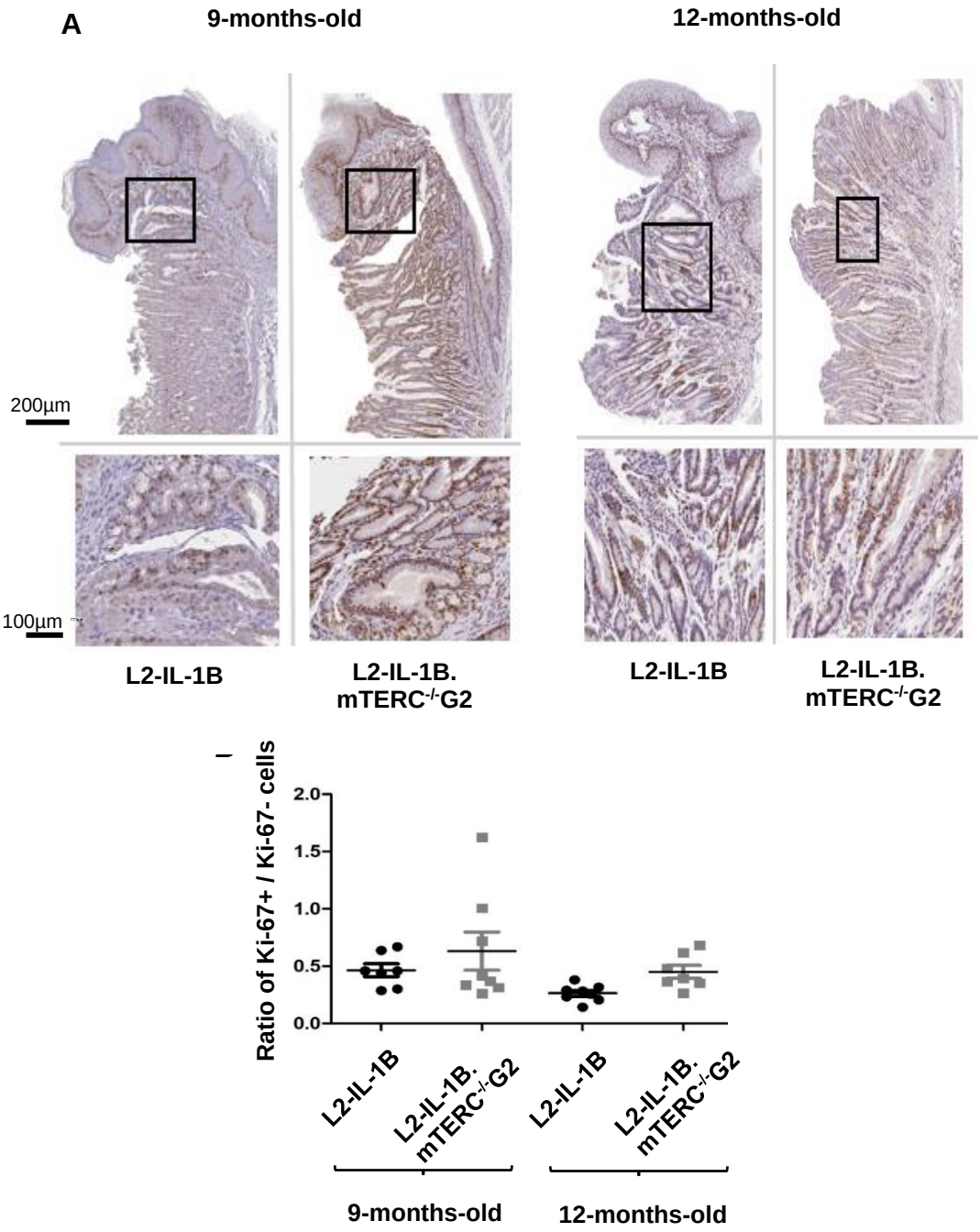

Figure 15 Ki-67-staining of murine SCJ tissue and assessment

*Graphic **A** shows exemplary scans of SCJ-tissue of L2-IL-1B- and L2-IL-1B.mTERC$^{-/-}$G2 mice stained for Ki-67. The upper images contain the whole SCJ with stratified esophageal epithelium at the top and columnar cardiac/gastric epithelium below. Framed areas are magnified in the images below. Dark brown stained nuclei show Ki-67 positive cells. In Graph **B** ratios of Ki-67- positive epithelial cells to unstained epithelial cells (Ki-67 negative) for groups subdivided by genotype and time point are plotted. Means and standard deviation are indicated by horizontal bars. There were no significant differences between the 4 groups after ($p<0.08$ one-way ANOVA, Tukey's post-hoc test), even after data of both time points were pooled to obtain a mere comparison between the two genotypes with a larger number of observations, no significant difference was seen ($p=0.12$, unpaired t-test).*

4.1.7 In vitro examination reveals stronger organoid formation capacity of L2-IL-1B.mTERC$^{-/-}$G2 SCJ cells compared to L2-IL-1B cells

Organoid culture was performed to measure in vitro growth of metaplastic SCJ tissue and give a more comprehensive overview of the phenotype induced by genome instability. Organoid culture has been established previously for SCJ tissue of the L2-IL-1B mouse model (Pastula et al., 2016). With respect to organoid phenotype there were no obvious differences, however organoid formation capacity was significantly stronger in L2-IL-1B.mTERC$^{-/-}$G2 model compared to L2-IL-1B model. Three age-matched (at least 9 months old) mice per genotype were analyzed. In the third passage, after normalizing for starting organoid count (see method section), mean organoid count after 48h of L2-IL-1B mice (n=3) was 119.7 whereas mean organoid count of L2-IL-1B.mTERC$^{-/-}$G2 mice (n=3) was 489.4 which marked a significant difference ($p<0.01$, unpaired t-test).

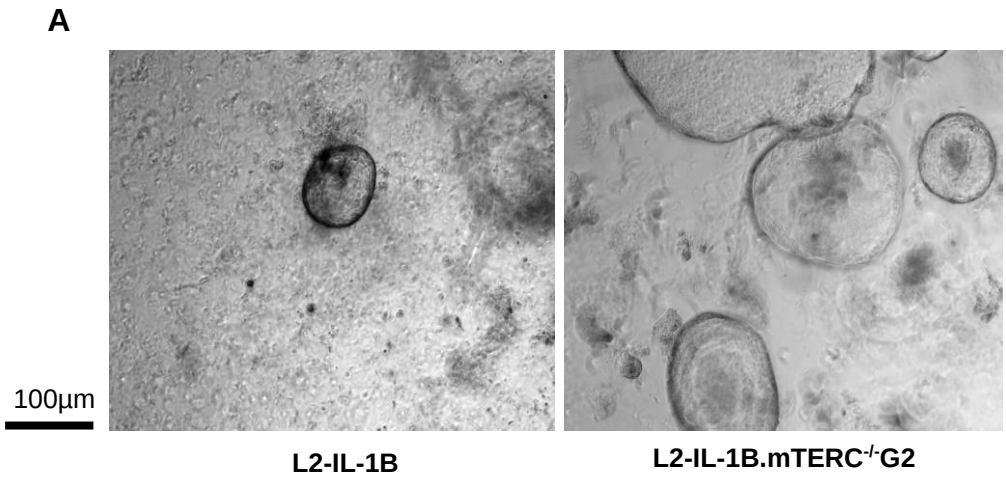

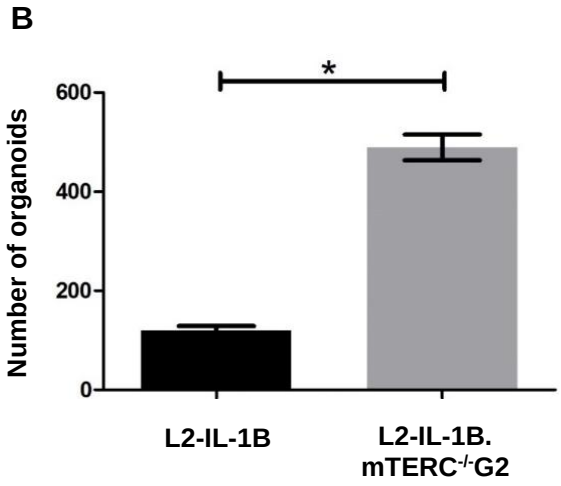

Figure 16 Organoid growth of SCJ isolates after 48h

*Figure **A** shows exemplary light microscopic photos of organoids, cultivated from SCJ cell isolations. Gross visible comparison yielded no differences in organoid morphology (size, organoid wall thickness). Graph **B** depicts number of organoids 48h after the third passage for both genotypes after correction for organoid number at the beginning of the third passage. Means and standard error of the means are indicated. The L2-IL-1B.mTERC$^{-/-}$G2 group presented with a significantly higher number of organoids ($p<0.01$, unpaired t-test).*

4.1.8 L2-IL-1B.mTERC$^{-/-}$G2.P53^{R172H} show similar macroscopic and microscopic changes to the tumor phenotype but no clear step-up compared to L2-IL-1B.mTERC$^{-/-}$G2 mice

To evaluate whether p53 abrogation has an additional effect on the tumor phenotype of the L2-IL-1B.mTERC-/-G2 mouse model we analyzed a preliminary number of 9 L2-IL-1B.mTERC-/-G2.P53R172H with an average age of 8.6 ± 1.7 months and compared those to the time-point pooled data of the other genotypes (L2-IL-1B and L2-IL-1B.mTERC-/-G2). In L2-IL-1B.mTERC-/-G2.P53^{R172H} mice we saw stronger morbidity which led to early deliverance of the mice due to preformed criteria.

L2-IL-1B.mTERC$^{-/-}$G2.P53^{R172H} mice presented with strong tumor coverage (3.3 ± 0.8 SD), more than the L2-IL-1B -group (3.0 ± 0.8 SD), but less than the L2-IL-1B.mTERC-/-G2 group (3.8 ± 0.4 SD), in both cases with no statistical significancy. Regarding tumor size L2-IL-1B.mTERC$^{-/-}$G2.P53^{R172H} (2.4 ± 0.9 SD) mice were on par with L2-IL-1B.mTERC$^{-/-}$G2 (2.4 ± 0.6 SD) mice and scored higher than the L2-IL-1B group (2.0 ± 0.8 SD) with no statistical difference between the three groups (p=0.3; one-way ANOVA).

Microscopic analysis revealed strong metaplasia in the L2-IL-1B.mTERC$^{-/-}$G2.P53^{R172H} group. All examined mice got the highest score of 3. This was also true for the L2-IL-1B.mTERC-/-G2 group. Only in the L2-IL-1B group three mice got a lower metaplasia rating of 2. Furthermore strong dysplasia was seen in L2-IL-1B.mTERC$^{-/-}$G2.P53^{R172H} (2.3 ± 0.7 SD), being only slightly topped by the L2-IL-1B.mTERC$^{-/-}$G2 group (2.5 ± 1.0 SD). The L2-IL-1B group scored the least: 1.6 ± 1.2 SD. A significant difference was only seen between the L2-IL-1B group and the L2-IL-1B.mTERC$^{-/-}$G2 group ($p<0.04$; one-way ANOVA). Inflammation was strongest in the L2-IL-1B.mTERC$^{-/-}$G2.P53^{R172H} group (3.0 ± 0.0 SD) and significantly stronger than in L2-IL-1B.mTERC$^{-/-}$G2 mice (2.6 ± 0.4 SD; $p<0.05$, one-way ANOVA) as well as L2-IL-1B mice (2.4 ± 0.4 SD, $p<0.001$ one-way ANOVA). Signs of intestinal metaplasia as measured by goblet cell ratio were lowest in the L2-IL-1B.mTERC$^{-/-}$G2.P53R172H group (38.9% ± 14.5 SD) compared to the L2-IL-1B.mTERC$^{-/-}$G2 group (50.6% ± 20.5 SD) and to the L2-IL-1B group (60.0% ± 21.0 SD). One-way ANOVA revealed a significant difference between the L2-IL-1B.mTERC$^{-/-}$G2.P53^{R172H} group and the L2-IL-1B group ($p<0.05$).

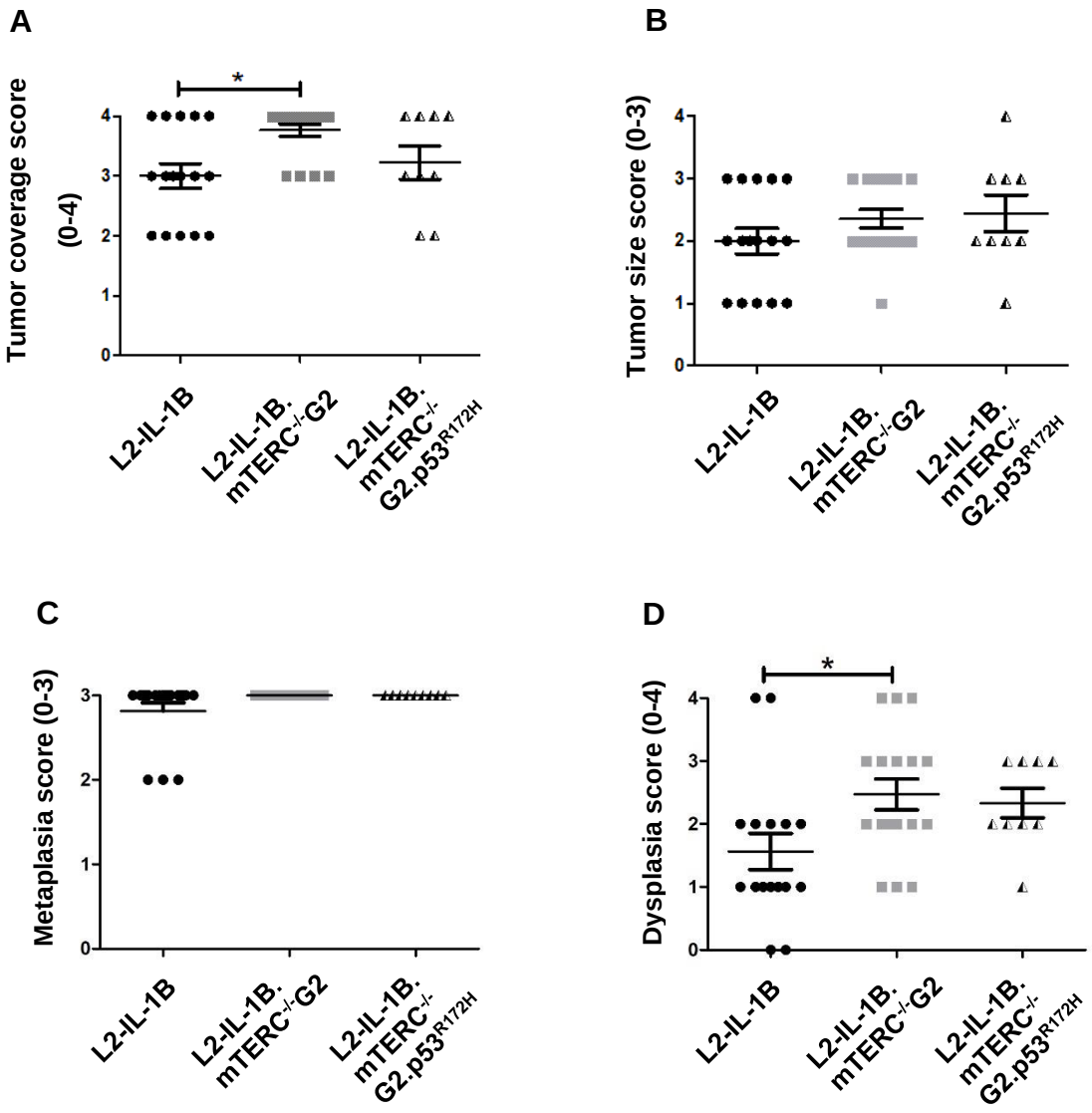

Figure 17 Macroscopic and microscopic comparison of all three genotypes

*Figure **A** depicts scores for tumor coverage of the three different genotypes with pooled time points. Means and standard deviation are indicated by horizontal bars, the asterisk marks a significant difference. Only the L2-IL-1B.mTERC$^{-/-}$G2 group exhibits significantly stronger tumor coverage than the L2-IL-1B group ($p<0.01$, one-way ANOVA, Tukey's post-test). In figure **B** scores for tumor size of all three genotypes are displayed with no significant differences $p=0.3$; one-way ANOVA. Graph **C** shows metaplasia scores of all three genotypes. Figure **D** shows dysplasia scores of SCJ-regions of all three genotypes. Both, the L2-IL-1B.mTERC$^{-/-}$G2 group and the L2-IL-1B.mTERC$^{-/-}$G2.p53^{R172H} group presented with strong dysplasia, a significant difference however was only seen between L2-IL-1B.mTERC$^{-/-}$G2 mice and L2-IL-1B mice.*

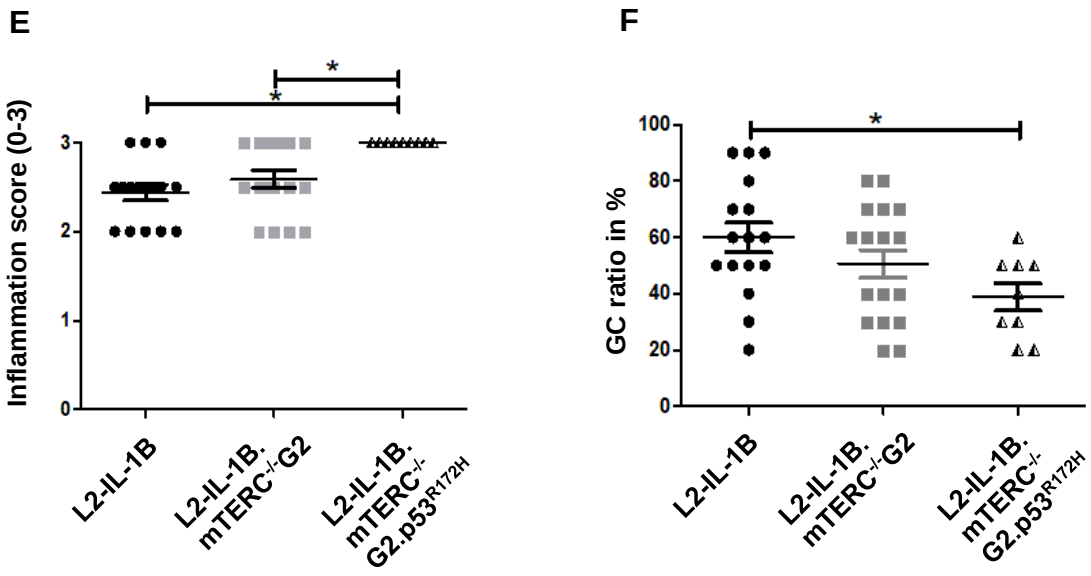

Figure 17 (continuation) Macroscopic and microscopic comparison of all three genotypes

*Figure **E** displays inflammation scores. Means and standard deviation are indicated by horizontal bars. L2-IL-1B.mTERC$^{-/-}$G2.p53^{R172H} mice exhibited stronger inflammation than both L2-IL-1B- and L2-IL-1B.mTERC$^{-/-}$G2 mice. Figure **F** depicts GC-ratios of all three genotypes. Mean and standard deviation are indicated by horizontal bars, the asterisk marks a significant difference. L2-IL-1B.mTERC$^{-/-}$G2.p53^{R172H} mice had less goblet cells than both other genotypes (p=0.05; one-way ANOVA).*

4.2 Results of telomere analysis on human tissue

4.2.1 Telomere measurement reveals consistent telomere erosion of epithelial cells in BE and low-grade dysplasia (LGD) compared to cardia tissue

25 histologic samples of eight individuals were assayed for telomere length. All individuals were male with a mean age of 70.6 ± 8.8 SD years. Per patient, one cardia sample and two or more samples of BE or more advanced stages of the disease, namely LGD or EAC were examined. An average of 5.2 ± 0.8 SD representative images of distinct areas within the same sample were selected. Each of which was subject to further analysis by telomere length measurement of 7.7 ± 3.1 SD epithelial nuclei and 5.9 ± 2.0 SD stromal nuclei. Telomere length of stromal nuclei was measured to get a ratio of epithelial cells to stromal cells which has been shown to yield more reproducible results (O'Sullivan et al., 2004). Furthermore, epithelial cells were – whenever possible – assigned to two groups: i) mucus-cells (i.e. goblet cells), which were identified as such by their characteristic vacuole auto-fluorescence pattern and ii) non-mucus cells (i.e. columnar lined epithelium), which lacked this fluorescence pattern. Results allowed us to create a “telomere profile” of each patient, depicting telomere length ratios for different histological stages (see Figure 18).

Telomere length ratios decreased in all eight patients from the cardia- to the BE- or LGD sample (see Figure 19). The mean telomere length ratio of cardia tissues was 0.87 ± 0.23 SD. Analysis of BE samples returned a mean telomere length ratio of 0.45 ± 0.18 SD, followed by LGD (0.41 ± 0.12 SD) and EAC (0.30 ± 0.14 SD). The EAC telomere length ratio of patient 1 (7.64) has been considered an outlier and therefore has been excluded in all calculations but was kept in Figure 18A and Figure 19.

Differences in telomere length ratios between BE- and LGD samples of the same patient returned a mixed picture: patient 5 (BE: 0.74; LGD: 0.51) and patient 8 (BE: 0.54; LGD 0.38) show a decrease in telomere length from BE to LGD while patient 3 (BE: 0.47; LGD: 0.54) shows an increase.

In order to evaluate telomere lengths of BE tissues in relationship to their location within the esophagus, we analyzed two separate BE samples at different locations of the esophagus in three patients. One sample close to the SCJ and one sample distant of it (see Figure 18B).

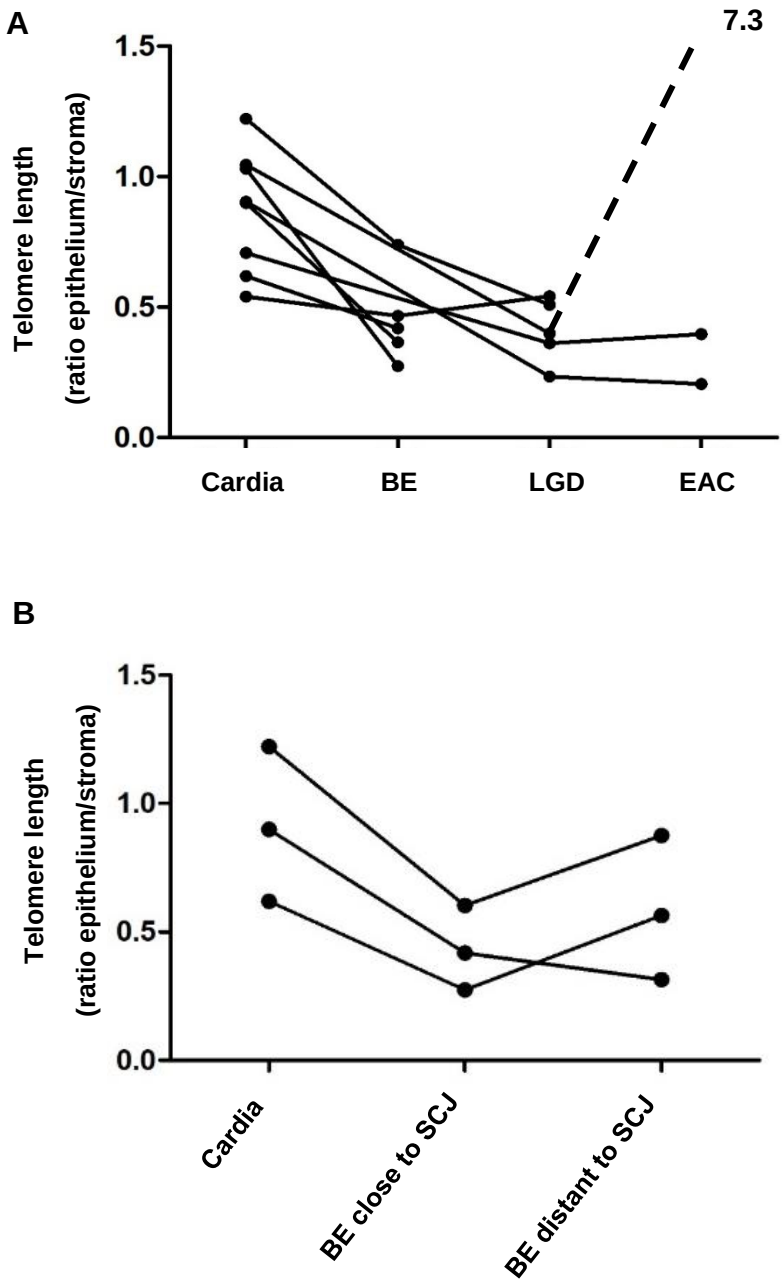

Figure 18 Telomere length profile of human samples

*In both graphs each point represents the calculated telomere length ratio of epithelial cells to stromal cells of a histologically defined sample. Connection of points indicates that samples originate from the same patient. Graph **A** shows telomere lengths according to tissue type, beginning with normal cardia tissue as a reference on the left with advancing stages of disease to the right. There is a consistent trend of telomere shortening in compared to the cardia reference tissue. Graph **B** shows data of three patients of whom two BE specimens were analyzed: one biopsied close to the SCJ and one more distant to it. In two out of these three patients mean epithelial telomere length in BE specimens distant to the SCJ was longer.*

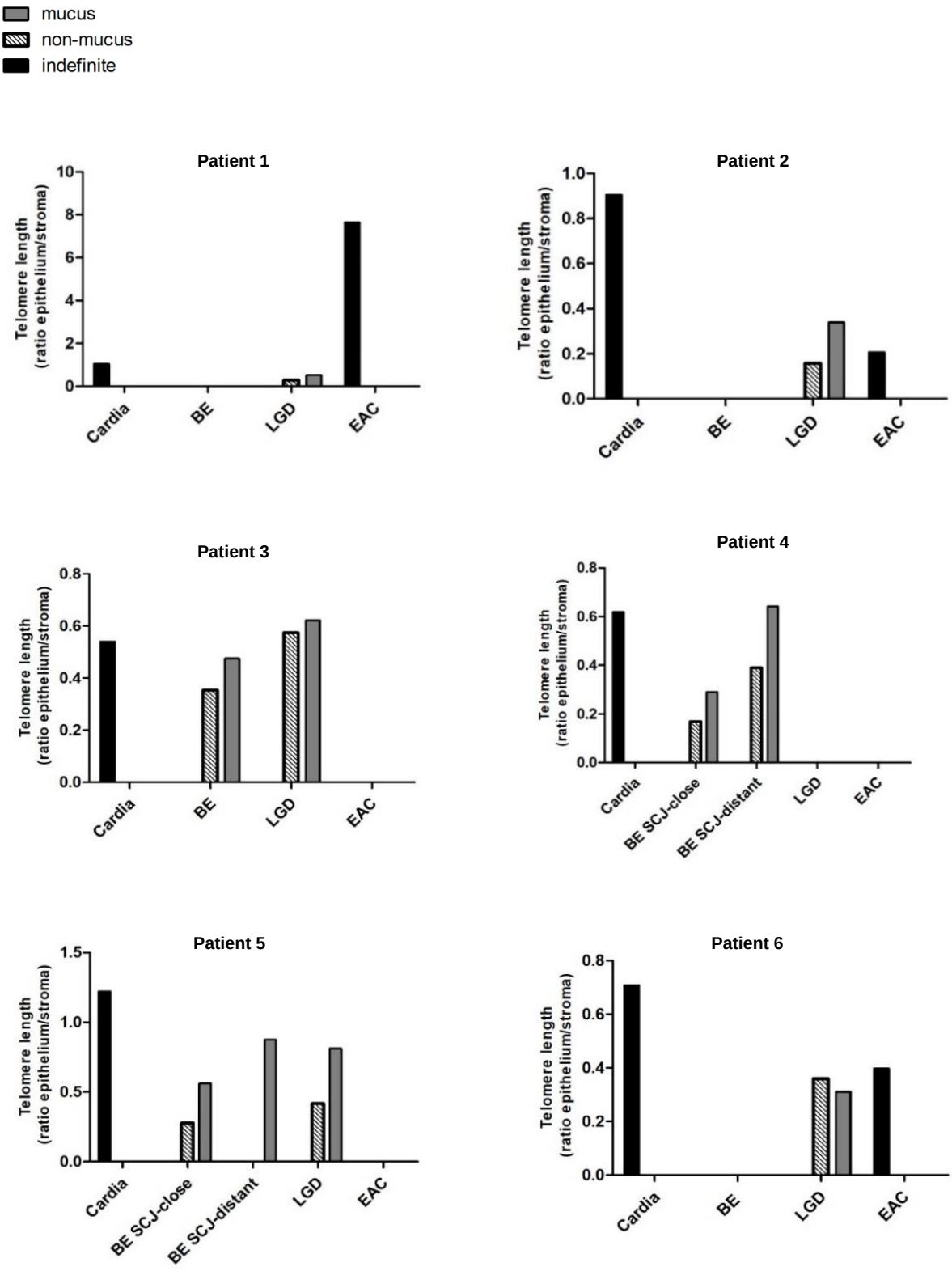

Figure 19 Telomere length measurements per individual patient

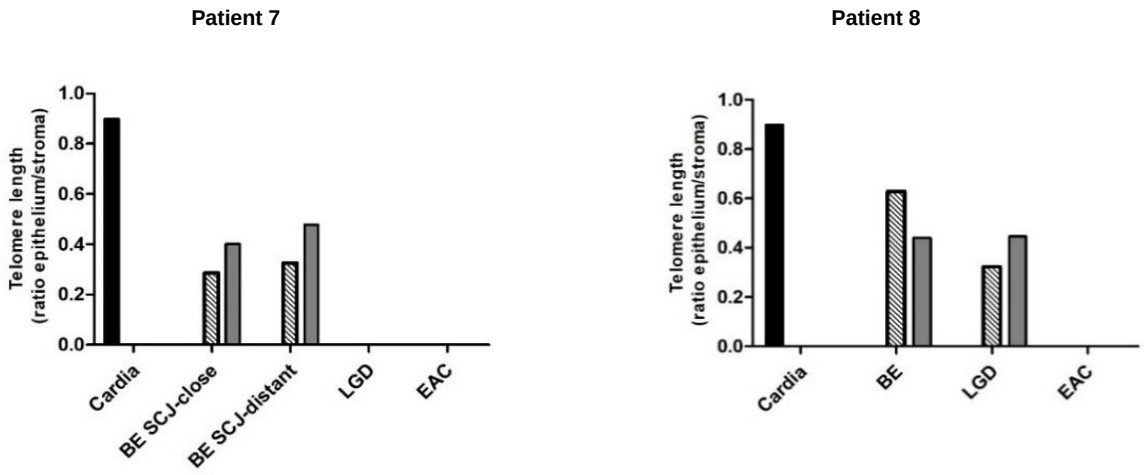

Figure 19 (continuation) Telomere length measurements per individual patient

This figure visualizes telomere length data according to tissue type of all eight patients individually with discrimination of mucus cells and non-mucus cells in BE- and LGD samples. Furthermore, in patients 4,5 and 7 two BE samples each were analyzed, one close to the SCJ, the other distant to it. Likewise to Figure 18A, there is a trend of shorter telomeres in BE and LGD tissues compared to the cardia samples. In all but one case (see patient 8, BE) the fraction of non-mucus cells presented with shorter telomeres compared to the mucus cell fraction of the very same histological samples.

4.2.2 Telomere lengths of non-mucus cells are shorter than mucus cells in BE- and LGD samples

Epithelial cells of human BE and LGD samples were categorized as either non-mucus cells, respectively columnar epithelium, or mucus with the typical vacuole-like auto-fluorescence pattern of goblet cells (see Figure 20). Telomere lengths were compared as a ratio of epithelial to stromal cells.

In BE samples there was a trend of a lower mean telomere length ratio (epithelium/stroma) in non-mucus cells (0.35 ± 0.14 SD) compared to mucus cells (0.47 ± 0.11 SD; p= 0.1, unpaired t-test, see Figure 22). In LGD-samples this trend became significant with mucus cells retaining a length value of 0.47 ± 0.20 SD and non-mucus cells showing a mean length of 0.33 ± 0.14 SD (p=0.05, paired t-test, see Figure 20).

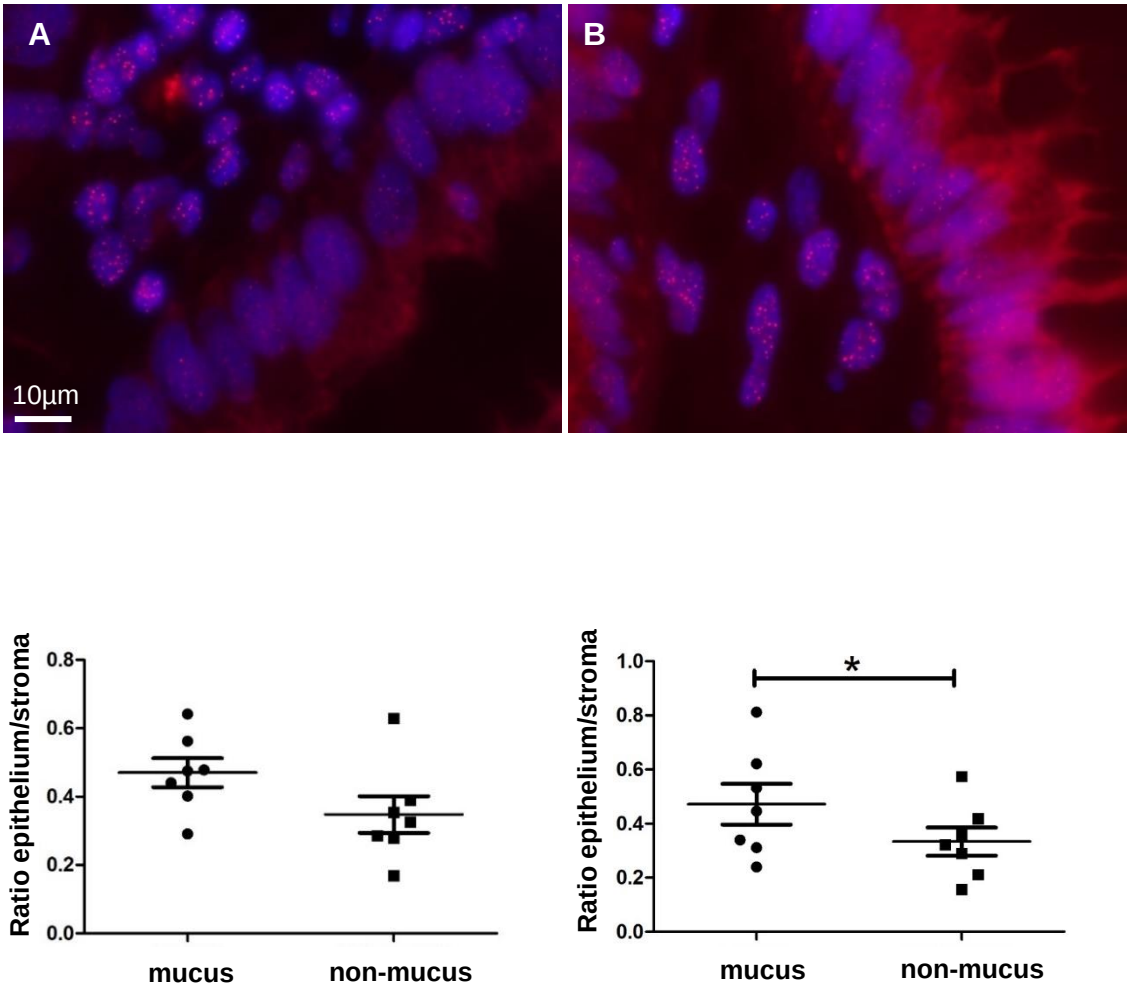

Figure 20 Images of telomere-FISH and differentiation between mucus- and non-mucus cells

*Graphic shows telomere-FISH images of a human LGD sample. The bottom right of image **A** displays part of a crypt with cells belonging to the non-mucus group due to lack of vacuoles. In **B** crypt cells possess goblet cell like vacuoles (mucus-group). Figure shows telomere length as a ratio of epithelial- to stromal- cell telomere length for both types of epithelial cells (mucus and non-mucus) in human BE- and LGD samples. Means and standard deviation are indicated, Asterisk implies significance. In BE samples there is a trend of shorter telomeres in non-mucus cells compared to mucus cells. In LGD-samples this trend becomes significant (p=0.05, paired t-test).*

4.2.3 Analysis of cell-to-cell telomere length variation (TLV) shows lower standard deviation in LGD samples

Cell-to-cell telomere length variation has been examined in other tumor entities and has been implicated as a predictor of progress (Hansel et al., 2006; Sun et al., 2015; Zhou et al., 2012). In the study at hand two measures of cell-to-cell variability were used on human cardia-, BE- LGD- and EAC tissues: i) standard deviation of epithelial cells' telomere length values; ii) coefficient of variation of epithelial cells' telomere length values.

Telomere length values of cardiac epithelial cells presented with the highest mean standard deviation of 17.39 ± 11.35 SD, followed by BE (14.14 ± 8.18 SD), EAC (10.23 ± 6.37 SD) and LGD (7.31 ± 2.35 SD). One-way ANOVA with Tukey's post-hoc test found mean standard deviation of LGD cells' telomere length values to be significantly lower compared to cardiac cells ($p= 0.03$, one-way ANOVA, Tukey's post-hoc test).

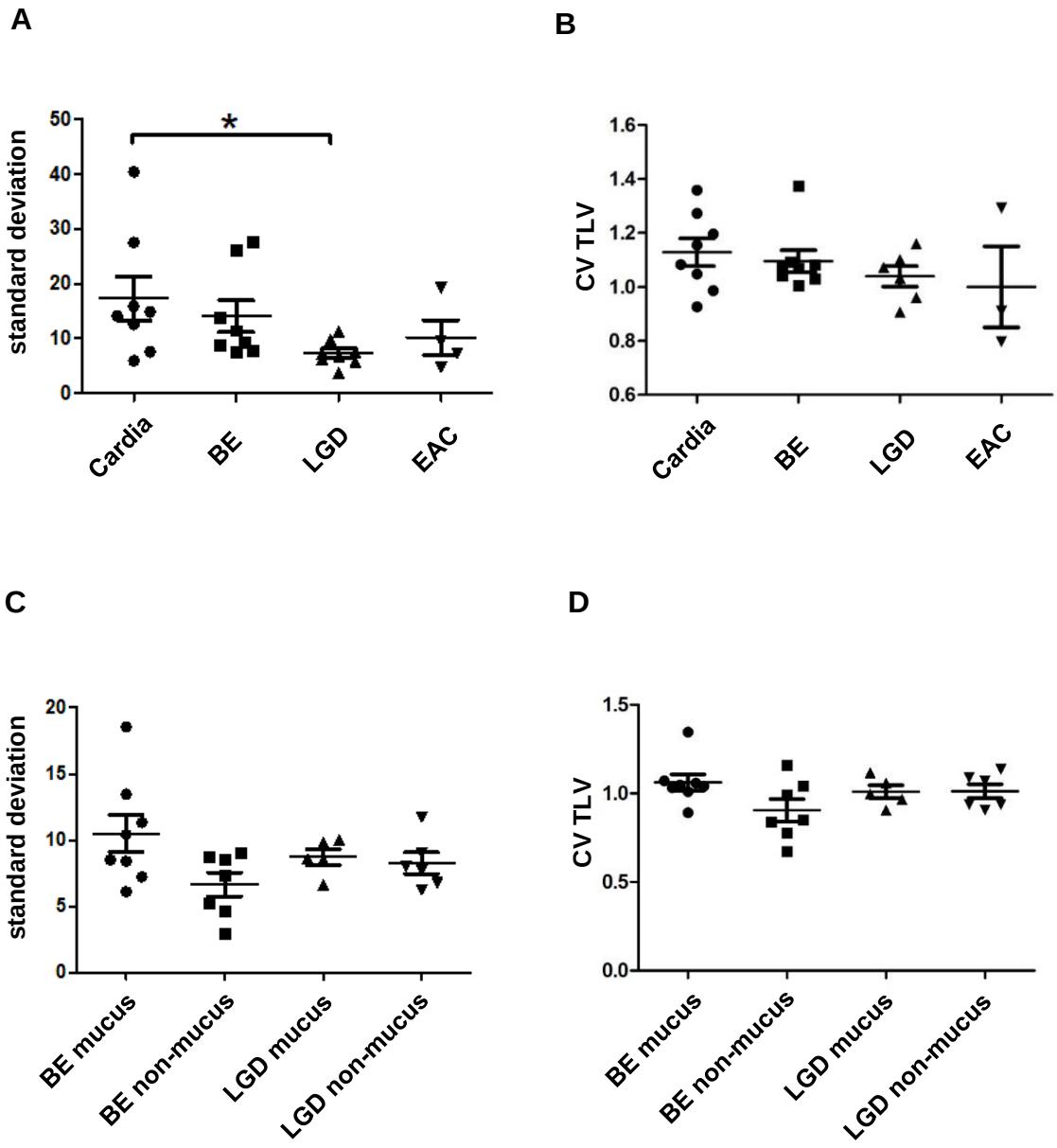

Figure 21 Measurements of cell-to-cell telomere length variation

*The graphs in this figure show measures of epithelial cell-to-cell telomere length variation of distinct histological areas or cell types. Graph **A** depicts standard deviation of epithelial cells' mean telomere lengths calculated per individual biological specimen and tissue type. Means and standard deviation are indicated by horizontal bars. The asterisk marks a significant difference. LGD epithelial cells presented with significantly lower standard deviation (p= 0.03, one-way ANOVA, Tukey's post-hoc test). Graph **B** shows calculated values for the coefficient of variation of epithelial cells' mean telomere lengths per individual specimen and tissue type. In **C** standard deviation of epithelial cells' mean telomere lengths calculated per individual biological specimen and cell type (mucus and non-mucus) of BE and LGD samples are presented. **D** shows the calculated coefficient of variation of the same data set as already shown in **C**.*

5 Discussion

5.1 Discussion of Results

5.1.1 Telomeres are shorter in L2-IL-1B.mTERC$^{-/-}$G2 mice compared to the L2-IL-1B model

Telomere shortening has been observed in human BE tissues (Finley et al., 2006; Letsolo et al., 2017; Shiraishi et al., 2009; Xing et al., 2009) and coincided with signs of genome instability (Finley et al., 2006; Shiraishi et al., 2009). In-situ telomere length measurements conducted in this work, showed a marked reduction in telomere length of epithelial cells at the SCJ in L2-IL-1B.mTERC$^{-/-}$G2 mice compared to L2-IL-1B mice. The decrease in telomere length was highly significant when viewed at cell-level. Hereby one telomere length value per cell was calculated (see Figure 10A). Telomere lengths however vary strongly between individual biological specimens. Therefore when telomere lengths were compared at the mouse-level (meaning one telomere length value per mouse), significant differences in mean telomere length values were only seen in the comparison between the 12-months-old L2-IL-1B.mTERC$^{-/-}$G2 group and both the 9-months-old and the 12-months-old L2-IL-1B groups (see Figure 10B). Notably, mean telomere lengths of the 9-months-old L2-IL-1B.mTERC$^{-/-}$G2 group did not differ significantly from any other group including both L2-IL-1B groups. This indicates that the sample size for each time point (n=8 or n=9) was too small to consistently yield significant differences in telomere lengths. Individual biological variation in telomere length and the accuracy of the FISH-method with subsequent analysis may be reasons for that. When data of both time points for each genotype were pooled to obtain a comparison between the two genotypes with a larger sample size (see Figure 10C), differences in telomere length were highly significant. This demonstrates that telomeres were shortened successfully in the SCJ area by means of mTERC knockout in the second generation. Furthermore, this validates the used protocol for FISH staining and subsequent image analysis. Interestingly there was a non-significant trend of shorter telomeres in 12-months-old L2-IL-1B.mTERC$^{-/-}$G2 mice compared to the 9-months-old group, whereas mean telomere length in L2-IL-1B mice was stable across both time points (see Figure 10B). This observation is in line with findings that telomeres of cells with mTERC knockout shorten measurably in the course of months (Blasco et al., 1997). Also, effects of telomere dysfunction are seen

earlier in tissues with high cell turnover like the gastrointestinal tract (Wong et al., 2000). This may suggest a good accuracy of telomere length assessment as well as strong proliferation in mouse SCJ tissue.

5.1.2 DNA damage increases in L2-IL-1B.mTERC$^{-/-}$G2 mice

Telomere shortening in mice leads to chromosomal instability in the form of chromosomal end-to-end fusions and anaphase bridging at mitosis and breakage-fusion-bridge cycles (Blasco et al., 1997; Hande et al., 1999). It has been shown that first effects in the mTERC mouse model are seen from generation two onwards (Blasco et al., 1997). In the work at hand, DNA damage was assayed with staining of γH2AX in SCJ specimens, which revealed more damage in L2-IL-1B.mTERC$^{-/-}$G2 mice compared to L2-IL-1B mice. This finding seems to affirm that parts of the differences in the macroscopic phenotype can be explained by a higher occurrence of DNA damage.

5.1.3 L2-IL-1B.mTERC$^{-/-}$G2 mice present with increased tumor coverage and dysplasia but not tumor size

Macroscopic evaluation of L2-IL-1B.mTERC$^{-/-}$G2 mice revealed a significant increase in tumor coverage at the SCJ but no significant increase in size of individual tumors. Upon histological assessment of these tumors, significantly higher levels of dysplasia were found in L2-IL-1B.mTERC$^{-/-}$G2 mice compared to the L2-IL-1B control group.

This is a remarkable finding since telomere shortening with loss of the protective function is generally known to exert a tumor suppressive function. Unlimited cell division, a hallmark of cancer cells, is only possible when an incipient cancer cell finds a way to add telomeric repeats onto its chromosomes, which is accomplished by expression of telomerase or activation of the ALT pathway (Sobinoff & Pickett, 2017). With activation of telomerase being off the table in mTERC knockout mice, this impairs the ability of an incipient cancer cell to gain immortality. Furthermore, when telomeres become dysfunctional the DDR system is activated which leads to p53 mediated senescence or apoptosis (Chin et al., 1999; Vaziri & Benchimol, 1996). Accordingly, in some other cancer prone mouse models mere introduction of dysfunctional telomeres by usage of mTERC knockout led to p53 mediated senescence or apoptosis and subsequently impaired tumor development (Gonzalez-Suarez, Samper, Flores, & Blasco, 2000; Greenberg et al., 1999). Only when p53 function was abrogated, additionally to

telomere dysfunction, tumor formation was increased. However, in the original mTERC$^{-/-}$ mouse model without additional genetic modification or treatment, increased incidence of spontaneous cancers occurred in later generations (Rudolph et al., 1999). Additionally, there have also been reports of an increase in tumor initiation in some cancer mouse models with mTERC knockout (Rudolph et al., 2001; Satyanarayana, Manns, & Rudolph, 2004): In the APCmin mouse model for intestinal carcinoma, mTERC knockout in the second generation led to a slight increase in macroscopic tumor formation and a marked increase in microscopic lesions as well as a reduced life span. At later mTERC$^{-/-}$ generations tumor formation decreased however (Rudolph et al., 2001). Similarly, in experiments with three different mouse models for hepatocellular carcinoma, researchers demonstrated that introduction of telomere dysfunction via mTERC knockout led to an increase in early microscopic lesions but a decrease in macroscopic lesions and late stage lesions in these mouse models (Farazi et al., 2003).

The effect of tumor initiation by telomere dysfunction and still intact p53 in mice has been elegantly shown by Begus-Nahrmann et al. (Begus-Nahrmann et al., 2012). Here the protective capacity of telomeres was abrogated by induction of *TRF2*$^{\Delta B \Delta M}$ (a dominant-negative truncation of TRF2) which leads to telomere fusions in a telomerase proficient background. Combined with a diethylnitrosamine (DEN) model for hepatocarcinogenesis (Solt et al., 1983), phenotype analysis showed that liver carcinogenesis was promoted in these mice. In their publication (Begus-Nahrmann et al., 2012) these mice were compared to other DEN mice with telomere dysfunction by mTERC knockout in the third generation. The model with mTERC mediated telomere dysfunction showed increased rates of microscopic tumor formation and increased DNA damage but smaller tumors overall and an increase of cell-cycle arrest and apoptosis. This trend of early tumor initiation but decrease in macroscopic tumors was overcome by the model with transient telomere dysfunction.

In consideration of these earlier findings in other cancer-prone mouse models, it seems plausible that telomere dysfunction through second generation mTERC knockout led to an increase in tumor initiation in the L2-IL-1B mouse model demonstrated in this dissertation. The increase of tumor coverage along the SCJ could be explained with an increase in microscopic tumor formation and only a

moderate and not significant increase in macroscopic tumors indicate that apoptosis and cell cycle arrest limit further progression. Rather surprisingly also the grade of dysplasia was significantly elevated in the group of L2-IL-1B.mTERC$^{-/-}$G2 mice compared to L2-IL-1B mice. This suggests that not only tumor initiation, but also early steps of tumor progression are promoted.

One might speculate that also in the L2-IL-1B mouse model transient telomere dysfunction in a telomerase-proficient background could yield similar results like it had on the DEN model for hepatocarcinogenesis. Of note, the study design with mTERC knockout only permits investigation of early carcinogenesis since activation of telomerase is not possible anymore after genetic disruption. Telomerase activation however is an important and common feature during esophageal carcinogenesis in BE, dysplasia and EAC and likely necessary for cancer growth. We did not specifically analyze ALT in our mouse model, but as we did not observe increased tumor growth and telomeres were consistently shorter in the mTERC$^{-/-}$G2 mice, it is likely that no ALT occurred.

5.1.4 Inflammation and intestinal metaplasia are similar in L2-IL1B.mTERC$^{-/-}$ G2- and L2-IL-1B mice

Inflammatory processes in the SCJ were analyzed compared to existing cohorts of L2-IL-1B mice and revealed no significant differences. Both mouse models exhibited strong inflammation at both time points. Telomere dysfunction by mTERC knockout affects all cells and therefore also inflammatory cells and wound healing in general (Rudolph et al., 1999; Song, Wang, et al., 2010; Victorelli & Passos, 2017). However, no closer analysis except for histological assessment was executed to evaluate inflammatory response.

Another phenotypic property of the L2-IL-1B mouse model is intestinal metaplasia marked by goblet-cell-like mucin producing cells. In both models GF-ratios were comparable which indicates that mTERC knockout does not alter intestinal metaplasia.

These data suggest that telomerase dysfunction is rather a cell intrinsic process that is not altering cellular differentiation as well as the host immune response.

5.1.5 Proliferation in vitro is increased in L2-IL-1B.mTERC$^{-/-}$G2 compared to L2-IL-1B while in situ proliferation is comparable

In vitro analysis of the two genotypes through organoid culture found no visible changes in organoid morphology (i.e. thickened organoid wall), however there was a significant increase in organoid proliferation in cell isolations of L2-IL-1B.mTERC$^{-/-}$G2 mice compared to L2-IL-1B mice. This indicates an accelerated division rate or increased organoid formation capacity of L2-IL-1B.mTERC$^{-/-}$G2 cells compared to L2-IL-1B SCJ cells. This result seems to reaffirm the already discussed macroscopic tumor formation properties of the L2-IL-1B.mTERC$^{-/-}$G2 model: In the context of telomere erosion, tumor initiation as indicated by stronger tumor coverage in the histologic evaluation is matched by stronger organoid proliferation.

Since telomere shortening with intact check points leads to senescence and/ or apoptosis (Artandi & DePinho, 2010) it can be assumed that telomeres of these cells either have not reached critical length or that an increased rate of genome instability led to inactivation of tumor suppressors or activation of oncogenes and show stronger proliferation in this in vitro organoid model.

In situ evaluation of proliferation in the SCJ zone by means of immunohistochemistry with the marker Ki-67 however found no significant difference between L2-IL-1B- and L2-IL-1B.mTERC$^{-/-}$G2 mice. This may be due to already strong proliferation in the L2-IL-1B mouse model, which makes it harder to detect possible increases in the L2-IL-1B.mTERC$^{-/-}$G2 model with the existing sample size. Nonetheless stronger proliferation in the in vitro organoid model affirms histologic evaluation that showed – as already discussed – stronger signs of dysplasia in L2-IL-1B.mTERC$^{-/-}$G2 mice compared to L2-IL-1B mice of the same age.

5.1.6 Preliminary data for the L2-IL-1B.mTERC$^{-/-}$G2.p53^{R172H} model show no increased carcinogenesis compared to L2-IL-1B.mTERC$^{-/-}$G2 mice

The role of telomere erosion and procarcinogenic effects has been tied to the lack of p53 function (Artandi & DePinho, 2010; Blackburn, Epel, & Lin, 2015; Vaziri & Benchimol, 1996). While telomere shortening alone can have a tumor suppressive effect, the combination of dysfunctional telomeres and a compromised p53-pathway was able to accelerate and/or aggravate the tumor

phenotypes of different murine cancer models (Artandi & DePinho, 2010; Chin et al., 1999).

In the small cohort of L2-IL-1B.mTERC$^{-/-}$G2.p53^{R172H} (n=9) we found that macro- and microscopic properties of the phenotype were similar to those of the L2-IL-1B.mTERC$^{-/-}$G2 cohort. Our results did however not provide evidence that carcinogenesis was accelerated. This may either be due to the small sample size of the L2-IL-1B.mTERC$^{-/-}$G2.p53^{R172H} cohort or may indicate that the p53^{R172H} mutation has no additional effect und carcinogenesis in the L2-IL-1B- mouse model.

5.1.7 Telomere length in human BE samples may function as biomarker

Telomere length or DNA content abnormalities as a proxy marker for genome instability have already been proposed as a tumor marker for a variety of solid tumors and implied as a useful addition to the classic TNM staging system (Bisoffi, Heaphy, & Griffith, 2006). Since telomere attrition is already observed in BE together with signs of chromosomal instability (Finley et al., 2006; Shiraishi et al., 2009), this offers the possibility of telomere length assessment as a tool of surveillance or risk prediction in addition to endoscopic surveillance for patients with BE. Furthermore the evidence of increased tumor initiation in the L2-IL-1B.mTERC$^{-/-}$G2 mice implies telomere dysfunction i.e. shortening as an early contributing factor to carcinogenesis.

Measurements of telomere length ratios between epithelium and stroma as conducted here revealed a significant decrease of telomere length in BE- and LGD samples compared to cardia samples. There was however no significant decrease between LGD- and BE samples in our data. One of the most comprehensive in-situ telomere length analyses of human BE was conducted by Finley et al. (Finley et al., 2006). In this study the researchers measured the telomere length of human BE samples at different stages of disease (BE, LGD, HGD and EAC) and stomach samples. They also found a decrease in telomere length in BE samples compared to stomach samples but could show a small, yet not significant increase of telomere length in LGD samples, which was even more pronounced but still not significant in HGD and EAC (Finley et al., 2006).

This does not align completely with our measurement results, since here we see a trend of lower telomere length in LGD compared to BE in most cases (see

Figure 19). There are at least two different explanations for this deviation: i) the sample size is too small: the trend we see (even shorter telomeres in LGD epithelium) might vanish with more data; ii) histological classification of samples is ambiguous with high inter-rater variability (Naini, Chak, Ali, & Odze, 2015; Yantiss, 2010): this might have led to erroneous LGD classification when the actual assessment should have been BE or HGD in either of the two studies.

Nonetheless, advantageous to our study design is the fact that samples of different histological grades of the same individual could be compared. That permitted the creation of a telomere profile for individual patients. BE- or LGD nuclei had shorter telomeres than the cardia tissue, which was used as a reference. However, the difference in telomere length between the two tissue types was variable between the patients. In patient 3 for example only a slight decrease was seen, whereas patient 7 displayed a greater difference in telomere length (see Figure 19). This leaves room for speculation as to whether a big difference has prognostic relevance.

Additionally, the in-situ approach made it possible to differentiate between mucus producing cells (i.e. goblet cells) and non-mucus cells (i.e. columnar lined epithelium). The finding that cells of the mucus producing fraction retrained longer telomeres than the non-mucus cells demands mentioning. This result possibly aligns with findings of a recent study describing bimodal distributions of telomere length within one sample using the STELA method, which was ascertained to heterogeneity of cells (Letsolo et al., 2017). A possible explanation for this sees already well differentiated goblet cells as the low cycling fraction of BE epithelial cells whereas CLE is proliferating more strongly: If oxidative damage as a cause for telomere erosion is considered equally strong in both cell types due to their proximity, the gap in telomere length could be explained by more cell divisions of CLE cells compared with goblet cells. According to this deliberation the gap in telomere length would depend on the proliferation rate of both cell types, time span and telomerase activity. Regarding the latter, previous studies have found that TERT expression is an early event in the development of EAC and can already be seen in non-dysplastic BE and telomerase activity as assayed with telomerase repeat assay protocol (TRAP) has shown to be rather common in BE (Going et al., 2004). Therefore, telomerase activity as a reason for differing telomere lengths must be taken into consideration.

In three out of the eight patients that were investigated, two BE samples were analyzed, one close to the SCJ and one distant of it. This was carried out to check the hypothesis of BE formation out of cardia-stem cells, which results from findings in the L2-IL-1B mouse model. Following this hypothesis, and assuming BE expansion beginning from the SCJ or cardia by cell division, one would expect BE cells further away from the SCJ to retain shorter telomeres after more cell divisions than cells close to the SCJ. There was however not a clear trend with two patients exhibiting shorter telomeres in the BE region close to the SCJ compared to the BE region distant of it and the third patient the other way around. In a study by Letsolo et al. (Letsolo et al., 2017) that used the STELA method to measure telomere lengths in human BE tissue also found no correlation between BE location and telomere length.

Standard deviation and the coefficient of variation was calculated for telomere length measurements of all measured human samples (see Figure 21). This was done to obtain a measure for cell to cell variability of telomere length, similar to which was previously described by Heaphy et al. for prostate cancer assessment (Heaphy et al., 2013). While the coefficient of variation showed no significant difference, standard deviation of epithelial cell measurements got lower in most BE samples and significantly lower in LGD samples compared to cardia tissue, therefore indicating lower cell to cell variability in telomere length in these tissues. This could possibly be explained with less heterogeneity/stronger monoclonality in LGD- than in cardia samples. Letsolo et al. measured telomere length in BE specimens with the STELA method and found patchy telomere erosion with certain areas of BE in which cells retain similar telomere length which was attributed to localized clonal expansion (Letsolo et al., 2017). This indicates that low standard deviation and therefore low cell-to-cell variability in telomere length might correlate with localized clonal expansion. However it must be noted that the STELA method is more precise in estimating telomere lengths than the Q-FISH method (Lai, Wright, & Shay, 2018) and it cannot be ruled out that the downward trend in standard deviation from BE to LGD is just an artifact that vanishes with the collection of more data. It has been shown that premalignant cells that acquire p53 and p16 mutations can expand and comprise whole BE segments and can function as progenitor cells for cancer (Barrett et al., 1999). Maley et al. conducted a prospective study in which genome instability in the form of loss of heterozygosity for p53 or p16, aneuploidy or tetraploidy was combined

with the size of clonal patches which together yielded a higher hazard ratio of progression than each factor alone (Maley et al., 2004). Following this notion there might be a benefit to calculating standard deviation of epithelial cells' telomere lengths to get a second readout of telomere length measurements.

In summary, the results of telomere measurements in the human study cohort may yield new insights and approaches in utilizing telomere length measurements for the assessment of BE. The created telomere profile shows for the first time that the cardia tissue might be a suitable reference tissue for telomere length measurements, since there was a considerable decline in telomere length between cardia tissue and BE or LGD tissue in all cases but one (see Patient 3, Figure). If the progenitor cell of BE and EAC has its origin from the cardia, then the difference in telomere length between BE- and cardia-cells could indicate the history of proliferation. Likewise, it could be speculated that the difference in telomere length between mucus cells and non-mucus cells is indicative of the history of proliferation assuming considerably lower levels of proliferation in mucus producing cells. If additionally, future studies can attribute the lower standard deviation to local clonal expansion then telomere measurement can yield a triple readout:

i) Short telomeres as a risk factor for CIN and therefore increasing probability of transformational mutations.

ii) Difference between telomere length measured between cardia samples and BE or difference in telomere length between mucus producing cells and non-mucus cells as an indicator of the history of proliferation.

iii) Low standard deviation within one sample as a marker for localized clonal expansion.

All these hypotheses are untested and need to be verified in bigger prospective studies.

5.1.8 Increase in tumor initiation in telomere dysfunctional background hints at dangers of telomerase inhibition as a treatment for EAC

Telomerase inhibitors have previously been proposed for EAC therapy (Shammas et al., 2005; Shammas et al., 2004; Shammas et al., 2008) since EAC cells show increased levels of telomerase activity (Lord et al., 2000) making

activation of telomerase a likely means of achieving immortality in this cancer type. The observation of increased levels of tumor initiation in L2-IL-1B.mTERC$^{-/-}$G2 mice however raises the possibility of adverse effects of short-term use of telomerase inhibitors for EAC treatment, since it may provoke the emergence of new mutant clones, a concern already put forward in a similar context for hepatocarcinogenesis (Wanat & Johnson, 2012). In the current model for development of BE, which puts forward chronic mucosal damage and wound healing in response to micro-traumata at the gastroesophageal junction and subsequent selection of cells that can cope with this harsh environment (Quante, Graham, & Jansen, 2018; Sayin et al., 2018), telomerase inhibition might accelerate this selection by an increase in chromosomal instability and accordingly transformational mutations.

5.2 Limitations

Due to the study setting there are several limitations regarding this work. Knowledge of them will help derive more precise conclusions from the results of the experiments that were conducted in this piece of work.

5.2.1 L2-IL-1B mouse model

L2-IL-1B mouse was used as a model for carcinogenesis of EAC through preneoplastic BE for this study at hand. Comprehensive characterization of the L2-IL-1B mouse model has been carried out previously (M. Quante, J. A. Abrams, et al., 2012; M. Quante, G. Bhagat, et al., 2012), which found striking similarities between murine BE and human BE but also significant differences. Due to differences in species and the artificial modelling of the disease, any insights of this model may not exactly translate to BE development and carcinogenesis in humans. Two main differences between this mouse model and BE in humans have to be considered: i) the murine esophagus and stomach differ anatomically from their human counterparts. Mice possess a forestomach which causes the SCJ to be found in the stomach rather than at the aboral end of the esophagus like it is the case in humans. Murine esophagus tissue also lacks submucosal glands. Since current research focuses on the progenitor cell of BE (see introduction), anatomical and consequently developmental differences must be taken into consideration and make insights not completely transferable to human EAC development; ii) the L2-IL-1B mouse shows – especially with addition of bile acids to their drinking water – increased levels of FF2, CCKBR, MUC5AC, CDX2,

K19 and Notch, indicating signs of intestinal differentiation (Quante et al., 2018). However, goblet cells, which are mandated by some guidelines as a sign of intestinal metaplasia for the classification of BE (Spechler et al., 2011; K. K. Wang & Sampliner, 2008) are missing. The reason for this being that in some studies progression to EAC has been reported only when goblet cells had been found (Chandrasoma et al., 2012; Westerhoff, Hovan, Lee, & Hart, 2012). Furthermore, some studies suggest that the lack of goblet cells in some human BE biopsies is due to insufficient sampling (Gatenby, Ramus, Caygill, Shepherd, & Watson, 2008; Harrison et al., 2007). On the other hand, it was demonstrated that CLE epithelium without goblet cells expresses immunohistochemical markers that are associated with intestinal differentiation like MUC-2, CDX2 and villin, similar to CLE with goblet cells. Likewise, comparable molecular and DNA content abnormalities have been found in both tissues (Chaves et al., 2005; Hahn et al., 2009; W. Liu, Hahn, Odze, & Goyal, 2009). Moreover, other studies found similar rates of progression to dysplasia and cancer regardless of intestinal metaplasia in the form of goblet cells (Gatenby et al., 2008; Kelty, Gough, Van Wyk, Stephenson, & Ackroyd, 2007). Another study investigated the type of epithelium next to early EAC (< 2cm), which proved to be of cardiac type in 70% of cases with no goblet cells (Takubo et al., 2009). In this study however there was no mentioning whether intestinal metaplasia was present at other areas of BE without EAC, which does not address the notion of receding intestinal metaplasia with disease progression. This is a reasonable assumption since it has been shown that goblet cell count as well as Tff2+ cell count get lower with disease progression (Schellnegger et al., 2017). To sum up, there is a still an ongoing debate whether goblet cells are necessary for BE classification and risk assessment, which is resembled by differing guidelines. Depending on the point of view taken, the lack of goblet cells in the L2-IL-1B mouse model may pose a significant shortcoming in that the model does not mimic the human disease well enough. Conversely one might argue that the induction of EAC in the L2-IL-1B mouse model swings the argument in favor of making the presence of goblet cells in BE not mandatory.

5.2.2 mTERC$^{-/-}$ mouse model

The mTERC-mouse model was created to study effects of telomere dysfunction in vivo and in combination with other genetic modification. The telomerase knockout has previously been introduced to other cancer prone mouse models.

Since it uses a full body knockout, all cells – i.e. from different organs – possess very short telomeres which might lead to confounding effects. As already mentioned in the introduction there are reports of delayed wound healing and decreased resistance against chemotherapeutics of mTERC mice (Rudolph et al., 1999). In this spirit the marked increase in BE-formation in L2-IL-1B.mTERC$^{-/-}$G2 mice could be due to decreased ability of wound healing in the inflamed SCJ of these mice rather than genome instability of the SCJ cells. Another factor that cannot be addressed with this mouse model is the fact that during carcinogenesis the neoplastic cell has to find a way to achieve immortality, which is done in the majority of cases by activation of telomerase (Hanahan & Weinberg, 2011). This is not possible in this mouse model so only very early stages of carcinogenesis are modeled. This becomes more important in the light of findings that hTERT expression is elevated early in BE and telomerase activity measured by TRAP can be detected (Going et al., 2004). Furthermore there are mouse models with inducible chromosomal instability that work by alteration of TRF2 (Begus-Nahrmann et al., 2012), a part of the shelterin complex that prevents telomere uncapping and recognition by the ATM kinase (Karlseder, Broccoli, Dai, Hardy, & de Lange, 1999) or an inducible mTERT allele (Z. Ding et al., 2012). With these newer models of inducible telomere based chromosomal instability, reactivation of telomerase in the process of carcinogenesis can be modelled, which arguably resembles carcinogenesis better.

5.2.3 Differences in telomere biology between mice and humans

There are several key differences in telomere biology between mice and humans. Telomeres of mice possess far longer telomeres and telomerase activity is more abundant within murine tissues (Horikawa et al., 2005). Also in humans there is a stronger checkpoint response to telomere dysfunction, since not only the p53 pathway but also the p16/INK4a pathway is activated (Khoo, Carrasco, Bosenberg, Paik, & Depinho, 2007; Smogorzewska & de Lange, 2002). This led researchers to believe that the tumor suppressive function of telomere dysfunction based checkpoint responses is more pronounced in humans and in part explains the approximately 10,000 fold higher incidence of cancer in mice after correction for cell divisions and life span (Wright & Shay, 2000).

5.2.4 Telomere length measurement

There are several methods of telomere length measurement (see introduction). The in-situ approach of telomere length measurement used in this study enabled the assessment of individual nuclei. This allowed the distinction of mucus producing cells (i.e. goblet cells) compared to nuclei of CLE in human BE tissue. However, goblet cells were only identified by their typical vacuole-like auto-fluorescence pattern. It cannot be ruled out that cells were assigned incorrectly. Furthermore, the telomere length analysis conducted in this work used a semi-quantitative approach since absolute length of individual telomeres was not measured. To each telomeric spot a certain TFI-value was assigned according to brightness and size and the default settings of the “Telometer” program. It is possible to calibrate telomere length measurement with use of fluorescent beads or comparison to telomere length of cultured cells with known telomere length. This permits inferring the length of telomeres in a resolution of several hundred base pairs from the measured signal intensity (G., I., J., & T., 2017).

However, in both, murine telomere length analysis as well as analysis of human samples, not lengths of single telomeres were compared but signals were combined to obtain a single TFI-value per nucleus. Therefore, resolution of telomere length is restricted to the cell level. It is however known that even a subset of dysfunctional telomeres can cause telomere attrition related effects (Hemann et al., 2001; Samper et al., 2001). If telomere lengths are heterogenous with very short telomeres and longer telomeres within one cell, the calculated TFI-value per nucleus may not reflect the extent of telomere dysfunctionality.

6 Conclusion and outlook

EAC is a carcinoma with very complex chromosomal rearrangements caused by excessive CIN and great resemblance to a CIN type gastric cancer ("Integrated genomic characterization of oesophageal carcinoma," 2017). It is assumed that BE and furthermore dysplasia and EAC is not caused by a single specific driver mutation but rather by opportunistic extension of cells most viable in the harsh conditions of inflammation and reflux due to cumulative mutations and DNA abnormalities (Ross-Innes et al., 2015; X. Wang et al., 2011). Presumably stem cells of the BE region acquire different genetic mutations, which can promote but do not guarantee carcinogenesis (Yamamoto et al., 2016). Therefore, measuring telomere length as a proxy marker for possible genome instability in the carcinogenesis of EAC can help identify an individual baseline of mutational capacity.

Shortening of telomeres in the L2-IL-1B mouse model for BE was able to accelerate tumor formation with microscopically more advanced stages of disease than the age matched L2-IL-1B mice with normal telomeres. An increase of γH2AX positive cells in the SCJ region indicates a surge in DNA damage and verifies involvement of dysfunctional telomeres in the carcinogenesis in this model. This is a remarkable finding as telomere shortening alone with intact p53 was previously found to rather impair tumor formation in cancer prone mouse models (Gonzalez-Suarez et al., 2000; Greenberg et al., 1999; Jaskelioff et al., 2009; W. Y. Kim & Sharpless, 2006; Rudolph et al., 2001) and only accelerate carcinogenesis when p53 was abrogated (Artandi & DePinho, 2010; Chin et al., 1999). On the other hand, there is evidence that in some mouse models an increase in microscopic tumor formation was observed with a p53 sufficient background which led to the notion of dysfunctional telomeres being implicated early in tumor initiation (Farazi et al., 2003; Rudolph et al., 2001). This notion was fostered with observations that transient telomere dysfunction strongly accelerated carcinogenesis in other mouse models (Begus-Nahrmann et al., 2012; Z. Ding et al., 2012). Preliminary macroscopic data of the L2-IL-1B.mTERC$^{-/-}$G2.p53^{R172H} however did not show the expected promotion of tumor development and growth.

Prior studies conducted on human BE samples could detect telomeres shortening in the epithelial cell fraction, correlated with signs of chromosomal instability (Finley et al., 2006). and that telomere lengths in BE samples are within a range where chromosomal fusion has been observed (Letsolo et al., 2017).

Together these insights – increased microscopic tumor initiation in the mouse model and previously described telomere shortening in human BE samples – prompted further investigation of telomere length patterns in human BE-, LGD-, and EAC samples. In situ telomere length measurements conducted in this work affirmed telomere shortening in BE samples compared to cardia tissue and verifies the latter as a possible reference tissue for telomere measurements. Furthermore, decreased standard deviation in LGD samples as a measure for cell-to-cell telomere length variability compared to cardia tissue might indicate a higher possibility for clonal expansion within LGD samples. The here measured differences in telomere length between mucus producing cells and CLE within the same biological specimen might yield a new approach in assessing BE since it may be a proxy marker for the maturity of the lesion.

Telomere length measurement of BE cells may provide useful to future risk assessment of EAC development. It may qualify as a biomarker since it can serve as a proxy marker for chromosomal instability which has shown to be mechanistically relevant in malignant transformation of BE to EAC.

Rather recently a novel form of genome instability has been discovered, chromothripsis, that leads to tens to hundreds of chromosomal rearrangements in a single catastrophic event (Rode et al., 2016; Stephens et al., 2011). It has been verified as a driver for tumorigenesis in a significant amount of EACs (Nones et al., 2014) and telomere shortening and subsequent chromosomal instability has been proposed as a possible mechanism of chromothripsis (Jones & Jallepalli, 2012; Nones et al., 2014; Rode et al., 2016; Sorzano et al., 2013). That might bring telomere length measurement into play as a tool to estimate the likelihood of chromothriptic events. However, further prospective studies are needed to verify the results of the work at hand and test the hypotheses mentioned here.

List of references

Abdallah, J., Maradey-Romero, C., Lewis, S., Perzynski, A., & Fass, R. (2015). The relationship between length of Barrett's oesophagus mucosa and body mass index. *Aliment Pharmacol Ther, 41*(1), 137-144. doi:10.1111/apt.12991

Abnet, C. C., Lai, B., Qiao, Y. L., Vogt, S., Luo, X. M., Taylor, P. R., . . . Dawsey, S. M. (2005). Zinc concentration in esophageal biopsy specimens measured by x-ray fluorescence and esophageal cancer risk. *J Natl Cancer Inst, 97*(4), 301-306. doi:10.1093/jnci/dji042

Abnet, C. C., Qiao, Y. L., Mark, S. D., Dong, Z. W., Taylor, P. R., & Dawsey, S. M. (2001). Prospective study of tooth loss and incident esophageal and gastric cancers in China. *Cancer Causes Control, 12*(9), 847-854.

Agoston, A. T., Strauss, A. C., Dulai, P. S., Hagen, C. E., Muzikansky, A., Fudman, D. I., . . . Srivastava, A. (2016). Predictors Of Treatment Failure After Radiofrequency Ablation For Intramucosal Adenocarcinoma in Barrett Esophagus: A Multi-institutional Retrospective Cohort Study. *Am J Surg Pathol, 40*(4), 554-562. doi:10.1097/pas.0000000000000566

Aguilera, A., & Gomez-Gonzalez, B. (2008). Genome instability: a mechanistic view of its causes and consequences. *Nat Rev Genet, 9*(3), 204-217. doi:10.1038/nrg2268

Allshire, R. C., Dempster, M., & Hastie, N. D. (1989). Human telomeres contain at least three types of G-rich repeat distributed non-randomly. *Nucleic Acids Res, 17*(12), 4611-4627.

Allsopp, R. C., Morin, G. B., DePinho, R., Harley, C. B., & Weissman, I. L. (2003). Telomerase is required to slow telomere shortening and extend replicative lifespan of HSCs during serial transplantation. *Blood, 102*(2), 517-520. doi:10.1182/blood-2002-07-2334

Arnold, M., Soerjomataram, I., Ferlay, J., & Forman, D. (2015). Global incidence of oesophageal cancer by histological subtype in 2012. *Gut, 64*(3), 381-387. doi:10.1136/gutjnl-2014-308124

Artandi, S. E., Chang, S., Lee, S. L., Alson, S., Gottlieb, G. J., Chin, L., & DePinho, R. A. (2000). Telomere dysfunction promotes non-reciprocal translocations and epithelial cancers in mice. *Nature, 406*(6796), 641-645. doi:10.1038/35020592

Artandi, S. E., & DePinho, R. A. (2010). Telomeres and telomerase in cancer. *Carcinogenesis, 31*(1), 9-18. doi:10.1093/carcin/bgp268

Aubert, G., Hills, M., & Lansdorp, P. M. (2012). Telomere length measurement-caveats and a critical assessment of the available technologies and tools. *Mutat Res, 730*(1-2), 59-67. doi:10.1016/j.mrfmmm.2011.04.003

Aurelio, O. N., Kong, X. T., Gupta, S., & Stanbridge, E. J. (2000). p53 mutants have selective dominant-negative effects on apoptosis but not growth arrest in human cancer cell lines. *Mol Cell Biol, 20*(3), 770-778. doi:10.1128/mcb.20.3.770-778.2000

Badillo, R., & Francis, D. (2014). Diagnosis and treatment of gastroesophageal reflux disease. *World J Gastrointest Pharmacol Ther, 5*(3), 105-112. doi:10.4292/wjgpt.v5.i3.105

Baird, D. M., Rowson, J., Wynford-Thomas, D., & Kipling, D. (2003). Extensive allelic variation and ultrashort telomeres in senescent human cells. *Nat Genet, 33*(2), 203-207. doi:10.1038/ng1084

Barbera, M., di Pietro, M., Walker, E., Brierley, C., MacRae, S., Simons, B. D., . . . Fitzgerald, R. C. (2015). The human squamous oesophagus has widespread capacity for clonal expansion from cells at diverse stages of differentiation. *Gut, 64*(1), 11-19. doi:10.1136/gutjnl-2013-306171

Barrett, M. T., Sanchez, C. A., Prevo, L. J., Wong, D. J., Galipeau, P. C., Paulson, T. G., . . . Reid, B. J. (1999). Evolution of neoplastic cell lineages in Barrett oesophagus. *Nat Genet, 22*(1), 106-109. doi:10.1038/8816

Begus-Nahrmann, Y., Hartmann, D., Kraus, J., Eshraghi, P., Scheffold, A., Grieb, M., . . . Rudolph, K. L. (2012). Transient telomere dysfunction induces chromosomal instability and promotes carcinogenesis. *J Clin Invest, 122*(6), 2283-2288. doi:10.1172/jci61745

Bhat, S. K., McManus, D. T., Coleman, H. G., Johnston, B. T., Cardwell, C. R., McMenamin, U., . . . Murray, L. J. (2015). Oesophageal adenocarcinoma and prior diagnosis of Barrett's oesophagus: a population-based study. *Gut, 64*(1), 20-25. doi:10.1136/gutjnl-2013-305506

Bisoffi, M., Heaphy, C. M., & Griffith, J. K. (2006). Telomeres: prognostic markers for solid tumors. *Int J Cancer, 119*(10), 2255-2260. doi:10.1002/ijc.22120

Bjorkdahl, O., Akerblad, P., Gjorloff-Wingren, A., Leanderson, T., & Dohlsten, M. (1999). Lymphoid hyperplasia in transgenic mice over-expressing a secreted form of the human interleukin-1beta gene product. *Immunology, 96*(1), 128-137.

Blackburn, E. H., Epel, E. S., & Lin, J. (2015). Human telomere biology: A contributory and interactive factor in aging, disease risks, and protection. *Science, 350*(6265), 1193-1198. doi:10.1126/science.aab3389

Blasco, M. A., Funk, W., Villeponteau, B., & Greider, C. W. (1995). Functional characterization and developmental regulation of mouse telomerase RNA. *Science, 269*(5228), 1267-1270.

Blasco, M. A., Lee, H. W., Hande, M. P., Samper, E., Lansdorp, P. M., DePinho, R. A., & Greider, C. W. (1997). Telomere shortening and tumor formation by mouse cells lacking telomerase RNA. *Cell, 91*(1), 25-34.

Brandtner, A. K., & Quante, M. (2016). Risk prediction in Barrett's esophagus - aspects of a combination of molecular and epidemiologic biomarkers reflecting alterations of the microenvironment. *Scand J Clin Lab Invest Suppl, 245*, S63-69. doi:10.1080/00365513.2016.1210327

Brown, L. M., Hoover, R., Silverman, D., Baris, D., Hayes, R., Swanson, G. M., . . . Fraumeni, J. F., Jr. (2001). Excess incidence of squamous cell esophageal cancer among US Black men: role of social class and other risk factors. *Am J Epidemiol, 153*(2), 114-122.

Bulsiewicz, W. J., Kim, H. P., Dellon, E. S., Cotton, C. C., Pasricha, S., Madanick, R. D., . . . Shaheen, N. J. (2013). Safety and efficacy of endoscopic mucosal therapy with radiofrequency ablation for patients with neoplastic Barrett's esophagus. *Clin Gastroenterol Hepatol, 11*(6), 636-642. doi:10.1016/j.cgh.2012.10.028

Cawthon, R. M., Smith, K. R., O'Brien, E., Sivatchenko, A., & Kerber, R. A. (2003). Association between telomere length in blood and mortality in people aged 60 years or older. *Lancet, 361*(9355), 393-395. doi:10.1016/s0140-6736(03)12384-7

Cesare, A. J., Quinney, N., Willcox, S., Subramanian, D., & Griffith, J. D. (2003). Telomere looping in P. sativum (common garden pea). *Plant J, 36*(2), 271-279.

Chak, A., Lee, T., Kinnard, M. F., Brock, W., Faulx, A., Willis, J., . . . Goddard, K. A. (2002). Familial aggregation of Barrett's oesophagus, oesophageal adenocarcinoma, and oesophagogastric junctional adenocarcinoma in Caucasian adults. *Gut, 51*(3), 323-328.

Chandrasoma, P., Wijetunge, S., DeMeester, S., Ma, Y., Hagen, J., Zamis, L., & DeMeester, T. (2012). Columnar-lined esophagus without intestinal metaplasia has no proven risk of adenocarcinoma. *Am J Surg Pathol, 36*(1), 1-7. doi:10.1097/PAS.0b013e31822a5a2c

Chaves, P., Cruz, C., Dias Pereira, A., Suspiro, A., de Almeida, J. C., Leitao, C. N., & Soares, J. (2005). Gastric and intestinal differentiation in Barrett's metaplasia and associated adenocarcinoma. *Dis Esophagus, 18*(6), 383-387. doi:10.1111/j.1442-2050.2005.00520.x

Chin, L., Artandi, S. E., Shen, Q., Tam, A., Lee, S. L., Gottlieb, G. J., . . . DePinho, R. A. (1999). p53 deficiency rescues the adverse effects of telomere loss and cooperates with telomere dysfunction to accelerate carcinogenesis. *Cell, 97*(4), 527-538.

Choudhury, A. R., Ju, Z., Djojosubroto, M. W., Schienke, A., Lechel, A., Schaetzlein, S., . . . Rudolph, K. L. (2007). Cdkn1a deletion improves stem cell function and lifespan of mice with dysfunctional telomeres without accelerating cancer formation. *Nat Genet, 39*(1), 99-105. doi:10.1038/ng1937

Cleal, K., Norris, K., & Baird, D. (2018). Telomere Length Dynamics and the Evolution of Cancer Genome Architecture. *Int J Mol Sci, 19*(2). doi:10.3390/ijms19020482

Coad, R. A., Woodman, A. C., Warner, P. J., Barr, H., Wright, N. A., & Shepherd, N. A. (2005). On the histogenesis of Barrett's oesophagus and its associated squamous islands: a three-dimensional study of their morphological relationship with native oesophageal gland ducts. *J Pathol, 206*(4), 388-394. doi:10.1002/path.1804

Counter, C. M., Avilion, A. A., LeFeuvre, C. E., Stewart, N. G., Greider, C. W., Harley, C. B., & Bacchetti, S. (1992). Telomere shortening associated with chromosome instability is arrested in immortal cells which express telomerase activity. *Embo j, 11*(5), 1921-1929.

Croagh, D., Phillips, W. A., Redvers, R., Thomas, R. J., & Kaur, P. (2007). Identification of candidate murine esophageal stem cells using a combination of cell kinetic studies and cell surface markers. *Stem Cells, 25*(2), 313-318. doi:10.1634/stemcells.2006-0421

Curvers, W. L., Alvarez Herrero, L., Wallace, M. B., Wong Kee Song, L. M., Ragunath, K., Wolfsen, H. C., . . . Bergman, J. J. (2010). Endoscopic tri-modal imaging is more effective than standard endoscopy in identifying early-stage neoplasia in Barrett's esophagus. *Gastroenterology, 139*(4), 1106-1114. doi:10.1053/j.gastro.2010.06.045

d'Adda di Fagagna, F., Reaper, P. M., Clay-Farrace, L., Fiegler, H., Carr, P., Von Zglinicki, T., . . . Jackson, S. P. (2003). A DNA damage checkpoint response in telomere-initiated senescence. *Nature, 426*(6963), 194-198. doi:10.1038/nature02118

Davelaar, A. L., Calpe, S., Lau, L., Timmer, M. R., Visser, M., Ten Kate, F. J., . . . Krishnadath, K. K. (2015). Aberrant TP53 detected by combining immunohistochemistry and DNA-FISH improves Barrett's esophagus progression prediction: a prospective follow-up study. *Genes Chromosomes Cancer, 54*(2), 82-90. doi:10.1002/gcc.22220

de Lange, T. (2005). Shelterin: the protein complex that shapes and safeguards human telomeres. *Genes Dev, 19*(18), 2100-2110. doi:10.1101/gad.1346005

De Stefani, E., Barrios, E., & Fierro, L. (1993). Black (air-cured) and blond (flue-cured) tobacco and cancer risk. III: Oesophageal cancer. *Eur J Cancer, 29a*(5), 763-766.

di Pietro, M., Alzoubaidi, D., & Fitzgerald, R. C. (2014). Barrett's esophagus and cancer risk: how research advances can impact clinical practice. *Gut Liver, 8*(4), 356-370. doi:10.5009/gnl.2014.8.4.356

Ding, C., & Cantor, C. R. (2004). Quantitative analysis of nucleic acids--the last few years of progress. *J Biochem Mol Biol, 37*(1), 1-10.

Ding, Z., Wu, C. J., Jaskelioff, M., Ivanova, E., Kost-Alimova, M., Protopopov, A., . . . DePinho, R. A. (2012). Telomerase reactivation following telomere dysfunction yields murine prostate tumors with bone metastases. *Cell, 148*(5), 896-907. doi:10.1016/j.cell.2012.01.039

Dittmer, D., Pati, S., Zambetti, G., Chu, S., Teresky, A. K., Moore, M., . . . Levine, A. J. (1993). Gain of function mutations in p53. *Nat Genet, 4*(1), 42-46. doi:10.1038/ng0593-42

Doupe, D. P., Alcolea, M. P., Roshan, A., Zhang, G., Klein, A. M., Simons, B. D., & Jones, P. H. (2012). A single progenitor population switches behavior to maintain and repair esophageal epithelium. *Science, 337*(6098), 1091-1093. doi:10.1126/science.1218835

Dulai, G. S., Guha, S., Kahn, K. L., Gornbein, J., & Weinstein, W. M. (2002). Preoperative prevalence of Barrett's esophagus in esophageal adenocarcinoma: a systematic review. *Gastroenterology, 122*(1), 26-33.

El-Serag, H. B., Sweet, S., Winchester, C. C., & Dent, J. (2014). Update on the epidemiology of gastro-oesophageal reflux disease: a systematic review. *Gut, 63*(6), 871-880. doi:10.1136/gutjnl-2012-304269

Engel, L. S., Chow, W. H., Vaughan, T. L., Gammon, M. D., Risch, H. A., Stanford, J. L., . . . Fraumeni, J. F., Jr. (2003). Population attributable risks of esophageal and gastric cancers. *J Natl Cancer Inst, 95*(18), 1404-1413.

Fabian, T., & Leung, A. (2021). Epidemiology of Barrett's Esophagus and Esophageal Carcinoma. *Surg Clin North Am, 101*(3), 381-389. doi:10.1016/j.suc.2021.03.001

Falk, G. W. (2016). Updated Guidelines for Diagnosing and Managing Barrett Esophagus. *Gastroenterol Hepatol (N Y), 12*(7), 449-451.

Fang, M., Lew, E., Klein, M., Sebo, T., Su, Y., & Goyal, R. (2004). DNA abnormalities as marker of risk for progression of Barrett's esophagus to adenocarcinoma: image cytometric DNA analysis in formalin-fixed tissues. *Am J Gastroenterol, 99*(10), 1887-1894. doi:10.1111/j.1572-0241.2004.30886.x

Fang, Y., Chen, X., Bajpai, M., Verma, A., Das, K. M., Souza, R. F., . . . Dvorak, K. (2013). Cellular origins and molecular mechanisms of Barrett's esophagus and esophageal adenocarcinoma. *Ann N Y Acad Sci, 1300*, 187-199. doi:10.1111/nyas.12249

Farazi, P. A., Glickman, J., Jiang, S., Yu, A., Rudolph, K. L., & DePinho, R. A. (2003). Differential impact of telomere dysfunction on initiation and progression of hepatocellular carcinoma. *Cancer Res, 63*(16), 5021-5027.

Farzaneh-Far, R., Cawthon, R. M., Na, B., Browner, W. S., Schiller, N. B., & Whooley, M. A. (2008). Prognostic value of leukocyte telomere length in patients with stable coronary artery disease: data from the Heart and Soul Study. *Arterioscler Thromb Vasc Biol, 28*(7), 1379-1384. doi:10.1161/atvbaha.108.167049

Finley, J. C., Reid, B. J., Odze, R. D., Sanchez, C. A., Galipeau, P., Li, X., . . . Rabinovitch, P. S. (2006). Chromosomal instability in Barrett's esophagus is related to telomere shortening. *Cancer Epidemiol Biomarkers Prev, 15*(8), 1451-1457. doi:10.1158/1055-9965.epi-05-0837

Fitzgerald, R. C., Abdalla, S., Onwuegbusi, B. A., Sirieix, P., Saeed, I. T., Burnham, W. R., & Farthing, M. J. (2002). Inflammatory gradient in Barrett's oesophagus: implications for disease complications. *Gut, 51*(3), 316-322.

Fitzgerald, R. C., di Pietro, M., Ragunath, K., Ang, Y., Kang, J. Y., Watson, P., . . . de Caestecker, J. (2014). British Society of Gastroenterology guidelines on the diagnosis and management of Barrett's oesophagus. *Gut, 63*(1), 7-42. doi:10.1136/gutjnl-2013-305372

Fitzgerald, R. C., Onwuegbusi, B. A., Bajaj-Elliott, M., Saeed, I. T., Burnham, W. R., & Farthing, M. J. (2002). Diversity in the oesophageal phenotypic response to gastro-oesophageal reflux: immunological determinants. *Gut, 50*(4), 451-459.

Fox, J. G., Beck, P., Dangler, C. A., Whary, M. T., Wang, T. C., Shi, H. N., & Nagler-Anderson, C. (2000). Concurrent enteric helminth infection modulates inflammation and gastric immune responses and reduces helicobacter-induced gastric atrophy. *Nat Med, 6*(5), 536-542. Retrieved from http://www.ncbi.nlm.nih.gov/entrez/query.fcgi?cmd=Retrieve&db=PubMed&dopt=Citation&list_uids=10802709. doi:10.1038/75015

Fumagalli, M., Rossiello, F., Clerici, M., Barozzi, S., Cittaro, D., Kaplunov, J. M., . . . d'Adda di Fagagna, F. (2012). Telomeric DNA damage is irreparable and causes persistent DNA-damage-response activation. *Nat Cell Biol, 14*(4), 355-365. doi:10.1038/ncb2466

G., J., I., J., J., F., & T., L. (2017). Telomere Length Measurement by FISH. doi:https://doi.org/10.1007/978-3-662-52959-1_14

Galipeau, P. C., Prevo, L. J., Sanchez, C. A., Longton, G. M., & Reid, B. J. (1999). Clonal expansion and loss of heterozygosity at chromosomes 9p and 17p in premalignant esophageal (Barrett's) tissue. *J Natl Cancer Inst, 91*(24), 2087-2095.

Gammon, M. D., Schoenberg, J. B., Ahsan, H., Risch, H. A., Vaughan, T. L., Chow, W. H., . . . Fraumeni, J. F., Jr. (1997). Tobacco, alcohol, and socioeconomic status

and adenocarcinomas of the esophagus and gastric cardia. *J Natl Cancer Inst, 89*(17), 1277-1284.

Gatenby, P. A., Ramus, J. R., Caygill, C. P., Shepherd, N. A., & Watson, A. (2008). Relevance of the detection of intestinal metaplasia in non-dysplastic columnar-lined oesophagus. *Scand J Gastroenterol, 43*(5), 524-530. doi:10.1080/00365520701879831

Goh, X. Y., Rees, J. R., Paterson, A. L., Chin, S. F., Marioni, J. C., Save, V., . . . Fitzgerald, R. C. (2011). Integrative analysis of array-comparative genomic hybridisation and matched gene expression profiling data reveals novel genes with prognostic significance in oesophageal adenocarcinoma. *Gut, 60*(10), 1317-1326. doi:10.1136/gut.2010.234179

Going, J. J., Fletcher-Monaghan, A. J., Neilson, L., Wisman, B. A., van der Zee, A., Stuart, R. C., & Keith, W. N. (2004). Zoning of mucosal phenotype, dysplasia, and telomerase activity measured by telomerase repeat assay protocol in Barrett's esophagus. *Neoplasia, 6*(1), 85-92.

Gong, J. G., Costanzo, A., Yang, H. Q., Melino, G., Kaelin, W. G., Jr., Levrero, M., & Wang, J. Y. (1999). The tyrosine kinase c-Abl regulates p73 in apoptotic response to cisplatin-induced DNA damage. *Nature, 399*(6738), 806-809. doi:10.1038/21690

Gonzalez-Suarez, E., Samper, E., Flores, J. M., & Blasco, M. A. (2000). Telomerase-deficient mice with short telomeres are resistant to skin tumorigenesis. *Nat Genet, 26*(1), 114-117. doi:10.1038/79089

Gopal, D. V., Lieberman, D. A., Magaret, N., Fennerty, M. B., Sampliner, R. E., Garewal, H. S., . . . Faigel, D. O. (2003). Risk factors for dysplasia in patients with Barrett's esophagus (BE): results from a multicenter consortium. *Dig Dis Sci, 48*(8), 1537-1541.

Greenberg, R. A., Chin, L., Femino, A., Lee, K. H., Gottlieb, G. J., Singer, R. H., . . . DePinho, R. A. (1999). Short dysfunctional telomeres impair tumorigenesis in the INK4a(delta2/3) cancer-prone mouse. *Cell, 97*(4), 515-525.

Greider, C. W., & Blackburn, E. H. (1985). Identification of a specific telomere terminal transferase activity in Tetrahymena extracts. *Cell, 43*(2 Pt 1), 405-413.

Griffith, J. D., Comeau, L., Rosenfield, S., Stansel, R. M., Bianchi, A., Moss, H., & de Lange, T. (1999). Mammalian telomeres end in a large duplex loop. *Cell, 97*(4), 503-514.

Grivennikov, S. I., Greten, F. R., & Karin, M. (2010). Immunity, inflammation, and cancer. *Cell, 140*(6), 883-899. doi:10.1016/j.cell.2010.01.025

Gupta, M., Iyer, P. G., Lutzke, L., Gorospe, E. C., Abrams, J. A., Falk, G. W., . . . Wang, K. K. (2013). Recurrence of esophageal intestinal metaplasia after endoscopic mucosal resection and radiofrequency ablation of Barrett's esophagus: results from a US Multicenter Consortium. *Gastroenterology, 145*(1), 79-86.e71. doi:10.1053/j.gastro.2013.03.008

Hahn, H. P., Blount, P. L., Ayub, K., Das, K. M., Souza, R., Spechler, S., & Odze, R. D. (2009). Intestinal differentiation in metaplastic, nongoblet columnar epithelium in the esophagus. *Am J Surg Pathol, 33*(7), 1006-1015. doi:10.1097/PAS.0b013e31819f57e9

Hajar, N., Castell, D. O., Ghomrawi, H., Rackett, R., & Hila, A. (2012). Impedance pH confirms the relationship between GERD and BMI. *Dig Dis Sci, 57*(7), 1875-1879. doi:10.1007/s10620-012-2131-6

Hanahan, D., & Weinberg, R. A. (2011). Hallmarks of cancer: the next generation. *Cell, 144*(5), 646-674. doi:10.1016/j.cell.2011.02.013

Hande, M. P., Samper, E., Lansdorp, P., & Blasco, M. A. (1999). Telomere length dynamics and chromosomal instability in cells derived from telomerase null mice. *J Cell Biol, 144*(4), 589-601.

Hansel, D. E., Meeker, A. K., Hicks, J., De Marzo, A. M., Lillemoe, K. D., Schulick, R., . . . Argani, P. (2006). Telomere length variation in biliary tract metaplasia, dysplasia, and carcinoma. *Mod Pathol, 19*(6), 772-779. doi:10.1038/modpathol.3800591

Harley, C. B., Futcher, A. B., & Greider, C. W. (1990). Telomeres shorten during ageing of human fibroblasts. *Nature, 345*(6274), 458-460. doi:10.1038/345458a0

Harrison, R., Perry, I., Haddadin, W., McDonald, S., Bryan, R., Abrams, K., . . . Jankowski, J. A. (2007). Detection of intestinal metaplasia in Barrett's esophagus: an observational comparator study suggests the need for a minimum of eight biopsies. *Am J Gastroenterol, 102*(6), 1154-1161. doi:10.1111/j.1572-0241.2007.01230.x

Hayakawa, Y., Sethi, N., Sepulveda, A. R., Bass, A. J., & Wang, T. C. (2016). Oesophageal adenocarcinoma and gastric cancer: should we mind the gap? *Nat Rev Cancer, 16*(5), 305-318. doi:10.1038/nrc.2016.24

Hayflick, L. (1965). THE LIMITED IN VITRO LIFETIME OF HUMAN DIPLOID CELL STRAINS. *Exp Cell Res, 37*, 614-636.

Heaphy, C. M., Yoon, G. S., Peskoe, S. B., Joshu, C. E., Lee, T. K., Giovannucci, E., . . . Meeker, A. K. (2013). Prostate cancer cell telomere length variability and stromal cell telomere length as prognostic markers for metastasis and death. *Cancer Discov, 3*(10), 1130-1141. doi:10.1158/2159-8290.cd-13-0135

Hemann, M. T., Strong, M. A., Hao, L. Y., & Greider, C. W. (2001). The shortest telomere, not average telomere length, is critical for cell viability and chromosome stability. *Cell, 107*(1), 67-77.

Horikawa, I., Chiang, Y. J., Patterson, T., Feigenbaum, L., Leem, S. H., Michishita, E., . . . Barrett, J. C. (2005). Differential cis-regulation of human versus mouse TERT gene expression in vivo: identification of a human-specific repressive element. *Proc Natl Acad Sci U S A, 102*(51), 18437-18442. doi:10.1073/pnas.0508964102

Hur, C., Choi, S. E., Rubenstein, J. H., Kong, C. Y., Nishioka, N. S., Provenzale, D. T., & Inadomi, J. M. (2012). The cost effectiveness of radiofrequency ablation for Barrett's esophagus. *Gastroenterology, 143*(3), 567-575. doi:10.1053/j.gastro.2012.05.010

Hutchinson, L., Stenstrom, B., Chen, D., Piperdi, B., Levey, S., Lyle, S., . . . Houghton, J. (2011). Human Barrett's adenocarcinoma of the esophagus, associated myofibroblasts, and endothelium can arise from bone marrow-derived cells after allogeneic stem cell transplant. *Stem Cells Dev, 20*(1), 11-17. doi:10.1089/scd.2010.0139

Hvid-Jensen, F., Pedersen, L., Drewes, A. M., Sorensen, H. T., & Funch-Jensen, P. (2011). Incidence of adenocarcinoma among patients with Barrett's esophagus. *N Engl J Med, 365*(15), 1375-1383. doi:10.1056/NEJMoa1103042

Integrated genomic characterization of oesophageal carcinoma. (2017). *Nature, 541*(7636), 169-175. doi:10.1038/nature20805

Jacobs, J. J., & de Lange, T. (2004). Significant role for p16INK4a in p53-independent telomere-directed senescence. *Curr Biol, 14*(24), 2302-2308. doi:10.1016/j.cub.2004.12.025

Jaskelioff, M., Song, W., Xia, J., Liu, C., Kramer, J., Koido, S., . . . Gong, J. (2009). Telomerase deficiency and telomere dysfunction inhibit mammary tumors induced by polyomavirus middle T oncogene. *Oncogene, 28*(48), 4225-4236. doi:10.1038/onc.2009.268

Jiang, M., Li, H., Zhang, Y., Yang, Y., Lu, R., Liu, K., . . . Que, J. (2017). Transitional basal cells at the squamous-columnar junction generate Barrett's oesophagus. *Nature, 550*(7677), 529-533. doi:10.1038/nature24269

Jones, M. J., & Jallepalli, P. V. (2012). Chromothripsis: chromosomes in crisis. *Dev Cell, 23*(5), 908-917. doi:10.1016/j.devcel.2012.10.010

Kahn, A., Kommineni, V., Callaway, J., Pannala, R., Fleischer, D., Ashman, J. B., . . . Ramirez, F. (2015). Long-term follow-up of patients with Barrett esophagus: Progression to high-grade dysplasia and esophageal adenocarcinoma according to histology at presentation. *Journal of Clinical Oncology, 33*(3_suppl), 20-20. Retrieved from http://ascopubs.org/doi/abs/10.1200/jco.2015.33.3_suppl.20. doi:10.1200/jco.2015.33.3_suppl.20

Kalabis, J., Oyama, K., Okawa, T., Nakagawa, H., Michaylira, C. Z., Stairs, D. B., . . . Rustgi, A. K. (2008). A subpopulation of mouse esophageal basal cells has

properties of stem cells with the capacity for self-renewal and lineage specification. *J Clin Invest, 118*(12), 3860-3869. doi:10.1172/jci35012

Kapoor, H., Lohani, K. R., Lee, T. H., Agrawal, D. K., & Mittal, S. K. (2015). Animal Models of Barrett's Esophagus and Esophageal Adenocarcinoma-Past, Present, and Future. *Clin Transl Sci, 8*(6), 841-847. doi:10.1111/cts.12304

Karlseder, J., Broccoli, D., Dai, Y., Hardy, S., & de Lange, T. (1999). p53- and ATM-dependent apoptosis induced by telomeres lacking TRF2. *Science, 283*(5406), 1321-1325.

Kastelein, F., Biermann, K., Steyerberg, E. W., Verheij, J., Kalisvaart, M., Looijenga, L. H., . . . Bruno, M. J. (2013). Aberrant p53 protein expression is associated with an increased risk of neoplastic progression in patients with Barrett's oesophagus. *Gut, 62*(12), 1676-1683. doi:10.1136/gutjnl-2012-303594

Kauer, W. K., Peters, J. H., DeMeester, T. R., Ireland, A. P., Bremner, C. G., & Hagen, J. A. (1995). Mixed reflux of gastric and duodenal juices is more harmful to the esophagus than gastric juice alone. The need for surgical therapy re-emphasized. *Ann Surg, 222*(4), 525-531; discussion 531-523.

Kelty, C. J., Gough, M. D., Van Wyk, Q., Stephenson, T. J., & Ackroyd, R. (2007). Barrett's oesophagus: intestinal metaplasia is not essential for cancer risk. *Scand J Gastroenterol, 42*(11), 1271-1274. doi:10.1080/00365520701420735

Khara, H. S., Jackson, S. A., Nair, S., Deftereos, G., Patel, S., Silverman, J. F., . . . Gross, S. A. (2014). Assessment of mutational load in biopsy tissue provides additional information about genomic instability to histological classifications of Barrett's esophagus. *J Gastrointest Cancer, 45*(2), 137-145. doi:10.1007/s12029-013-9570-y

Khoo, C. M., Carrasco, D. R., Bosenberg, M. W., Paik, J. H., & Depinho, R. A. (2007). Ink4a/Arf tumor suppressor does not modulate the degenerative conditions or tumor spectrum of the telomerase-deficient mouse. *Proc Natl Acad Sci U S A, 104*(10), 3931-3936. doi:10.1073/pnas.0700093104

Kim, N. W., Piatyszek, M. A., Prowse, K. R., Harley, C. B., West, M. D., Ho, P. L., . . . Shay, J. W. (1994). Specific association of human telomerase activity with immortal cells and cancer. *Science, 266*(5193), 2011-2015.

Kim, W. Y., & Sharpless, N. E. (2006). The regulation of INK4/ARF in cancer and aging. *Cell, 127*(2), 265-275. doi:10.1016/j.cell.2006.10.003

Kimura, M., Stone, R. C., Hunt, S. C., Skurnick, J., Lu, X., Cao, X., . . . Aviv, A. (2010). Measurement of telomere length by the Southern blot analysis of terminal restriction fragment lengths. *Nat Protoc, 5*(9), 1596-1607. doi:10.1038/nprot.2010.124

Kipling, D., & Cooke, H. J. (1990). Hypervariable ultra-long telomeres in mice. *Nature, 347*(6291), 400-402. doi:10.1038/347400a0

Klobutcher, L. A., Swanton, M. T., Donini, P., & Prescott, D. M. (1981). All gene-sized DNA molecules in four species of hypotrichs have the same terminal sequence and an unusual 3' terminus. *Proc Natl Acad Sci U S A, 78*(5), 3015-3019.

Konda, V. J. A., & Souza, R. F. (2018). Biomarkers of Barrett's Esophagus: From the Laboratory to Clinical Practice. *Dig Dis Sci, 63*(8), 2070-2080. doi:10.1007/s10620-018-5088-2

Koop, H., Fuchs, K. H., Labenz, J., Lynen Jansen, P., Messmann, H., Miehlke, S., . . . Wenzl, T. G. (2014). [S2k guideline: gastroesophageal reflux disease guided by the German Society of Gastroenterology: AWMF register no. 021-013]. *Z Gastroenterol, 52*(11), 1299-1346. doi:10.1055/s-0034-1385202

Krejci, K., & Koch, J. (1998). Improved detection and comparative sizing of human chromosomal telomeres in situ. *Chromosoma, 107*(3), 198-203.

Kurz, D. J., Decary, S., Hong, Y., Trivier, E., Akhmedov, A., & Erusalimsky, J. D. (2004). Chronic oxidative stress compromises telomere integrity and accelerates the onset of senescence in human endothelial cells. *J Cell Sci, 117*(Pt 11), 2417-2426. doi:10.1242/jcs.01097

Lagergren, J., Bergstrom, R., Adami, H. O., & Nyren, O. (2000). Association between medications that relax the lower esophageal sphincter and risk for esophageal adenocarcinoma. *Ann Intern Med, 133*(3), 165-175.

Lagergren, J., Bergstrom, R., Lindgren, A., & Nyren, O. (1999). Symptomatic gastroesophageal reflux as a risk factor for esophageal adenocarcinoma. *N Engl J Med, 340*(11), 825-831. doi:10.1056/nejm199903183401101

Lai, T. P., Wright, W. E., & Shay, J. W. (2018). Comparison of telomere length measurement methods. *Philos Trans R Soc Lond B Biol Sci, 373*(1741). doi:10.1098/rstb.2016.0451

Lambert, R., & Hainaut, P. (2007). The multidisciplinary management of gastrointestinal cancer. Epidemiology of oesophagogastric cancer. *Best Pract Res Clin Gastroenterol, 21*(6), 921-945. doi:10.1016/j.bpg.2007.10.001

Lang, G. A., Iwakuma, T., Suh, Y. A., Liu, G., Rao, V. A., Parant, J. M., . . . Lozano, G. (2004). Gain of function of a p53 hot spot mutation in a mouse model of Li-Fraumeni syndrome. *Cell, 119*(6), 861-872. doi:10.1016/j.cell.2004.11.006

Lansdorp, P. M., Verwoerd, N. P., van de Rijke, F. M., Dragowska, V., Little, M. T., Dirks, R. W., . . . Tanke, H. J. (1996). Heterogeneity in telomere length of human chromosomes. *Hum Mol Genet, 5*(5), 685-691.

Lee, C. H., Wu, D. C., Lee, J. M., Wu, I. C., Goan, Y. G., Kao, E. L., . . . Wu, M. T. (2007). Carcinogenetic impact of alcohol intake on squamous cell carcinoma risk of the oesophagus in relation to tobacco smoking. *Eur J Cancer, 43*(7), 1188-1199. doi:10.1016/j.ejca.2007.01.039

Lee, H. W., Blasco, M. A., Gottlieb, G. J., Horner, J. W., 2nd, Greider, C. W., & DePinho, R. A. (1998). Essential role of mouse telomerase in highly proliferative organs. *Nature, 392*(6676), 569-574. doi:10.1038/33345

Lee, M. K., Teoh, W. W., Phang, B. H., Tong, W. M., Wang, Z. Q., & Sabapathy, K. (2012). Cell-type, dose, and mutation-type specificity dictate mutant p53 functions in vivo. *Cancer Cell, 22*(6), 751-764. doi:10.1016/j.ccr.2012.10.022

Lee, Y., Urbanska, A. M., Hayakawa, Y., Wang, H., Au, A. S., Luna, A. M., . . . Wang, T. C. (2017). Gastrin stimulates a cholecystokinin-2-receptor-expressing cardia progenitor cell and promotes progression of Barrett's-like esophagus. *Oncotarget, 8*(1), 203-214. doi:10.18632/oncotarget.10667

Leedham, S. J., Preston, S. L., McDonald, S. A., Elia, G., Bhandari, P., Poller, D., . . . Wright, N. A. (2008). Individual crypt genetic heterogeneity and the origin of metaplastic glandular epithelium in human Barrett's oesophagus. *Gut, 57*(8), 1041-1048. doi:10.1136/gut.2007.143339

Letsolo, B. T., Jones, R. E., Rowson, J., Grimstead, J. W., Keith, W. N., Jenkins, G. J., & Baird, D. M. (2017). Extensive telomere erosion is consistent with localised clonal expansions in Barrett's metaplasia. *PLoS One, 12*(3), e0174833. doi:10.1371/journal.pone.0174833

Levine, D. S., Blount, P. L., Rudolph, R. E., & Reid, B. J. (2000). Safety of a systematic endoscopic biopsy protocol in patients with Barrett's esophagus. *Am J Gastroenterol, 95*(5), 1152-1157. doi:10.1111/j.1572-0241.2000.02002.x

Li, X., Galipeau, P. C., Paulson, T. G., Sanchez, C. A., Arnaudo, J., Liu, K., . . . Reid, B. J. (2014). Temporal and spatial evolution of somatic chromosomal alterations: a case-cohort study of Barrett's esophagus. *Cancer Prev Res (Phila), 7*(1), 114-127. doi:10.1158/1940-6207.capr-13-0289

Liu, G., McDonnell, T. J., Montes de Oca Luna, R., Kapoor, M., Mims, B., El-Naggar, A. K., & Lozano, G. (2000). High metastatic potential in mice inheriting a targeted p53 missense mutation. *Proc Natl Acad Sci U S A, 97*(8), 4174-4179. doi:10.1073/pnas.97.8.4174

Liu, W., Hahn, H., Odze, R. D., & Goyal, R. K. (2009). Metaplastic esophageal columnar epithelium without goblet cells shows DNA content abnormalities similar to goblet cell-containing epithelium. *Am J Gastroenterol, 104*(4), 816-824. doi:10.1038/ajg.2009.85

Lord, R. V., Salonga, D., Danenberg, K. D., Peters, J. H., DeMeester, T. R., Park, J. M., . . . Danenberg, P. V. (2000). Telomerase reverse transcriptase expression is

increased early in the Barrett's metaplasia, dysplasia, adenocarcinoma sequence. *J Gastrointest Surg, 4*(2), 135-142.

Lu, X., Liu, D. P., & Xu, Y. (2013). The gain of function of p53 cancer mutant in promoting mammary tumorigenesis. *Oncogene, 32*(23), 2900-2906. doi:10.1038/onc.2012.299

Lundblad, V. (1997). The end replication problem: more than one solution. *Nat Med, 3*(11), 1198-1199.

Maciejowski, J., & de Lange, T. (2017). Telomeres in cancer: tumour suppression and genome instability. *Nat Rev Mol Cell Biol, 18*(3), 175-186. doi:10.1038/nrm.2016.171

Maciejowski, J., Li, Y., Bosco, N., Campbell, P. J., & de Lange, T. (2015). Chromothripsis and Kataegis Induced by Telomere Crisis. *Cell, 163*(7), 1641-1654. doi:10.1016/j.cell.2015.11.054

Macke, R. A., Nason, K. S., Mukaisho, K., Hattori, T., Fujimura, T., Sasaki, S., . . . Jobe, B. (2011). Barrett's esophagus and animal models. *Ann N Y Acad Sci, 1232*, 392-400. doi:10.1111/j.1749-6632.2011.06061.x

Maley, C. C., Galipeau, P. C., Li, X., Sanchez, C. A., Paulson, T. G., Blount, P. L., & Reid, B. J. (2004). The combination of genetic instability and clonal expansion predicts progression to esophageal adenocarcinoma. *Cancer Res, 64*(20), 7629-7633. doi:10.1158/0008-5472.can-04-1738

McClintock, B. (1939). The Behavior in Successive Nuclear Divisions of a Chromosome Broken at Meiosis. *Proc Natl Acad Sci U S A, 25*(8), 405-416.

McClintock, B. (1941). The Stability of Broken Ends of Chromosomes in Zea Mays. *Genetics, 26*(2), 234-282.

McGrath, M., Wong, J. Y., Michaud, D., Hunter, D. J., & De Vivo, I. (2007). Telomere length, cigarette smoking, and bladder cancer risk in men and women. *Cancer Epidemiol Biomarkers Prev, 16*(4), 815-819. doi:10.1158/1055-9965.epi-06-0961

Meeker, A. K., Gage, W. R., Hicks, J. L., Simon, I., Coffman, J. R., Platz, E. A., . . . De Marzo, A. M. (2002). Telomere length assessment in human archival tissues: combined telomere fluorescence in situ hybridization and immunostaining. *The American journal of pathology, 160*(4), 1259-1268. doi:10.1016/s0002-9440(10)62553-9

Meena, J., Rudolph, K. L., & Gunes, C. (2015). Telomere Dysfunction, Chromosomal Instability and Cancer. *Recent Results Cancer Res, 200*, 61-79. doi:10.1007/978-3-319-20291-4_3

Meyerson, M., Counter, C. M., Eaton, E. N., Ellisen, L. W., Steiner, P., Caddle, S. D., . . . Weinberg, R. A. (1997). hEST2, the putative human telomerase catalytic subunit gene, is up-regulated in tumor cells and during immortalization. *Cell, 90*(4), 785-795.

Mirkovic, J., Howitt, B. E., Roncarati, P., Demoulin, S., Suarez-Carmona, M., Hubert, P., . . . Herfs, M. (2015). Carcinogenic HPV infection in the cervical squamo-columnar junction. *J Pathol, 236*(3), 265-271. doi:10.1002/path.4533

Miwa, K., Sahara, H., Segawa, M., Kinami, S., Sato, T., Miyazaki, I., & Hattori, T. (1996). Reflux of duodenal or gastro-duodenal contents induces esophageal carcinoma in rats. *Int J Cancer, 67*(2), 269-274. doi:10.1002/(sici)1097-0215(19960717)67:2<269::aid-ijc19>3.0.co;2-6

Montpetit, A. J., Alhareeri, A. A., Montpetit, M., Starkweather, A. R., Elmore, L. W., Filler, K., . . . Jackson-Cook, C. K. (2014). Telomere length: a review of methods for measurement. *Nurs Res, 63*(4), 289-299. doi:10.1097/nnr.0000000000000037

Morton, J. P., Timpson, P., Karim, S. A., Ridgway, R. A., Athineos, D., Doyle, B., . . . Sansom, O. J. (2010). Mutant p53 drives metastasis and overcomes growth arrest/senescence in pancreatic cancer. *Proc Natl Acad Sci U S A, 107*(1), 246-251. doi:10.1073/pnas.0908428107

Münch, N. S., Fang, H. Y., Ingermann, J., Maurer, H. C., Anand, A., Kellner, V., . . . Quante, M. (2019). High-Fat Diet Accelerates Carcinogenesis in a Mouse Model of Barrett's Esophagus via Interleukin 8 and Alterations to the Gut Microbiome. *Gastroenterology, 157*(2), 492-506.e492. doi:10.1053/j.gastro.2019.04.013

Munoz-Jordan, J. L., Cross, G. A., de Lange, T., & Griffith, J. D. (2001). t-loops at trypanosome telomeres. *Embo j, 20*(3), 579-588. doi:10.1093/emboj/20.3.579

Naini, B. V., Chak, A., Ali, M. A., & Odze, R. D. (2015). Barrett's oesophagus diagnostic criteria: endoscopy and histology. *Best Pract Res Clin Gastroenterol, 29*(1), 77-96. doi:10.1016/j.bpg.2014.11.004

Nakagawa, H., Wang, T. C., Zukerberg, L., Odze, R., Togawa, K., May, G. H., . . . Rustgi, A. K. (1997). The targeting of the cyclin D1 oncogene by an Epstein-Barr virus promoter in transgenic mice causes dysplasia in the tongue, esophagus and forestomach. *Oncogene, 14*(10), 1185-1190. doi:10.1038/sj.onc.1200937

Nason, K. S., Wichienkuer, P. P., Awais, O., Schuchert, M. J., Luketich, J. D., O'Rourke, R. W., . . . Jobe, B. A. (2011). Gastroesophageal reflux disease symptom severity, proton pump inhibitor use, and esophageal carcinogenesis. *Arch Surg, 146*(7), 851-858. doi:10.1001/archsurg.2011.174

Nones, K., Waddell, N., Wayte, N., Patch, A. M., Bailey, P., Newell, F., . . . Barbour, A. P. (2014). Genomic catastrophes frequently arise in esophageal adenocarcinoma and drive tumorigenesis. *Nat Commun, 5*, 5224. doi:10.1038/ncomms6224

Noone AM, H. N., Krapcho M, Miller D, Brest A, Yu M, Ruhl J, Tatalovich Z, Mariotto A, Lewis DR, Chen HS, Feuer EJ, Cronin KA (eds). SEER Cancer Statistics Review, 1975-2015, National Cancer Institute. Bethesda, MD, https://seer.cancer.gov/csr/1975_2015/, based on November 2017 SEER data submission, posted to the SEER web site, April 2018.

O'Neil, A., Petersen, C. P., Choi, E., Engevik, A. C., & Goldenring, J. R. (2017). Unique Cellular Lineage Composition of the First Gland of the Mouse Gastric Corpus. *J Histochem Cytochem, 65*(1), 47-58. doi:10.1369/0022155416678182

O'Riordan, J. M., Abdel-latif, M. M., Ravi, N., McNamara, D., Byrne, P. J., McDonald, G. S., . . . Reynolds, J. V. (2005). Proinflammatory cytokine and nuclear factor kappa-B expression along the inflammation-metaplasia-dysplasia-adenocarcinoma sequence in the esophagus. *Am J Gastroenterol, 100*(6), 1257-1264. doi:10.1111/j.1572-0241.2005.41338.x

O'Sullivan, J. N., Finley, J. C., Risques, R. A., Shen, W. T., Gollahon, K. A., Moskovitz, A. H., . . . Rabinovitch, P. S. (2004). Telomere length assessment in tissue sections by quantitative FISH: image analysis algorithms. *Cytometry A, 58*(2), 120-131. Retrieved from http://www.ncbi.nlm.nih.gov/pubmed/15057965. doi:10.1002/cyto.a.20006

Olive, K. P., Tuveson, D. A., Ruhe, Z. C., Yin, B., Willis, N. A., Bronson, R. T., . . . Jacks, T. (2004). Mutant p53 gain of function in two mouse models of Li-Fraumeni syndrome. *Cell, 119*(6), 847-860. doi:10.1016/j.cell.2004.11.004

Olivier, M., Eeles, R., Hollstein, M., Khan, M. A., Harris, C. C., & Hainaut, P. (2002). The IARC TP53 database: new online mutation analysis and recommendations to users. *Hum Mutat, 19*(6), 607-614. doi:10.1002/humu.10081

Pan, Q., Nicholson, A. M., Barr, H., Harrison, L. A., Wilson, G. D., Burkert, J., . . . Jankowski, J. A. (2013). Identification of lineage-uncommitted, long-lived, label-retaining cells in healthy human esophagus and stomach, and in metaplastic esophagus. *Gastroenterology, 144*(4), 761-770. doi:10.1053/j.gastro.2012.12.022

Pastula, A., Middelhoff, M., Brandtner, A., Tobiasch, M., Hohl, B., Nuber, A. H., . . . Quante, M. (2016). Three-Dimensional Gastrointestinal Organoid Culture in Combination with Nerves or Fibroblasts: A Method to Characterize the Gastrointestinal Stem Cell Niche. *Stem Cells Int, 2016*, 3710836. doi:10.1155/2016/3710836

Paull, A., Trier, J. S., Dalton, M. D., Camp, R. C., Loeb, P., & Goyal, R. K. (1976). The histologic spectrum of Barrett's esophagus. *N Engl J Med, 295*(9), 476-480. doi:10.1056/nejm197608262950904

Pennathur, A., Gibson, M. K., Jobe, B. A., & Luketich, J. D. (2013). Oesophageal carcinoma. *Lancet, 381*(9864), 400-412. doi:10.1016/s0140-6736(12)60643-6

Postlethwait, R. W. (1983). Carcinoma of the thoracic esophagus. *Surg Clin North Am, 63*(4), 933-940.

Pouw, R. E., Wirths, K., Eisendrath, P., Sondermeijer, C. M., Ten Kate, F. J., Fockens, P., . . . Bergman, J. J. (2010). Efficacy of radiofrequency ablation combined with endoscopic resection for barrett's esophagus with early neoplasia. *Clin Gastroenterol Hepatol, 8*(1), 23-29. doi:10.1016/j.cgh.2009.07.003

Quante, M., Abrams, J. A., Lee, Y., & Wang, T. C. (2012). Barrett esophagus: what a mouse model can teach us about human disease. *Cell Cycle, 11*(23), 4328-4338. doi:10.4161/cc.22485

Quante, M., Bhagat, G., Abrams, J. A., Marache, F., Good, P., Lee, M. D., . . . Wang, T. C. (2012). Bile Acid and Inflammation Activate Gastric Cardia Stem Cells in a Mouse Model of Barrett-Like Metaplasia. *Cancer Cell, 21*(1), 36-51. Retrieved from http://dx.doi.org/10.1016/j.ccr.2011.12.004. doi:10.1016/j.ccr.2011.12.004

Quante, M., Bhagat, G., Abrams, J. A., Marache, F., Good, P., Lee, M. D., . . . Wang, T. C. (2012). Bile acid and inflammation activate gastric cardia stem cells in a mouse model of Barrett-like metaplasia. *Cancer Cell, 21*(1), 36-51. doi:10.1016/j.ccr.2011.12.004

Quante, M., Graham, T. A., & Jansen, M. (2018). Insights Into the Pathophysiology of Esophageal Adenocarcinoma. *Gastroenterology, 154*(2), 406-420. doi:10.1053/j.gastro.2017.09.046

Quante, M., & Wang, T. C. (2008). Inflammation and stem cells in gastrointestinal carcinogenesis. *Physiology (Bethesda), 23*, 350-359. doi:10.1152/physiol.00031.2008

Qureshi, A. P., Stachler, M. D., Haque, O., & Odze, R. D. (2018). Biomarkers for Barrett's esophagus - a contemporary review. *Expert Rev Mol Diagn, 18*(11), 939-946. doi:10.1080/14737159.2018.1538793

Rabinovitch, P. S., Reid, B. J., Haggitt, R. C., Norwood, T. H., & Rubin, C. E. (1989). Progression to cancer in Barrett's esophagus is associated with genomic instability. *Lab Invest, 60*(1), 65-71.

Rasband, W. S., ImageJ, U. S. National Institutes of Health, Bethesda, Maryland, USA, https://imagej.nih.gov/ij/, 1997-2018.

Reichert, S., & Stier, A. (2017). Does oxidative stress shorten telomeres in vivo? A review. *Biol Lett, 13*(12). doi:10.1098/rsbl.2017.0463

Reid, B. J., Li, X., Galipeau, P. C., & Vaughan, T. L. (2010). Barrett's oesophagus and oesophageal adenocarcinoma: time for a new synthesis. *Nat Rev Cancer, 10*(2), 87-101. doi:10.1038/nrc2773

Riboni, R., Casati, A., Nardo, T., Zaccaro, E., Ferretti, L., Nuzzo, F., & Mondello, C. (1997). Telomeric fusions in cultured human fibroblasts as a source of genomic instability. *Cancer Genet Cytogenet, 95*(2), 130-136.

Richter, J. E., & Rubenstein, J. H. (2018). Presentation and Epidemiology of Gastroesophageal Reflux Disease. *Gastroenterology, 154*(2), 267-276. doi:10.1053/j.gastro.2017.07.045

Risques, R. A., Vaughan, T. L., Li, X., Odze, R. D., Blount, P. L., Ayub, K., . . . Rabinovitch, P. S. (2007). Leukocyte telomere length predicts cancer risk in Barrett's esophagus. *Cancer Epidemiol Biomarkers Prev, 16*(12), 2649-2655. doi:10.1158/1055-9965.epi-07-0624

Rode, A., Maass, K. K., Willmund, K. V., Lichter, P., & Ernst, A. (2016). Chromothripsis in cancer cells: An update. *Int J Cancer, 138*(10), 2322-2333. doi:10.1002/ijc.29888

Roger, L., Jones, R. E., Heppel, N. H., Williams, G. T., Sampson, J. R., & Baird, D. M. (2013). Extensive telomere erosion in the initiation of colorectal adenomas and its association with chromosomal instability. *J Natl Cancer Inst, 105*(16), 1202-1211. doi:10.1093/jnci/djt191

Ross-Innes, C. S., Becq, J., Warren, A., Cheetham, R. K., Northen, H., O'Donovan, M., . . . Fitzgerald, R. C. (2015). Whole-genome sequencing provides new insights into the clonal architecture of Barrett's esophagus and esophageal adenocarcinoma. *Nat Genet, 47*(9), 1038-1046. doi:10.1038/ng.3357

Rubenstein, J. H., Mattek, N., & Eisen, G. (2010). Age- and sex-specific yield of Barrett's esophagus by endoscopy indication. *Gastrointest Endosc, 71*(1), 21-27. doi:10.1016/j.gie.2009.06.035

Rubenstein, J. H., Morgenstern, H., Appelman, H., Scheiman, J., Schoenfeld, P., McMahon, L. F., Jr., . . . Inadomi, J. M. (2013). Prediction of Barrett's esophagus among men. *Am J Gastroenterol, 108*(3), 353-362. doi:10.1038/ajg.2012.446

Rudolph, K. L., Chang, S., Lee, H. W., Blasco, M., Gottlieb, G. J., Greider, C., & DePinho, R. A. (1999). Longevity, stress response, and cancer in aging telomerase-deficient mice. *Cell, 96*(5), 701-712.

Rudolph, K. L., Millard, M., Bosenberg, M. W., & DePinho, R. A. (2001). Telomere dysfunction and evolution of intestinal carcinoma in mice and humans. *Nat Genet, 28*(2), 155-159. doi:10.1038/88871

Samper, E., Flores, J. M., & Blasco, M. A. (2001). Restoration of telomerase activity rescues chromosomal instability and premature aging in Terc-/- mice with short telomeres. *EMBO Rep, 2*(9), 800-807. doi:10.1093/embo-reports/kve174

Sarosi, G., Brown, G., Jaiswal, K., Feagins, L. A., Lee, E., Crook, T. W., . . . Spechler, S. J. (2008). Bone marrow progenitor cells contribute to esophageal regeneration and metaplasia in a rat model of Barrett's esophagus. *Dis Esophagus, 21*(1), 43-50. doi:10.1111/j.1442-2050.2007.00744.x

Satyanarayana, A., Manns, M. P., & Rudolph, K. L. (2004). Telomeres and telomerase: a dual role in hepatocarcinogenesis. *Hepatology, 40*(2), 276-283. doi:10.1002/hep.20308

Sayin, S. I., Baumeister, T., Wang, T. C., & Quante, M. (2018). Origins of Metaplasia in the Esophagus: Is This a GE Junction Stem Cell Disease? *Dig Dis Sci, 63*(8), 2013-2021. doi:10.1007/s10620-018-5152-y

Schellnegger, R., Quante, A., Rospleszcz, S., Schernhammer, M., Hohl, B., Tobiasch, M., . . . Quante, M. (2017). Goblet Cell Ratio in Combination with Differentiation and Stem Cell Markers in Barrett Esophagus Allow Distinction of Patients with and without Esophageal Adenocarcinoma. *Cancer Prev Res (Phila), 10*(1), 55-66. doi:10.1158/1940-6207.capr-16-0117

Seery, J. P., & Watt, F. M. (2000). Asymmetric stem-cell divisions define the architecture of human oesophageal epithelium. *Curr Biol, 10*(22), 1447-1450.

Serrano, M., Lee, H., Chin, L., Cordon-Cardo, C., Beach, D., & DePinho, R. A. (1996). Role of the INK4a locus in tumor suppression and cell mortality. *Cell, 85*(1), 27-37.

Shaheen, N. J., Falk, G. W., Iyer, P. G., & Gerson, L. B. (2016). ACG Clinical Guideline: Diagnosis and Management of Barrett's Esophagus. *Am J Gastroenterol, 111*(1), 30-50; quiz 51. doi:10.1038/ajg.2015.322

Shaheen, N. J., Sharma, P., Overholt, B. F., Wolfsen, H. C., Sampliner, R. E., Wang, K. K., . . . Lightdale, C. J. (2009). Radiofrequency ablation in Barrett's esophagus with dysplasia. *N Engl J Med, 360*(22), 2277-2288. doi:10.1056/NEJMoa0808145

Shammas, M. A. (2011). Telomeres, lifestyle, cancer, and aging. *Curr Opin Clin Nutr Metab Care, 14*(1), 28-34. doi:10.1097/MCO.0b013e32834121b1

Shammas, M. A., Koley, H., Batchu, R. B., Bertheau, R. C., Protopopov, A., Munshi, N. C., & Goyal, R. K. (2005). Telomerase inhibition by siRNA causes senescence and apoptosis in Barrett's adenocarcinoma cells: mechanism and therapeutic potential. *Mol Cancer, 4*, 24. doi:10.1186/1476-4598-4-24

Shammas, M. A., Koley, H., Beer, D. G., Li, C., Goyal, R. K., & Munshi, N. C. (2004). Growth arrest, apoptosis, and telomere shortening of Barrett's-associated adenocarcinoma cells by a telomerase inhibitor. *Gastroenterology, 126*(5), 1337-1346.

Shammas, M. A., Qazi, A., Batchu, R. B., Bertheau, R. C., Wong, J. Y., Rao, M. Y., . . . Goyal, R. K. (2008). Telomere maintenance in laser capture microdissection-purified Barrett's adenocarcinoma cells and effect of telomerase inhibition in vivo. *Clin Cancer Res, 14*(15), 4971-4980. doi:10.1158/1078-0432.ccr-08-0473

Sharma, P., Morales, T. G., & Sampliner, R. E. (1998). Short segment Barrett's esophagus--the need for standardization of the definition and of endoscopic

criteria. *Am J Gastroenterol, 93*(7), 1033-1036. doi:10.1111/j.1572-0241.1998.00324.x

Shippen-Lentz, D., & Blackburn, E. H. (1990). Functional evidence for an RNA template in telomerase. *Science, 247*(4942), 546-552.

Shiraishi, H., Mikami, T., Aida, J., Nakamura, K., Izumiyama-Shimomura, N., Arai, T., . . . Takubo, K. (2009). Telomere shortening in Barrett's mucosa and esophageal adenocarcinoma and its association with loss of heterozygosity. *Scand J Gastroenterol, 44*(5), 538-544. doi:10.1080/00365520902718705

Singh, S., Sharma, A. N., Murad, M. H., Buttar, N. S., El-Serag, H. B., Katzka, D. A., & Iyer, P. G. (2013). Central adiposity is associated with increased risk of esophageal inflammation, metaplasia, and adenocarcinoma: a systematic review and meta-analysis. *Clin Gastroenterol Hepatol, 11*(11), 1399-1412.e1397. doi:10.1016/j.cgh.2013.05.009

Smogorzewska, A., & de Lange, T. (2002). Different telomere damage signaling pathways in human and mouse cells. *Embo j, 21*(16), 4338-4348.

Sobinoff, A. P., & Pickett, H. A. (2017). Alternative Lengthening of Telomeres: DNA Repair Pathways Converge. *Trends Genet, 33*(12), 921-932. doi:10.1016/j.tig.2017.09.003

Solt, D. B., Cayama, E., Tsuda, H., Enomoto, K., Lee, G., & Farber, E. (1983). Promotion of liver cancer development by brief exposure to dietary 2-acetylaminofluorene plus partial hepatectomy or carbon tetrachloride. *Cancer Res, 43*(1), 188-191.

Song, Z., von Figura, G., Liu, Y., Kraus, J. M., Torrice, C., Dillon, P., . . . Lenhard Rudolph, K. (2010). Lifestyle impacts on the aging-associated expression of biomarkers of DNA damage and telomere dysfunction in human blood. *Aging Cell, 9*(4), 607-615. doi:10.1111/j.1474-9726.2010.00583.x

Song, Z., Wang, J., Guachalla, L. M., Terszowski, G., Rodewald, H. R., Ju, Z., & Rudolph, K. L. (2010). Alterations of the systemic environment are the primary cause of impaired B and T lymphopoiesis in telomere-dysfunctional mice. *Blood, 115*(8), 1481-1489. doi:10.1182/blood-2009-08-237230

Sorzano, C. O., Pascual-Montano, A., Sanchez de Diego, A., Martinez, A. C., & van Wely, K. H. (2013). Chromothripsis: breakage-fusion-bridge over and over again. *Cell Cycle, 12*(13), 2016-2023. doi:10.4161/cc.25266

Souza, R. F. (2010). Biomarkers in Barrett's Esophagus. *Tech Gastrointest Endosc, 12*(2), 116-1212. doi:10.1016/j.tgie.2010.02.006

Spechler, S. J. (2013). Barrett esophagus and risk of esophageal cancer: a clinical review. *Jama, 310*(6), 627-636. doi:10.1001/jama.2013.226450

Spechler, S. J., Sharma, P., Souza, R. F., Inadomi, J. M., & Shaheen, N. J. (2011). American Gastroenterological Association medical position statement on the management of Barrett's esophagus. *Gastroenterology, 140*(3), 1084-1091. doi:10.1053/j.gastro.2011.01.030

Spechler, S. J., & Souza, R. F. (2014). Barrett's esophagus. *N Engl J Med, 371*(9), 836-845. doi:10.1056/NEJMra1314704

Stephens, P. J., Greenman, C. D., Fu, B., Yang, F., Bignell, G. R., Mudie, L. J., . . . Campbell, P. J. (2011). Massive genomic rearrangement acquired in a single catastrophic event during cancer development. *Cell, 144*(1), 27-40. doi:10.1016/j.cell.2010.11.055

Stiewe, T., & Putzer, B. M. (2001). p73 in apoptosis. *Apoptosis, 6*(6), 447-452.

Sun, B., Wang, Y., Kota, K., Shi, Y., Motlak, S., Makambi, K., . . . Zheng, Y. L. (2015). Telomere length variation: A potential new telomere biomarker for lung cancer risk. *Lung Cancer, 88*(3), 297-303. doi:10.1016/j.lungcan.2015.03.011

Takai, H., Smogorzewska, A., & de Lange, T. (2003). DNA damage foci at dysfunctional telomeres. *Curr Biol, 13*(17), 1549-1556.

Takubo, K., Aida, J., Naomoto, Y., Sawabe, M., Arai, T., Shiraishi, H., . . . Vieth, M. (2009). Cardiac rather than intestinal-type background in endoscopic resection specimens of minute Barrett adenocarcinoma. *Hum Pathol, 40*(1), 65-74. doi:10.1016/j.humpath.2008.06.008

Taylor, J. B., & Rubenstein, J. H. (2010). Meta-analyses of the effect of symptoms of gastroesophageal reflux on the risk of Barrett's esophagus. *Am J Gastroenterol, 105*(8), 1729, 1730-1727; quiz 1738. doi:10.1038/ajg.2010.194

Taylor, P. R., Qiao, Y. L., Abnet, C. C., Dawsey, S. M., Yang, C. S., Gunter, E. W., . . . Mark, S. D. (2003). Prospective study of serum vitamin E levels and esophageal and gastric cancers. *J Natl Cancer Inst, 95*(18), 1414-1416.

Telometer (Version: 3.0.5) last published: 2020-08-28. https://demarzolab.pathology.jhmi.edu/telometer/index.html, 25.06.2021. Last Published: 2020-08-28.

Tu, S., Bhagat, G., Cui, G., Takaishi, S., Kurt-Jones, E. A., Rickman, B., . . . Wang, T. C. (2008). Overexpression of interleukin-1beta induces gastric inflammation and cancer and mobilizes myeloid-derived suppressor cells in mice. *Cancer Cell, 14*(5), 408-419. doi:10.1016/j.ccr.2008.10.011

Valdes, A. M., Andrew, T., Gardner, J. P., Kimura, M., Oelsner, E., Cherkas, L. F., . . . Spector, T. D. (2005). Obesity, cigarette smoking, and telomere length in women. *Lancet, 366*(9486), 662-664. doi:10.1016/s0140-6736(05)66630-5

Vargas, A. J., & Harris, C. C. (2016). Biomarker development in the precision medicine era: lung cancer as a case study. *Nat Rev Cancer, 16*(8), 525-537. doi:10.1038/nrc.2016.56

Vaughan, T. L., Davis, S., Kristal, A., & Thomas, D. B. (1995). Obesity, alcohol, and tobacco as risk factors for cancers of the esophagus and gastric cardia: adenocarcinoma versus squamous cell carcinoma. *Cancer Epidemiol Biomarkers Prev, 4*(2), 85-92.

Vaziri, H., & Benchimol, S. (1996). From telomere loss to p53 induction and activation of a DNA-damage pathway at senescence: the telomere loss/DNA damage model of cell aging. *Exp Gerontol, 31*(1-2), 295-301.

Vera, E., & Blasco, M. A. (2012). Beyond average: potential for measurement of short telomeres. *Aging (Albany NY), 4*(6), 379-392. doi:10.18632/aging.100462

Victorelli, S., & Passos, J. F. (2017). Telomeres and Cell Senescence - Size Matters Not. *EBioMedicine, 21*, 14-20. doi:10.1016/j.ebiom.2017.03.027

von Holzen, U., & Enders, G. H. (2012). A surprise cell of origin for Barrett's esophagus. *Cancer Biol Ther, 13*(8), 588-591. doi:10.4161/cbt.20088

von Zglinicki, T. (2002). Oxidative stress shortens telomeres. *Trends Biochem Sci, 27*(7), 339-344.

von Zglinicki, T., Saretzki, G., Ladhoff, J., d'Adda di Fagagna, F., & Jackson, S. P. (2005). Human cell senescence as a DNA damage response. *Mech Ageing Dev, 126*(1), 111-117. doi:10.1016/j.mad.2004.09.034

Vulliamy, T., Marrone, A., Goldman, F., Dearlove, A., Bessler, M., Mason, P. J., & Dokal, I. (2001). The RNA component of telomerase is mutated in autosomal dominant dyskeratosis congenita. *Nature, 413*(6854), 432-435. doi:10.1038/35096585

Wanat, J. J., & Johnson, F. B. (2012). Telomere stability and carcinogenesis: an off-again, on-again relationship. *J Clin Invest, 122*(6), 1962-1965. doi:10.1172/jci63979

Wang, K. K., & Sampliner, R. E. (2008). Updated guidelines 2008 for the diagnosis, surveillance and therapy of Barrett's esophagus. *Am J Gastroenterol, 103*(3), 788-797. doi:10.1111/j.1572-0241.2008.01835.x

Wang, X., Ouyang, H., Yamamoto, Y., Kumar, P. A., Wei, T. S., Dagher, R., . . . McKeon, F. (2011). Residual embryonic cells as precursors of a Barrett's-like metaplasia. *Cell, 145*(7), 1023-1035. doi:10.1016/j.cell.2011.05.026

Wani, S., Rubenstein, J. H., Vieth, M., & Bergman, J. (2016). Diagnosis and Management of Low-Grade Dysplasia in Barrett's Esophagus: Expert Review From the Clinical Practice Updates Committee of the American Gastroenterological Association. *Gastroenterology, 151*(5), 822-835. doi:10.1053/j.gastro.2016.09.040

Westerhoff, M., Hovan, L., Lee, C., & Hart, J. (2012). Effects of dropping the requirement for goblet cells from the diagnosis of Barrett's esophagus. *Clin Gastroenterol Hepatol, 10*(11), 1232-1236. doi:10.1016/j.cgh.2012.05.013

Weusten, B., Bisschops, R., Coron, E., Dinis-Ribeiro, M., Dumonceau, J. M., Esteban, J. M., . . . di Pietro, M. (2017). Endoscopic management of Barrett's esophagus: European Society of Gastrointestinal Endoscopy (ESGE) Position Statement. *Endoscopy, 49*(2), 191-198. doi:10.1055/s-0042-122140

Wong, K. K., Chang, S., Weiler, S. R., Ganesan, S., Chaudhuri, J., Zhu, C., . . . DePinho, R. A. (2000). Telomere dysfunction impairs DNA repair and enhances sensitivity to ionizing radiation. *Nat Genet, 26*(1), 85-88. doi:10.1038/79232

Wright, W. E., & Shay, J. W. (2000). Telomere dynamics in cancer progression and prevention: fundamental differences in human and mouse telomere biology. *Nat Med, 6*(8), 849-851. doi:10.1038/78592

Xing, J., Ajani, J. A., Chen, M., Izzo, J., Lin, J., Chen, Z., . . . Wu, X. (2009). Constitutive short telomere length of chromosome 17p and 12q but not 11q and 2p is associated with an increased risk for esophageal cancer. *Cancer Prev Res (Phila), 2*(5), 459-465. doi:10.1158/1940-6207.capr-08-0227

Yamamoto, Y., Wang, X., Bertrand, D., Kern, F., Zhang, T., Duleba, M., . . . Xian, W. (2016). Mutational spectrum of Barrett's stem cells suggests paths to initiation of a precancerous lesion. *Nat Commun, 7*, 10380. doi:10.1038/ncomms10380

Yang, E. J., Quick, M. C., Hanamornroongruang, S., Lai, K., Doyle, L. A., McKeon, F. D., . . . Herfs, M. (2015). Microanatomy of the cervical and anorectal squamocolumnar junctions: a proposed model for anatomical differences in HPV-related cancer risk. *Mod Pathol, 28*(7), 994-1000. doi:10.1038/modpathol.2015.54

Yang, Z., Huang, X., Jiang, H., Zhang, Y., Liu, H., Qin, C., . . . Ju, Z. (2009). Short telomeres and prognosis of hypertension in a chinese population. *Hypertension, 53*(4), 639-645. doi:10.1161/hypertensionaha.108.123752

Yantiss, R. K. (2010). Diagnostic challenges in the pathologic evaluation of Barrett esophagus. *Arch Pathol Lab Med, 134*(11), 1589-1600. doi:10.1043/2009-0547-rar1.1

Yousef, F., Cardwell, C., Cantwell, M. M., Galway, K., Johnston, B. T., & Murray, L. (2008). The incidence of esophageal cancer and high-grade dysplasia in Barrett's esophagus: a systematic review and meta-analysis. *Am J Epidemiol, 168*(3), 237-249. doi:10.1093/aje/kwn121

Yu, W. Y., Slack, J. M., & Tosh, D. (2005). Conversion of columnar to stratified squamous epithelium in the developing mouse oesophagus. *Dev Biol, 284*(1), 157-170. doi:10.1016/j.ydbio.2005.04.042

Zakian, V. A. (1989). Structure and function of telomeres. *Annu Rev Genet, 23*, 579-604. doi:10.1146/annurev.ge.23.120189.003051

Zhou, X., Meeker, A. K., Makambi, K. H., Kosti, O., Kallakury, B. V., Sidawy, M. K., . . . Zheng, Y. L. (2012). Telomere length variation in normal epithelial cells adjacent to tumor: potential biomarker for breast cancer local recurrence. *Carcinogenesis, 33*(1), 113-118. doi:10.1093/carcin/bgr248

Zou, Y., Sfeir, A., Gryaznov, S. M., Shay, J. W., & Wright, W. E. (2004). Does a sentinel or a subset of short telomeres determine replicative senescence? *Mol Biol Cell, 15*(8), 3709-3718. doi:10.1091/mbc.e04-03-0207

List of figures

List of tables

List of abbreviations and acronyms

+/-	Heterozygous knockout
-/-	Homozygous knockout
γH2AX	Phosphorylated H2A histone family member X
ABC	Avidin-Biotin complex
ALT	Alternative lengthening of telomeres
BE	Barrett's esophagus
BFB cylce	Breakage-fusion-bridge- cycle
BMDC	Bone-marrow derived cells
BMI	Body mass index
Bp	Base pairs
CCKBR	Cholecystokinin B receptor
CDK	Cyclin-dependent kinase
CIN	Chromosomal instability
CLE	Columnar lined epithelium
CM	Complete medium
Wnt-CCM	Wnt-Conditioned Complete Medium
CM w/o GF	Complete Medium without Growth Factors
CAN	Copy number alteration
DAB	3,3′-Diaminobenzidin
Dclk1	Doublecortin like kinase 1
DDR	DNA-damage response
DEN	Diethylnitrosamine
DMEM	Dulbecco’s Modified Eagle Medium
DNA	Deoxyribonucleic acid

DSB	Double strand break
EAC	Esophageal adenocarcinoma
EDTA	Ethylenediaminetetraacetic acid
EGF	Epidermal growth factor
EGTA	Ethylene glycol-bis(β-aminoethyl ether)-*N*,*N*,*N′*,*N′*-tetraacetic acid
ERD	Erosive reflux disease
EMR	Endomucosal resection
ENR	Epidermal Growth Factor/Noggin/R-spondin
FBS	Heat inactivated fetal bovine serum
FCS	Fetal calf serum
FELASA	Federation of European Laboratory Animal Science Associations
FFPE	Formalin fixed paraffin embedded
FISH	Fluorescence in situ hybridization
G	Generation
GC-ratio	Ratio of goblet-like cells to Columnar lined epithelium cells
GERD	Gastroesophageal reflux disease
GF	Growth factor
H&E	Hematoxylin and Eosin staining
H2AX	H2A histone family member X
HEPES	4-(2-hydroxyethyl)-1-piperazineethanesulfonic acid
HGD	High grade dysplasia
IHC	Immunohistochemistry
IL-1β	Interleukin 1beta

IL-6	Interleukin 6
LGD	Low grade dysplasia
Lgr5	Leucine-rich repeat-containing G-protein coupled receptor 5
LOH	Loss of heterozygosity
Min	Minutes
MRI	Klinikum rechts der Isar of the Technische Universität München
NERD	Non-erosive reflux disease
Nt	Nucleotide
PAS	Periodic Acid-Schiff
PBS	Phosphate buffered saline
PCR	Polymerase chain reaction
POT1	Protection of telomeres 1
Q-FISH	Quantitative fluorescence in situ hybridisation
RAP1	Repressor activator protein 1
RFA	Radiofrequency ablation
RNA	Ribonucleic acid
SCC	squamous cell carcinoma
SCJ	Squamocolumnar junction
SD	Standard deviation
SOX2	Sex determining region Y-box 2
SPF	Specific pathogen free
STELA	Single telomere length analysis
TBST	Tris-buffered saline with Tween20
mTERC	Murine telomerase RNA component

TERT	Telomerase reverse transcriptase
TFI	Telomere fluorescence intensity
TIN 2	TRF1-interacting factor
TNFα	Tumor necrosis factor alpha
TNM	Tumor, lymph nodes, metastasis
TPP1	TRF1-interacting factor (TIN2) - interacting protein 1
TRAP	Telomerase repeat assay protocol
TRF	Terminal restriction fragment
TRF1	Telomeric repeat factor 1
TRF2	Telomeric repeat binding factor 2
US	United States (of America)
Wnt-CCM with GF and ENR	Wnt-conditioned complete medium with growth factors and epidermal growth factor/Noggin/R-spondin

Appendix

Danksagung

Die vorliegende Arbeit entstand als Forschungsprojekt der II. Medizinischen Klinik der TU München und wurde durch die Deutsche Krebshilfe im Rahmen des Mildred-Scheel-Doktorandenstipendiums gefördert. Ich möchte allen meinen Dank aussprechen, die zum Gelingen dieser Arbeit beigetragen haben und mich bei der Erstellung dieser Dissertation auf unterschiedlichste Weise unterstützt haben.

An erster Stelle möchte ich mich bei meinem Doktorvater, Prof. Dr. med. Michael Quante, für die Überlassung des Themas, die freundliche Aufnahme in das Labor, die Unterstützung bei der Durchführung der Experimente sowie für die vielen konstruktiven Gespräche bedanken, die maßgeblich zum Gelingen dieser Arbeit beigetragen haben.

Weiterhin möchte ich Prof. Dr. med. Roland Schmid danken, der in seiner Rolle als Klinikdirektor mit besonderem Einsatz für die Grundlagenforschung ein produktives Umfeld geschaffen hat.

Großer Dank gilt der Deutschen Krebshilfe, welche mich finanziell und fachlich gefördert hat.

Großer Dank gilt zudem den Mitgliedern der AG Quante, welche mich ausführlich in die Labormethoden eingearbeitet und zu deren Verbesserung beigetragen haben. Hierbei möchte ich besonders Dr. Carlo Maurer, Dr. Natascha Münch, Dr. Bettina Kunze und Dr. Theresa Baumeister danken.

Besonderen Dank möchte ich Dr. Akanksha Anand aussprechen für das Mitwirken bei der Durchführung der in-vitro Experimenten. Hervorheben möchte ich außerdem die große Unterstützung, die ich von Dr. Jonas Ingermann erhalten habe. Ohne seine Unterstützung und seine fachliche Kenntnis wäre die vorliegende Arbeit nur schwer möglich gewesen.

Zu guter Letzt möchte ich meiner Familie und meinen Freunden für ihre Unterstützung über die Jahre hinweg meinen Dank aussprechen.

Publications and Presentations

Parts of this thesis have been presented on international conferences and published in a peer reviewed journal. Furthermore, related projects have been published:

Telomere shortening accelerates tumor initiation in the L2-IL1B mouse model of Barrett esophagus and emerges as a possible biomarker

Vincenz Sahm, Carlo Maurer, Theresa Baumeister, Akanksha Anand, Julia Strangmann, Roland M Schmid, Timothy C Wang, Michael Quante **Oncotarget 2022**

Shortening of telomeres accelerates carcinogenesis in a mouse model for Barrett's esophagus and emerges as a biomarker for progression to esophageal adenocarcinoma

Oral presentation at UEG 2018, Vienna

Related projects:

High-Fat Diet Accelerates Carcinogenesis in a Mouse Model of Barrett's Esophagus via Interleukin 8 and Alterations to the Gut Microbiome. Natasha Stephens Münch*, Hsin-Yu Fang*, Jonas Ingermann*, H. Carlo Maurer, Akanksha Anand, Victoria Kellner, **Vincenz Sahm**, Maria Wiethaler, Theresa Baumeister, Frederik Wein, Henrik Einwächter, Florian Bolze, Martin Klingenspor, Dirk Haller, Maria Kavanagh, Joanne Lysaght, Richard Friedman, Andrew J. Dannenberg, Michael Pollak, Peter R. Holt, Sureshkumar Muthupalani, James G. Fox, Mark T. Whary, Yoomi Lee, Tony Y. Ren, Rachael Elliot, Rebecca Fitzgerald, Katja Steiger, Roland M. Schmid, Timothy C. Wang, Michael Quante. **Gastroenterology (2019)** *Authors share co-first authorship

Notch Signaling Mediates Differentiation in Barrett's Esophagus and Promotes Progression to Adenocarcinoma.

Kunze B, Wein F, Fang HY, Anand A, Baumeister T, Strangmann J, Gerland S, Ingermann J, Münch NS, Wiethaler M, **Sahm V**, Hidalgo-Sastre A, Lange S, Lightdale CJ, Bokhari A, Falk GW, Friedman RA, Ginsberg GG, Iyer PG, Jin Z, Nakagawa H, Shawber CJ, Nguyen T, Raab WJ, Dalerba P, Rustgi AK, Sepulveda AR, Wang KK, Schmid RM, Wang TC, Abrams JA, Quante M. **Gastroenterology (2020)**